GRID-FRIENDLY SERVICES OF SMART INVERTER AND BATTERY ENERGY STORAGE SYSTEM FOR SOLAR PV INTEGRATION IN ADVANCED DISTRIBUTION NETWORKS

by

Mahfuz Ali Shuvra

A dissertation submitted to the faculty of
The University of North Carolina at Charlotte
In partial fulfillment of the requirements
for the degree of Doctor of Philosophy in
Electrical Engineering

Charlotte

2018

Approved by:

Dr. Badrul Chowdhury

Dr. Valentina Cecchi

Dr. Madhav Manjrekar

Dr. M. Yasin Raja

ABSTRACT

MAHFUZ ALI SHUVRA. Grid-friendly Services of Smart Inverter and Battery Energy Storage System for Solar PV Integration in Advanced Distribution Networks. (Under the direction of DR. BADRUL CHOWDHURY)

Solar Photovoltaic (PV) power plants are changing the landscape of the electric power industry. The smart inverter is well-known for its versatility to integrate PV resources into the utility in a 'grid-friendly' manner. BESS deployment on the power grid facilitates this highly variable energy penetration by reducing the intermittency of PV resources. However, finding new applications of solar-storage combination would be needed to make it a cost-effective and reliable solution. In this context, voltage and frequency regulation, power quality and bulk-grid support applications are addressed in this work. At first, a droop-based BESS control is developed for grid-connected and islanded modes. Then, a distributed approach for regulating the voltage profile is proposed which utilizes volt-var control of smart inverter. Frequency regulation and coordination using frequency-watt control feature is also presented. After that, it is shown that power quality in terms of selective harmonic compensation, may be extended to be effective even under grid side fault events. A novel reconfigurable and flexible voltage control strategy is also proposed and shown to be effective to mitigate voltage fluctuations in a distribution network. As a bulk grid support application, low voltage ride through technique is discussed in detail. A novel inverter reference current calculation is proposed based on the Karush-Kuhn-Tucker optimal conditions. Different case scenarios are investigated with its intended application. The results found for each application demonstrate the effectiveness of the theoretical formulations presented and finally, provide future research challenges in this area.

DEDICATION

To my mother, Gulshan Ara Begum

ACKNOWLEDGMENTS

I would like to express my gratitude to my advisor, Dr. Badrul Chowdhury. He has been very supportive, and his guidance helped me complete this work. I would also like to thank my committee members, Dr. Valentina Cecchi, Dr. Madhav Manjrekar and Dr. M. Yasin Raja, for their advice and constructive feedback.

This work has been partially supported by the Energy Production & Infrastructure Center (EPIC) Research Assistantship (RA) funding. This work is also supported by Department of Electrical and Computer Engineering (ECE) at the University of North Carolina at Charlotte (UNCC) through Graduate Assistant Support Plan (GASP) award.

My sincere thanks go to my course instructors, colleagues, family and friends who have encouraged me to finish this research. I would also like to thank my beloved wife Fahmida Shamsuddin for her constant support and continued patience during this work.

TABLE OF CONTENTS

LIST OF FIGURES

LIST OF TABLES

LIST OF ABBREVIATIONS

BESS	Battery Energy Storage Systems
BMS	Battery Management System
BPF	Band Pass Filter
DERMS	Distributed Energy Resource Management System
DG/ DER	Distributed Generation/ Distributed Energy Resource
DMS	Distribution Management System
DNO/DSO	Distributed Network Operator/Distribution System Operator
DVCC	Dual Vector Current Control
EOL	End of the Line
FFT	Fast Fourier Transformation
FRT/LVRT	Fault Ride Through/Low Voltage Ride Through
FWC	Frequency-Watt Control
GC	Grid Code
HC	Hosting Capacity
HIL	Hardware-in-the-Loop
IDMT	Inverse Definite Minimum Time
KKT	Karush-Kuhn-Tucker
LDC	Line Drop Compensator
LV/MV	Low Voltage/Medium Voltage
MCCF	Multiple-Complex-Coefficient-Filter
MPPT	Maximum Power Point Tracking
NPC	Neutral Point Clamped

OLTC	On-load Tap Changer
PCC	Point of Common Coupling
PCS	Power Conditioning System
PF	Power Factor
PI	Proportional-Integral
PLL	Phase Locked Loop
PR	Proportional-Resonant
RCF	Real-Coefficient Filter
RPS	Renewable Portfolio Standard
SAPF	Shunt Active Power Filter
SHC	Selective Harmonic Compensation
SOC	State of Charge
SRF	Synchronous Reference Frame
SVR	Step Voltage Regulator
THD	Total Harmonic Distortion
VSC/VSI	Voltage Source Converter/Inverter
VVC	Volt-Var Control

CHAPTER 1: INTRODUCTION

1.1 Motivation

In recent years, the aging of electricity infrastructure and instances of cascading blackouts in different parts of the world have challenged the electric utility industry. It has generally led to increased calls for a smarter grid. The sun produces enough power that can now be harvested by solar panels in a distributed fashion (e.g. rooftop solar) for a significant portion of our electrical energy needs. This kind of installation has gained more attention because of the recent improvement in solar cell technologies. The efficiency of certain solar cells has now reached 46% in the lab compared to 25.6% just a few years ago [1]. In the last decade, a variety of reasons have led to an increase in the capacity of solar electric plants on the grid. U.S. installations of solar energy plants have grown by about 1000% since 2008. It is currently estimated to be 13 GW, or 1% of the nation's electricity generating capacity [2]. The cost of solar electricity is also steadily decreasing and becoming economically competitive with traditional energy sources in several states. The US Department of Energy's SunShot program has set aggressive targets for reducing overall cost of solar electricity by 2020 [3].

As expected, Distributed Generation (DG) like solar Photovoltaic (PV) is changing the electric power industry landscape in a rapid manner. A power electronic interface, especially a Neutral-Point-Clamped (NPC) Voltage Source Converter (VSC), is the core component in a DG. It aids the high penetration of these sparsely populated energy resources in proper coordination with the existing grid infrastructure. Controlling the active power (P) and reactive power (Q) independently is one of the reasons utilities are interested in this technology. For grid integration purpose, Distributed Energy Resources (DER) like solar

PV systems continue to make inroads into Low Voltage (LV) and Medium Voltage (MV) distribution networks. Unlike many European countries, higher penetration of PV is planned to be accommodated as a utility asset in the US [4], which requires a large capital expenditure and continuing operating expense to successfully manage the grid of the future. With the advancement of smart PV inverter capabilities, e.g. volt-var control, volt-watt control, fixed Power Factor (PF) control, etc., utilities are now more interested to allow high penetration from DERs into the distribution feeders. The IEEE 1547a-2018 S*tandard for Interconnection and Interoperability of Distributed Energy Resources with Associated Electric Power Systems Interfaces* [5] sets the regulation policy. Higher PV penetration assists in several grid and environment-friendly features, e.g. reduction in fossil fuel costs, reduction of line losses, voltage profile improvement, etc. However, active power (P) injection from these DERs can present a challenge for the traditional voltage regulation schemes when implemented in a Distribution Management System (DMS). Therefore, voltage control is one of the fundamental issues that needs to be resolved to get maximum benefit from high PV penetration. This leads to the requirement of a separate DER Management System (DERMS).

Moreover, the impact of large scale solar photovoltaic (PV) generating stations on the grid frequency is no longer insignificant [6]. With the deployment of distributed, large scale PV; frequency regulation is becoming more of a challenge. Conventional synchronous generator-based power systems have an advantage of high inertia, which is not the case for Voltage Source Inverter (VSI) interfaced energy resources like solar PV. Therefore, it is critical to clear, as quickly as possible, any abnormal frequency event which leads to transient frequency instability in a low-inertia grid [7], [8].

1.2 Literature review

In this section, a comprehensive review on existing works is provided. The literature review in this thesis covers two broad areas: utility applications of grid connected smart inverters with Battery Energy Storage Systems (BESS) and control of smart inverters during grid disturbance events. In the first part, existing solutions on the grid connected smart inverter control and application are reviewed. Then, a literature review on the control of smart inverters during grid side fault event is provided in the second sub-section.

1.2.1 Existing work on application of grid connected smart PV inverters and BESS

Different control strategies can be implemented to use the smart inverter for advanced functionalities. However, the goal is to emulate the behavior of a conventional synchronous generator [7]. A smart inverter is a powerful tool that can successfully mimic the control of a synchronous generator in a low-inertia system. As DGs can work in grid connected or islanded modes, the controller design differs based on the intended purpose. When DGs are connected to the grid, voltage (V) and frequency (f) are imposed by the grid network [9], [10]. In the islanded mode, the BESS is responsible for maintaining the voltage and frequency inside the micro-grid. Therefore, the BESS-side inverter control mode shifts to V-f scheme [11], [12]. During islanding, typical response time of BESS is in the order of 50-100ms [13]. Once the voltage and frequency are restored after subsequent islanding, all other DGs can continue to operate on power exchange (PQ) mode. Typically, PV sources connected far from the substation experience higher voltage problems which can cause serious system damage and/or voltage instability problem [14]–[16]. DMS uses communication protocols to send control signals to remotely operate the field devices. In the past, fixed and switching capacitors were the only assets to correct the voltage deviation

caused by inductive reactive power loading. On-load Tap Changers (OLTC) or Step Voltage Regulators (SVR) were used to mitigate the voltage deviation caused by the resistive active power loading [17]. Line Drop Compensators (LDC) were commanded from the centralized substation to keep the voltage profile within allowable limits. The problem with this centralized approach to send control signals and receive data from field devices are mainly twofold - single point of failure and high cost. To overcome these problems, a distributed voltage control scheme has been introduced in the literature [18]–[20]. The voltage control devices have sluggish response which poses a real challenge to solve the voltage rise problem due to high and intermittent PV penetration. Starting from IEEE 1547a-2014 standard [21], smart inverters can exchange reactive power with the grid to actively control the voltage at the Point of Common Coupling (PCC). This aids the utility industry to better manage and coordinate multiple smart inverters through integrated Volt-Var Control (VVC) which makes the DMS more aware of the network. This still requires a communication network to connect to DMS to update status.

On a different note, power systems operate on a principle in balancing generation and load at any point of time. If the generation becomes more than the load demand, an over-frequency event occurs. On the contrary, if demand is high compared to generation, an under-frequency event is recorded. Historically, a Distribution System Operator (DSO) coordinates with a power plant operator to increase or decrease the fuel consumption for controlling the grid frequency. However, PV generation is dependent on the weather condition and fluctuates throughout the day. Also, high PV penetration usually happens around sunny mid-days and typically creates an over-frequency event. From the DSO perspective, this is a problem that impedes further PV penetration into the distribution feeder

despite having enough Hosting Capacity (HC) remaining. In the US, not utilizing the HC directly affects the goal to meet the Renewable Portfolio Standard (RPS) in different states. Therefore, there is a greater call for advanced frequency regulation support from the smart inverters which benefits both the utility, federal government and customers.

To solve this classical problem, researchers have proposed different control strategies [22]–[25]. One way to solve the case is to use a BESS in association with the PV plant using a DC-coupler or a separate inverter. It provides a virtual inertia and a tight frequency regulation by controlling the DC link voltage [26]. Moreover, in an over-frequency event, PV power can be curtailed and stored in the BESS which can be used when needed, such as, in an under-frequency event. In this way, frequency regulation can be ensured for bulk power system support. Although good, this requires large scale BESS deployment, which makes it a costly solution [27]. A better, cost-effective solution is to use an advanced control strategy from smart PV inverters popularly known as Frequency-Watt Control (FWC). This type of control does not require costly infrastructure to communicate with the system operator. The reason behind it is that the FWC is inherently a droop-based control which is like a conventional governor-droop control. Also, FWC control can respond to an abnormal frequency event within a sub-second time scale [28]. Today, smart inverters are manufactured with FWC features which assist in high penetration scenario. In these inverters, the FWC is designed to respond primarily for over-frequency events as under-frequency events need extra active power (P) generation.

1.2.2 Existing work on the control of smart inverters during grid side fault

There have been concerns about the control strategy of VSIs during grid side disturbances. PV system sizes may vary from several kW to several hundred MW; yet, several technical

issues related to the impact of system conditions have to be taken into consideration before these plants can be considered ‘grid-friendly’. One of the concerns is Low Voltage Ride Through (LVRT) implementation which is an essential feature to maintain stability during various grid faults. In the meantime, string connections with embedded miniature inverters have gained popularity. It is already proposed to be mandatory in the IEEE 1547a-2018 standard to have Fault Ride Through (FRT) feature enabled in smart inverters.

Previously, PV plants using inverters that are IEEE Std. 1547/UL 1741 compliant do not have LVRT capability since these plants were required to disconnect in the event of a disturbance on the utility system [29]. Large penetration levels of PV plants using these types of inverter at the distribution voltage level can affect the grid stability. New inverter designs with reactive power and FRT capability and other ‘grid friendly’ features are expected to be required in new plant design during the planning stage. Therefore, implementing the FRT capability has been investigated as obvious from the literature. A LVRT capable 5 kW grid tie solar inverter is simulated in [30]. The control system is based on a Proportional-Resonant (PR) controller that can track sinusoidal signals at its resonance frequency. A 2 MW plant is simulated in [31] with boost converter topology and dynamic MPPT tracking algorithm. However, it does not consider micro-level performance of the system. Performance of a large PV plant is simulated under various balanced and unbalanced grid faults in [32]. Grid Codes (GC) govern the connection between conventional grid and DER at the PCC. According to the existing grid codes, solar panels cannot actively control the voltage and frequency in case of a fault on the grid side at the PCC. As soon as a fault occurs, the inverters must be tripped off. But German GC has already mentioned in their updated guidelines that PV panels can contribute reactive power

at times of a grid fault to improve the voltage sag. The requirements are also adopted in the US and Spain [33].

As mentioned earlier, DGs or BESS need a power electronic interface for interfacing with the electric power system. Typically, the interface is designed by VSI which works quite well in normal operating condition. These interfacing inverters are required to maintain several power quality standards at the PCC. IEEE 519-1992 is such a standard for harmonics control [34]. One of the attractive features of the VSI is that it can be used as a Shunt Active Power Filter (SAPF) to compensate harmonic currents arising from non-linear loads [35]. As the VSI, the grid, and the load are all connected in a parallel fashion at the PCC; the VSI can be used to supply harmonic current (I_h). There are various methods for harmonic detection and selective harmonic compensation that are reported in the literature [36], [37]. All of them work well under normal operating conditions. However, in case of an unbalanced grid fault, the voltage at the PCC is unbalanced, and might get distorted by harmonics even with a linear load. Harmonics control requirements standardized by IEEE 519 (1992 and 2014) - *IEEE Recommended Practices and Requirements for Harmonic Control in Electrical Power Systems*; provide guidelines for specific harmonic control during normal operating conditions. However, under abnormal or unbalanced operating conditions on the grid side, the limits may not apply [38]–[40]. Maintaining power quality e.g. harmonic control during fault events is therefore also quite ambitious at this point of time. In future, smart inverters might be required to have this capability because of the concern for improving system efficiency while incorporating higher penetration of renewable energy resources. In such a scenario, the harmonic detection and compensation technique in SAPF is one of the key factors that will need to be modified [41].

1.3 Novelty and contribution

This dissertation is divided into 6 chapters. Chapter 2 describes control and application of smart inverters in voltage and frequency regulation. Chapter 3 focuses on grid support application of smart inverter and BESS during grid faults. Chapter 4 discusses a novel reconfigurable and flexible voltage control strategy with integrated BESS for advanced distribution networks. Chapter 5 proposed a distributed dynamic grid support using smart PV inverters during unbalanced grid faults. Chapter 6 concludes the work by summarizing the findings followed by future research work in this area. The novelty and contribution of this work are summarized below-

Chapter 2: The proposed unified P-f and Q-V control supports remote on/off feature of the smart inverter with adjustable droop settings. The previous approaches often did not consider these two things. The unified approach can enable voltage and frequency regeneration via secondary control layer in islanded/microgrid mode and simultaneously supports “local” voltage and frequency regulation. Unified Q-V droop control can also correct power factor locally working as a switched capacitor bank. Next, it is shown that a unique yet simple OLTC and inverter coordination based on the leading and lagging var direction can be achieved that mitigates voltage rise or drop effectively and allow high PV penetration. Most of the existing methodologies used costly and complex communication infrastructure with a single point-of-failure. Finally, a coordinated FWC scheme for multiple inverters is proposed which mimics the principle of inverse definite minimum time (IDMT) characteristics for frequency regulation aiding bulk grid in the upstream. The novelty of this work lies in the fact that the existing frequency regulation approaches require BESS and a centralized communication network to solve this classical issue.

Chapter 3: Dynamic voltage support and low voltage ride through using dc link voltage stabilization with BESS is proposed. The novelty of this work is in the application of BESS for extended period of operation in strong and weak grid conditions which is not considered in existing literature. Investigation on PLL performance under fault condition found room for improvement inside its structure for synchronization and sequence extraction which is solved by MCCF. The contribution is in the value proposition of using smart inverter as shunt active power filter to improve power quality during normal and faulty condition.

Chapter 4: A reconfigurable voltage control strategy is proposed for the two-stage utility owned PV and integrated BESS technology. Then, a novel topology is introduced to incorporate a BESS which is safe and easy to reconfigure from an operational standpoint, not possible in existing literature and industry practice. The proposed algorithm is implemented by device level controllers and local voltage control is guaranteed. Flexible voltage control can be achieved using active and reactive power in a network cognizant manner.

Chapter 5: A dynamic voltage support strategy using smart inverters for a two-stage PV inverter architecture, which can be applied to different feeders with different X/R ratios, is proposed. Karush–Kuhn–Tucker (KKT) condition is implemented at the heart of the proposed approach to calculate and optimize the required active and reactive current references in both positive and negative sequence frames during a fault. A new distributed coordination approach among multiple inverters to ride through the same fault event based on fundamental positive and negative sequence voltage support is also proposed which is non-existent in current literature.

CHAPTER 2: CONTROL AND APPLICATION OF SMART INVERTERS IN VOLTAGE AND FREQUENCY REGULATION

In this chapter, first, a droop based autonomous control for the smart inverter interface in grid connected and islanded mode is presented. The controller is implemented in dq0 reference frame so that active and reactive power control can be decoupled. The proposed controllers can easily be scaled up for a larger network with many DGs connected to any location. The MATLAB/SIMSCAPE POWER SYSTEMS package is used for simulation purpose. Conventional P-f and Q-V droops are implemented and extensively discussed in the context of their application in different scenarios.

Secondly, based on the grid connected control scheme of the inverter, a distributed voltage control scheme for MV distribution networks is proposed. The proposed scheme requires minimal information exchange between the nearby existing voltage control devices like On Load Tap Changer (OLTC), capacitor banks, etc. and three-phase smart inverters that may be connected at the far End-of-the-Line (EOL) in high PV penetration scenarios. A leading and lagging power factor (PF)-based algorithm is developed to properly coordinate these multiple inverters. Advanced Volt-Var characteristics of the smart inverter equipped with extended reactive power reserve is used to mitigate the voltage rise issue. A theoretical framework is also developed for setting the inverter control parameters.

Finally, the classical frequency regulation problem of the same MV distribution network with high PV penetration is addressed. The methodology, using multiple distributed smart inverters, is discussed thoroughly. The frequency control strategy shown here, is primarily based on the advanced Frequency-Watt Control (FWC) feature of the Voltage Source

Inverter (VSI). This feature mimics the governor droop control of conventional synchronous generator and doesn't require costly communication infrastructure. Dead band coordination is discussed and a low-cost coordination strategy for multiple smart PV inverters is also proposed based on the Inverse Definite Minimum Time (IDMT) principle. Dynamic frequency regulation on a modified IEEE-13 bus test system is simulated and analyzed to verify the effectiveness of the proposed solution. Simulation results from a modified IEEE 13 bus test system verify the effectiveness of these proposed control methods.

2.1 Autonomous control of smart inverters in grid connected and islanded mode

For simplicity, a small medium voltage distribution feeder equipped with one solar PV panel and one BESS is used for validating the controller performance. Two different types of controllers are shown-one for the PV system and another for the BESS. Two different autonomous control algorithms for proper coordination and power sharing among a 100kW solar PV, an 80 kW Li-Ion BESS and the grid network are presented with the focus on inverter control strategy. One control strategy is used for active power droop and other for reactive power droop. The proposed system is shown in Figure 2-1. The BESS is installed with a separate Power Conditioning System (PCS) for maintaining the power balance during the transition. Droop control method is utilized to share the power with respect to voltage and frequency deviation [42]. Another approach with back-to-back converter is presented in [43].

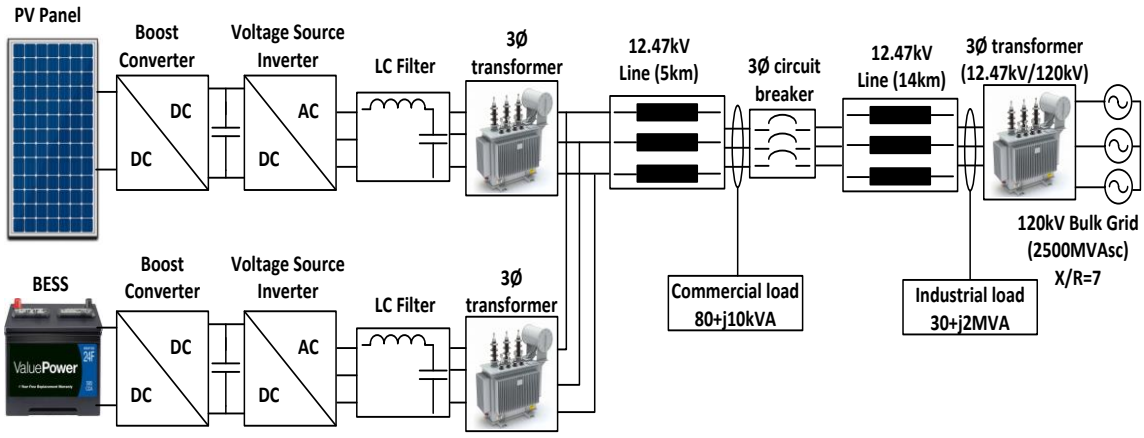

Figure 2-1: Studied MV distribution network

2.1.1 Solar PV system

The parameters used for the PV system are listed in Table 2-1. From a VSI operational point of view, the DC-link voltage control is the primary concern for any successful

interconnection. Solar energy is intermittent in nature. Therefore, it cannot maintain the voltage at the DC side. Moreover, the voltage at the output of the PV panels is at a different level than that needed for connecting to the grid via smart inverter interface. So, a DC/DC boost converter is usually deployed at the front end of the inverter. The purpose of the boost converter is twofold- a) maximum power point tracking (MPPT) and b) voltage boost to match the inverter input. For this work, the incremental conductance method is used for MPPT operation. The relationship between DC and AC side voltages is given in (2.1).

$$V_{dc} = \frac{2\sqrt{2}V_{LL}}{\sqrt{3}\mathrm{M_a}} \tag{2.1}$$

where, M_a is the amplitude modulation index of the inverter. For a sinusoidal PWM generation scheme it is limited to maximum value of 1 [44]. V_{dc} is the DC-link voltage and V_{LL} is the AC side line-to-line voltage in rms. As a 12.47 kV medium voltage distribution system is considered, a 0.48/12.47kV step-up transformer is needed to match the grid voltage. Essentially, it becomes a two-stage transformer-connected PV system and the leakage reactance of the transformer is considered while designing the controller.

Table 2-1: Solar PV system parameters

Parameters	**Values**
Module type	Sun power SPR-305-WHT (96 cells)
Open circuit voltage (V_{oc})	64.2 V
Short circuit current (I_{sc})	5.96 A
Voltage at MPP (V_{mpp})	54.7 V
Current at MPP (I_{mpp})	5.58 A
Number of series connected modules (N_s)	5
Number of parallel connected modules (N_p)	66

The capacitor at the front end of the PV inverter is the primary source of inertia of the system. To maintain the instantaneous power balance between PV side and AC grid,

capacitor charge balance is needed, which is the key concept for driving the inverter. Energy conservation on both sides leads to-

$$P_{dc} = \mathrm{P}_{AC} \tag{2.2}$$

$$V_{dc}\mathrm{I}_{\mathrm{dc}} = \mathrm{V}_{\mathrm{pu}} I_{pu} \tag{2.3}$$

Equation (2.2) and (2.3) shows that the AC current can be controlled in a way such that the DC link voltage remains constant. So, controlling the output AC current based on the DC link voltage stabilization is the main goal for PV inverters. Injecting the active power into the system in this way is efficient and independent of reactive power output. The governing equations for P and Q in a synchronous reference frame is as follows [45]-

$$\mathrm{P} = \frac{3}{2} V_d I_d \tag{2.4}$$

$$Q = -\frac{3}{2} V_d I_q \tag{2.5}$$

Equation (2.4) shows that the active power can be controlled by the d-axis grid current component (I_d) and whereas (2.5) shows that Q can be controlled by q-axis grid current component (I_q). These components are decoupled and independent of each other's influence. Two separate PI controllers are designed and tuned for reference tracking as shown in Table 2-2.

Table 2-2: DC voltage controller parameters

Parameters	**Values**
Outer voltage controller, [K_p, K_i]	[7, 800]
Inner current controller, [K_p, K_i]	[0.3, 20]

Such a controller is designed which consists of an outer DC voltage control loop and an inner AC current control loop. Figure 2-2 shows the cascaded configuration of the controller.

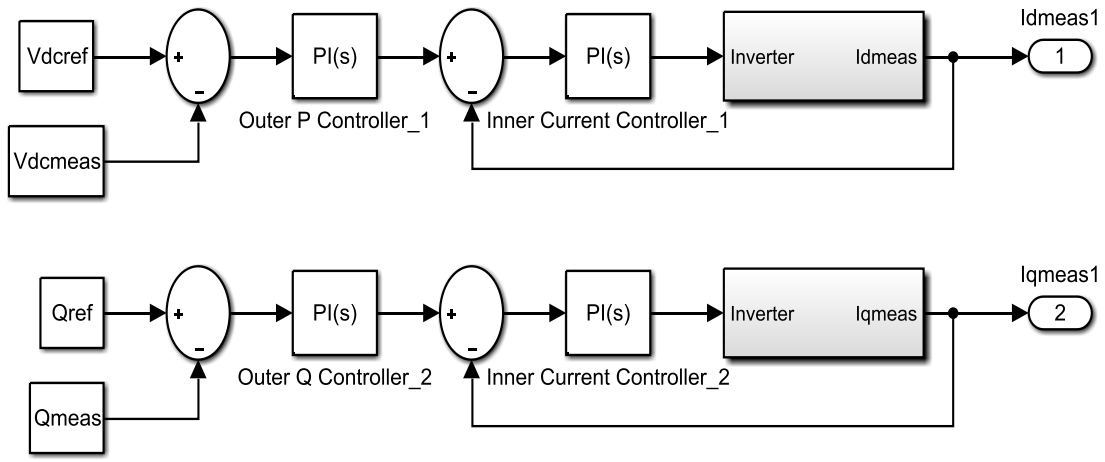

Figure 2-2: PV inverter control strategy

2.1.2 Battery energy storage system (BESS)

BESS can maintain the voltage in the input side of the inverter. To match up the voltage, a DC/DC boost converter on the DC side and a 0.48/12.47kV transformer on the AC side are also deployed. The idea of using a separate inverter for the BESS is to use it as a complete energy source when needed. In grid connected mode, the battery can be charged by the excess PV generation or by the grid in PQ mode. It can also be discharged to support any deficiency of power from the PV system. Thus, the whole system can work as a dispatch able source. During islanded mode, voltage and frequency can be restored by utilizing faster response from BESS to support the transient event. The parameters used for the BESS is shown in Table 2-3.

Table 2-3: Battery energy storage system parameters

Parameters	Values
Nominal voltage (V_{nom})	400V
Nominal ampere-hour rating (I_{nom})	200Ah
Initial state-of-charge (SOC)	100%
Outer voltage controller, [$K_{p,}$ K_i]	[1, 0]
Inner current controller, [$K_{p,}$ K_i]	[0.0177, 45.7]

The control system for the BESS is shown in Figure 2-3. The only difference between Figure 2-2 and Figure 2-3 is that the BESS controller injects the power based on a P_{ref} command. The DC voltage at the inverter input holds a stable value if the battery State-of-Charge (SOC) is in an acceptable range.

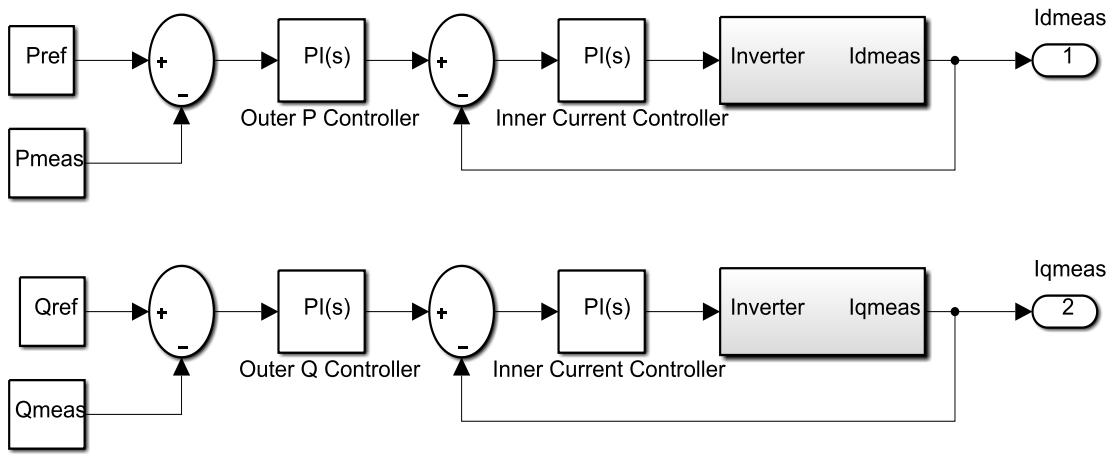

Figure 2-3: BESS inverter control strategy

2.2 Proposed control algorithm

In a synchronous generator, droop characteristics show that active power flow can be controlled by controlling the frequency which is known as P-f droop. Similarly, Q-V droop can also be found as the synchronous generator adjusts the voltage by using its excitation control. However, this relationship holds true for those networks which have a higher X/R ratio [46] as is the case for medium voltage distribution systems. In our case, the X/R ratio is 7 and the following equations hold true for our case-

$$f_{ref} = f_{nom} - m(P - P_0) \tag{2.6}$$

$$V_{ref} = V_{nom} - n(Q - Q_0). \tag{2.7}$$

where, f_{ref} and V_{ref} are reference frequency and voltage magnitude respectively for the DG, f_{nom} and V_{nom} are the frequency and voltage magnitude respectively when $P=P_0$ and $Q=Q_0$; m and n are the droop coefficients, which are typically in the range of 2-5% [47]. As the inverter interface has two modes of operation, two different droop settings can be applied, which are discussed in the following sections.

2.2.1 P-f Droop

In grid connected mode, grid frequency is generally set to 60 Hz as per US standard. Any change in instantaneous frequency is measured accurately by Phase Locked Loop (PLL) inside the inverter control system. The droop control can be set using a proportional controller. We have used 5% droop coefficient in case of grid connected operation. If there is any change in grid frequency, the output power of the DGs will be adjusted according to (2.6). In the transition process from grid connected to autonomous islanded mode, droop settings could be set to a lower value so that DGs do not experience a major change in their

output power. Doing so, the burden on secondary control can be reduced to reestablish the frequency in an islanded microgrid seamlessly. To eliminate the steady state error, an integral controller along with the proportional term is implemented for calculating the droop coefficient in microgrid application. We have used 2% droop for islanded microgrid case. Figure 2-4 shows the flowchart of the proposed scheme.

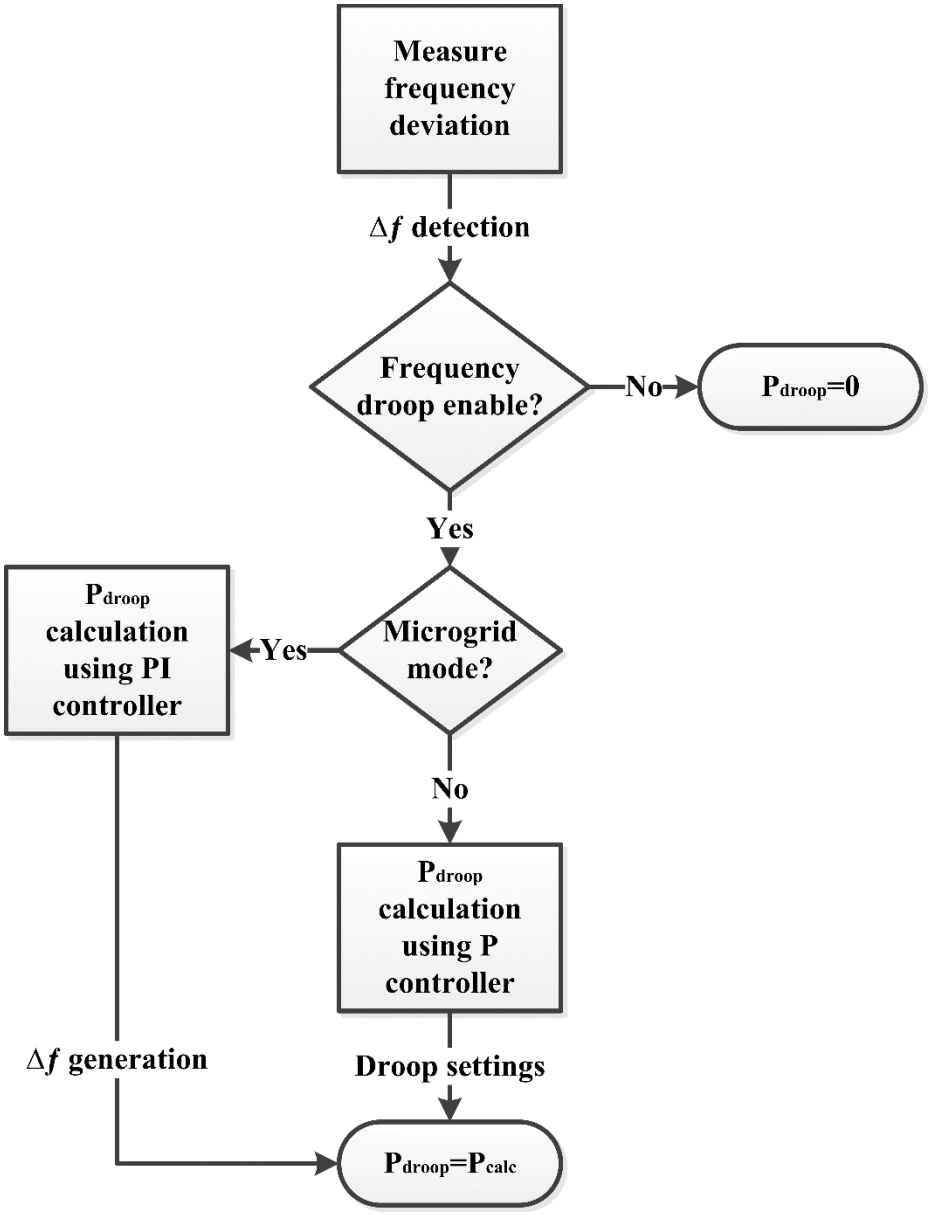

Figure 2-4: Proposed P-f droop control scheme

2.2.2 Q-V Droop

Using smart inverter reactive power capability, two different operations can be possible. The first one is unity power factor (PF) operation. Setting the Q_{ref} to zero in Figure 2-2 and Figure 2-3 guarantees unity PF operation in case of properly tuned PI controllers. But the availability of Q in inverters comes in two different forms vis-a-vis:

$$Q_{max} = \sqrt{S^2 - P^2} \tag{2.8}$$

$$Q = P\tan\theta \tag{2.9}$$

Equation (2.8) shows the maximum Q that can be extracted considering S as the inverter rating and P as the active power that is supplied by the DG. For any given PF, (2.9) provides the available Q that can be supplied without violating the inverter rating, S. Alternately, reactive power can be injected/absorbed by the inverter by setting Q_{ref} to any value other than zero. This scheme helps the utilities to achieve automatic and fast voltage control from the DGs that are connected to the network. Both the schemes have dependencies on voltage deviation as seen from (2.7). Figure 2-5 shows the flowchart of the proposed Q-V scheme.

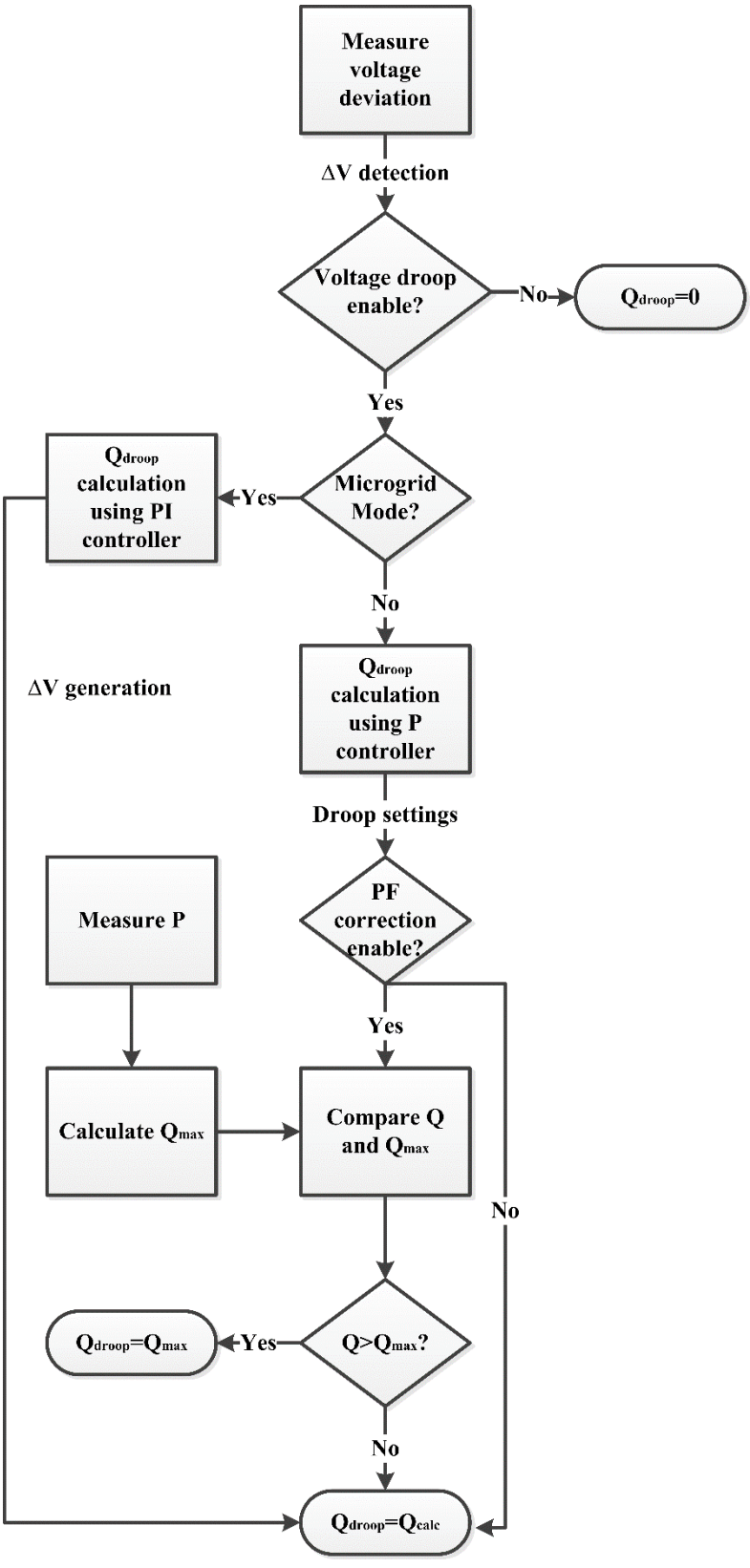

Figure 2-5: Proposed Q-V droop control scheme

2.3 Simulation results and analysis

Simulation results are presented case wise in the following two sections-

2.3.1 Operation without droop controller

Operation without a droop controller enabled shows the active and reactive power sharing between PV, BESS and grid. Initially, a small load of 80+j10 kVA is served in grid connected mode. Figure 2-6(a) shows the irradiance and temperature profile for the solar PV system. Figure 2-6(b) demonstrates that PV and BESS contribute to supply the load. No active power comes from the grid; instead, the grid supplies only the reactive power demand, as shown. Figure 2-6(c) shows that a dynamic load change can also be accommodated with the help of the grid supplying the excess demand. Figure 2-7 depicts the same case as Figure 2-6(b) in islanded condition, where an intentional islanding is simulated at 1.25 sec. After islanding, the BESS can restore the voltage, frequency, and power sharing in islanded mode, which is seamless as seen from the Figure 2-7.

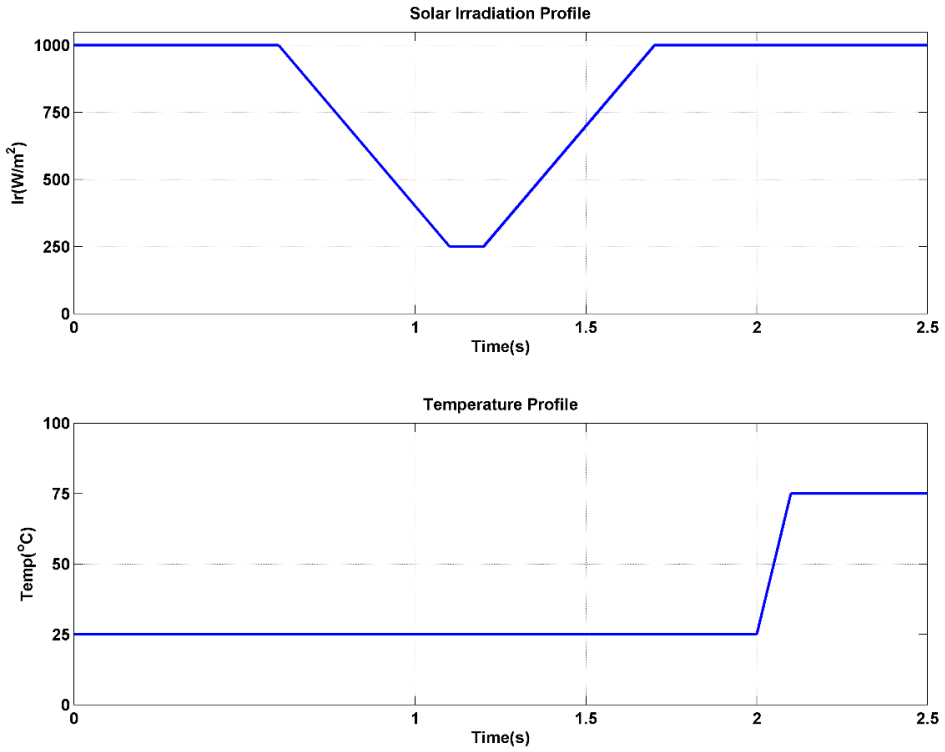

(a) Irradiance and temperature profile considered for solar panels

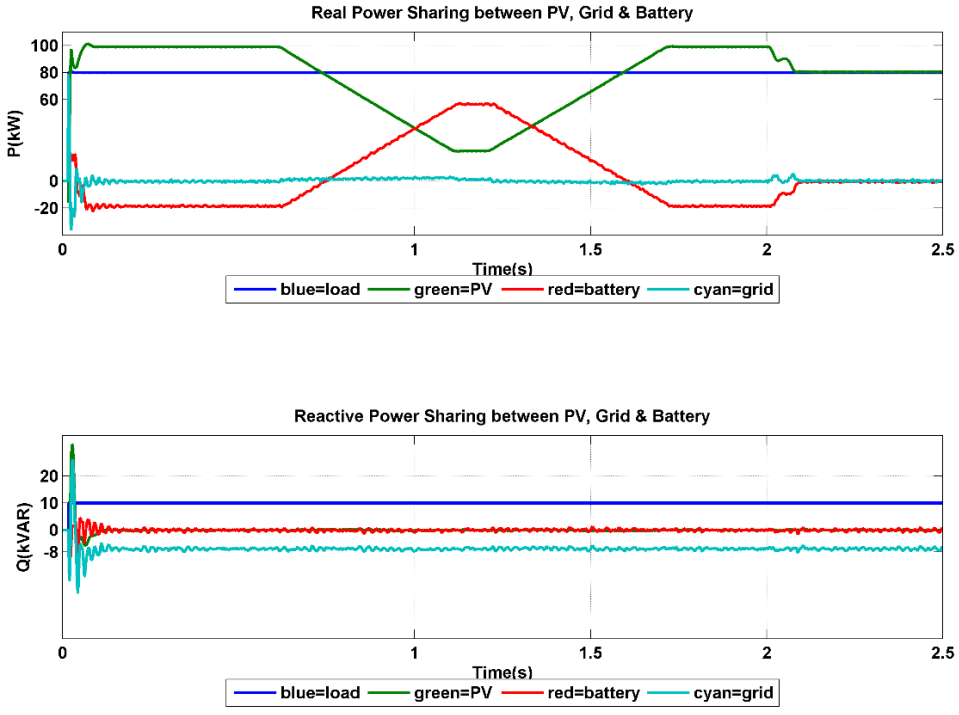

(b) Active and reactive power sharing in grid connected mode (constant load profile)

Figure 2-6: Controller effectiveness in grid connected mode

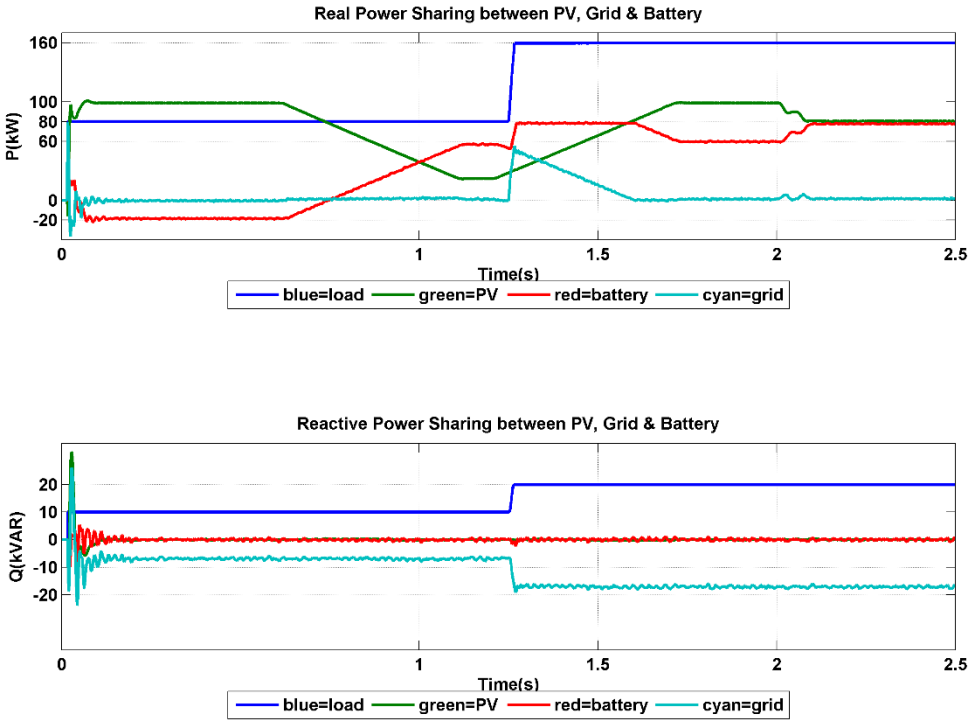

(c) Active and reactive power sharing in grid connected mode
(load demand doubled at 1.25 sec)
Figure 2-6: Controller effectiveness in grid connected mode

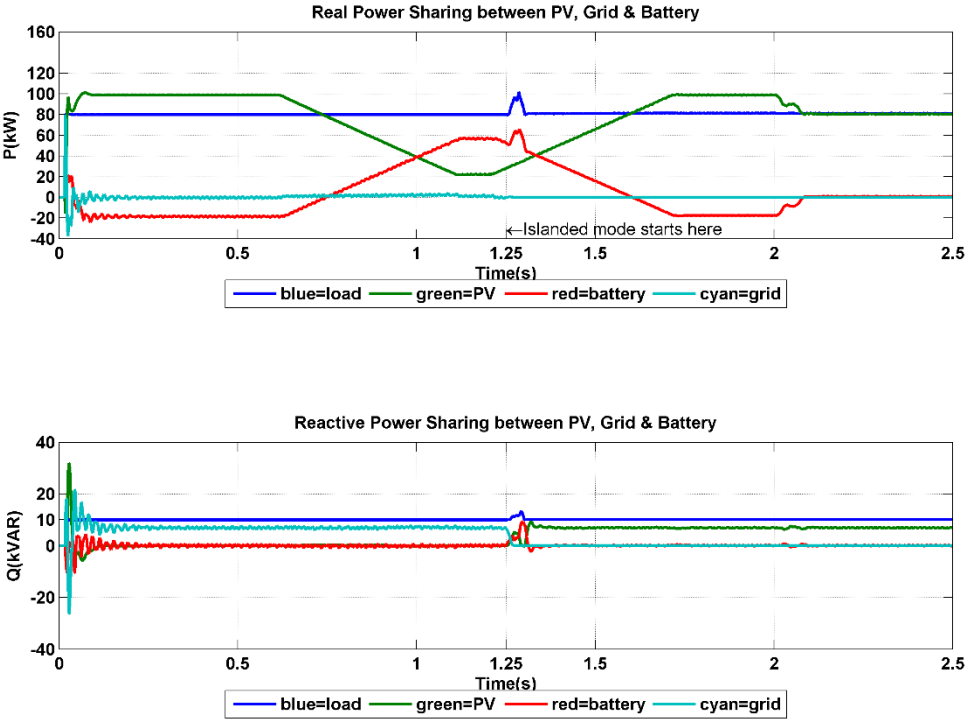

Figure 2-7: Active and reactive power sharing in islanded mode (Q supply from PV)

2.3.2 Operation with droop controller

In the second case, battery inverter is implemented with a droop controller as shown in Figure 2-4 and Figure 2-5. The load is changed to 200+j5 KVA. Both the droop coefficients for P and Q are set to 5%. When the grid frequency changes to 60.2 Hz, the active power supplied drops to 196 kW. Reactive power exchange is not affected in this process as shown in Figure 2-8(a). Similarly, Figure 2-8(b) shows the performance of Q-V droop where active power is not affected when the grid voltage rises to 12.72 kV. Figure 2-9(a) and Figure 2-9(b) show the proposed droop controller performance in the islanded mode. It is worth mentioning that the voltage restoration happens within 40 ms of islanding. Frequency returns to 60Hz in 100 ms. In case of islanding transition, even a 2% droop setting for *P* and *Q* provides a large variation, which is not desirable from the system's operational point of view. In addition, if the controllers are not properly tuned for the rapid transition case, there is a chance of voltage and frequency instability. Therefore, it would be better to disable the droop controllers in the transition period from grid connected to islanded mode for the sake of quick voltage and frequency restoration.

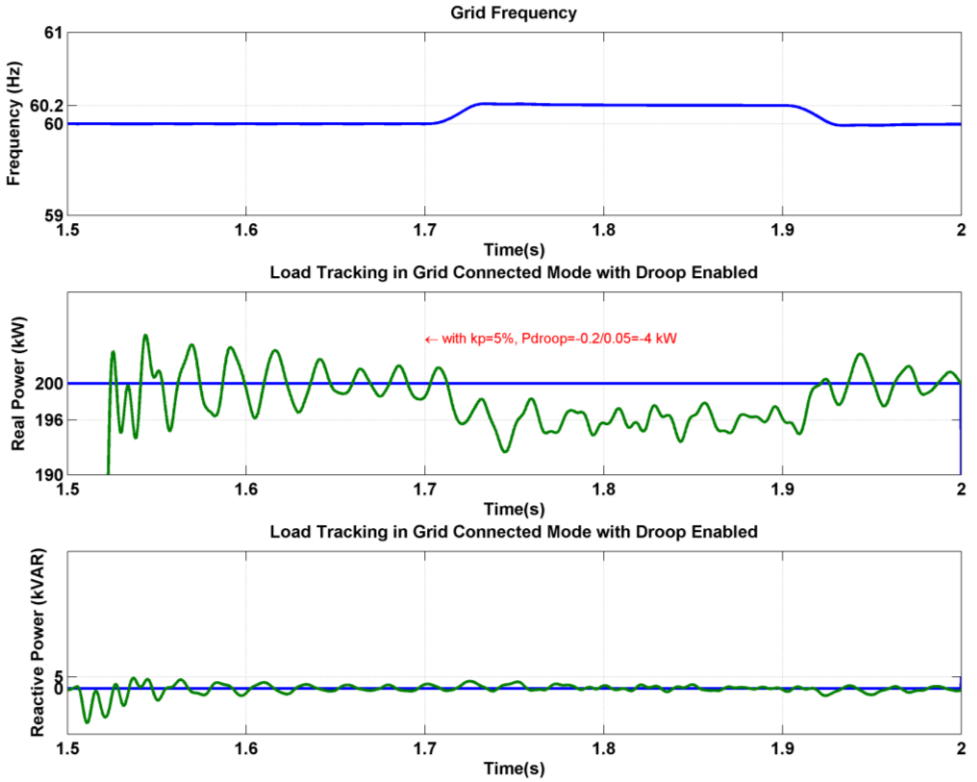

(a) P-f droop

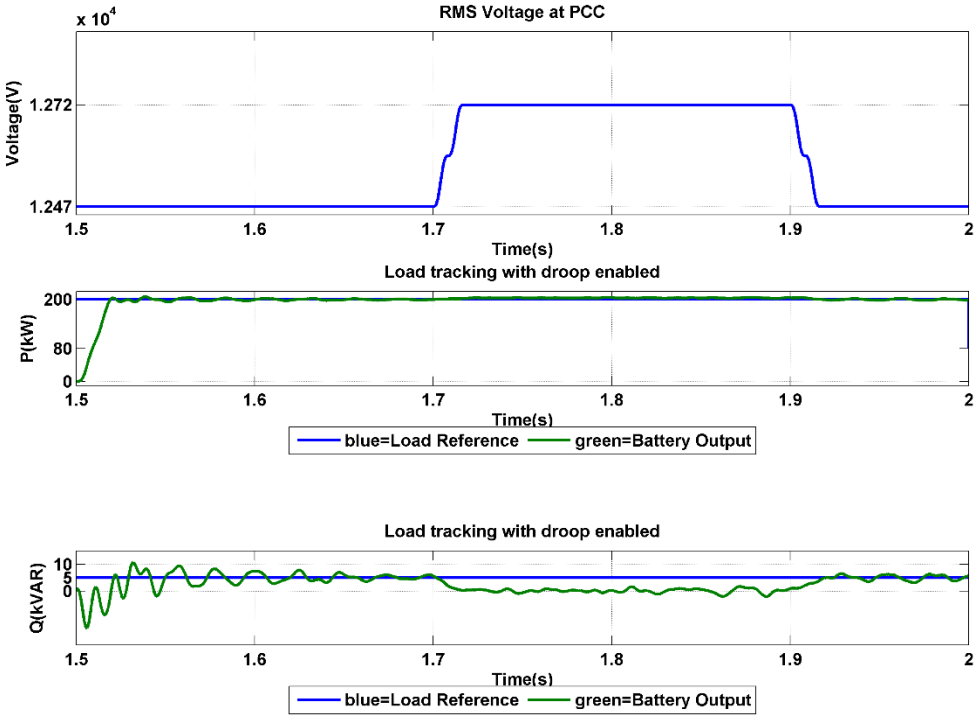

(b) Q-V droop

Figure 2-8: Proposed droop control operation in grid connected mode

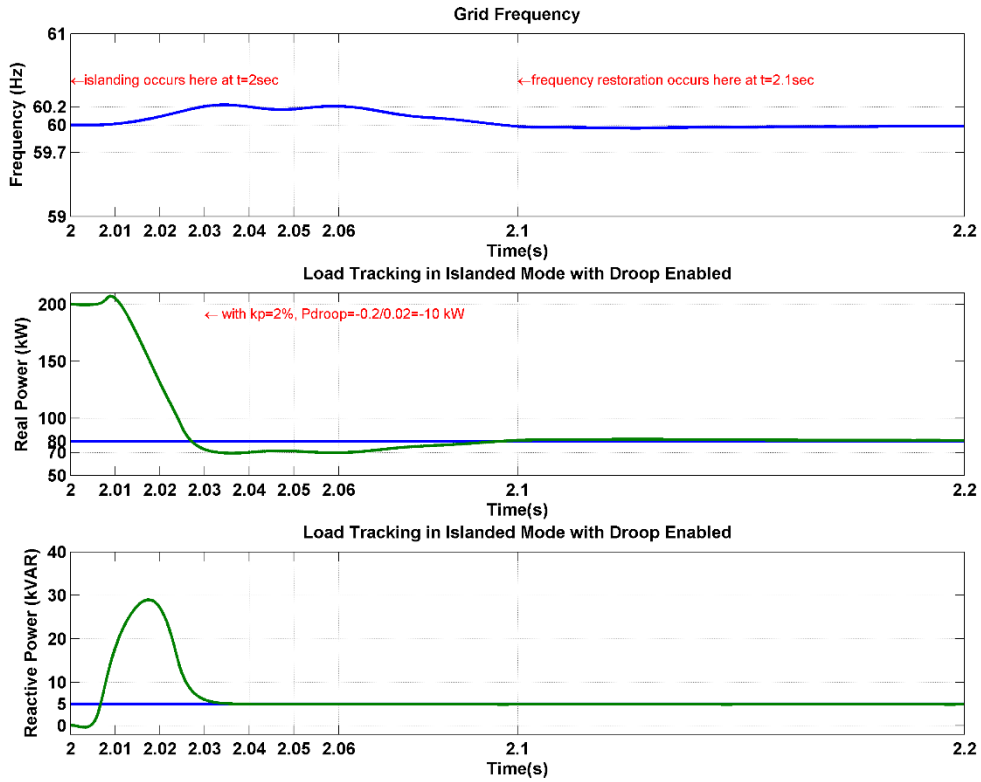

(a) P-f droop

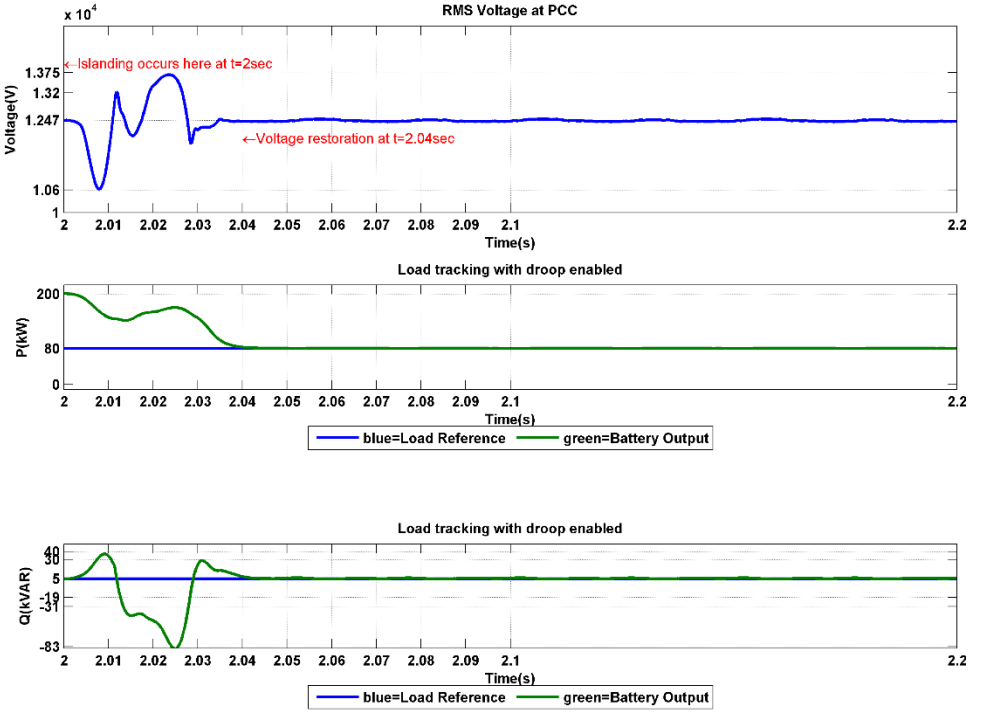

(b) Q-V droop

Figure 2-9: Proposed droop control operation in islanded mode

2.4 Distributed voltage control of active MV distribution networks in the presence of high PV penetration

This section first discusses the voltage rise problem formulation. Next, advanced Volt-Var capabilities of the smart PV inverters are analyzed. It is also shown that a slightly oversized inverter becomes essential for coordination among multiple inverters. After that, a distributed voltage control scheme is proposed which does not require a costly central communication infrastructure. Instead, it uses the concept of micro-management of each inverter with minimal information from the nearby voltage control devices using local measurements only. Finally, a modified IEEE 13-bus MV test feeder is used to verify the effectiveness of the proposed scheme. The contribution of this research lies in a distributed control scheme that is tasked with maximizing the PV penetration at low implementation cost, and which is faster when compared to the traditional voltage control devices.

2.4.1 Voltage control problem

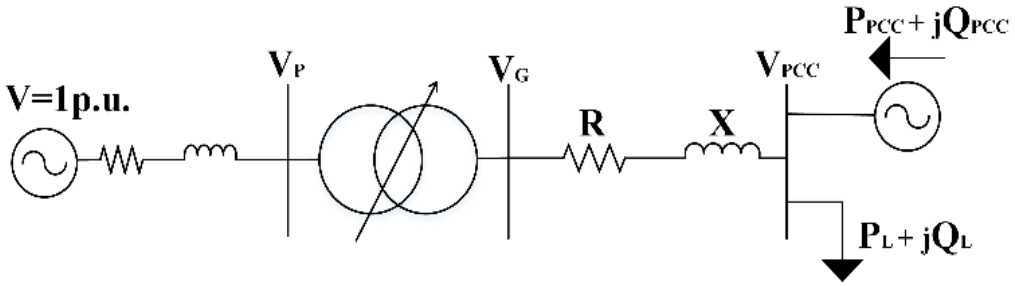

Figure 2-10: Single-line diagram of two generating stations

In a radial system as shown in Figure 2-10, the voltage at the PCC can be expressed as [48]-

$$V_{PCC} \approx V_G + \frac{RP+XQ}{V_{PCC}^*}. \quad (2.10)$$

Where, V_G is the substation bus voltage, $P=P_{PCC}-P_L$ and $Q= Q_{PCC}-Q_L$ are the active and reactive powers injected at the PCC respectively, and R and X are the feeder resistance and reactance respectively. To compensate for the voltage, rise/drop caused by P, i.e. to make $V_{PCC} \approx V_G$, the required Q is given by-

$$\frac{Q}{P} \approx -\frac{R}{X} \tag{2.11}$$

In case of (2.11), three cases can be considered- (i) R<X (ii) R=X and (iii) R>X. For case (i), reactive power (Q) injection is the desired choice for voltage control. Typically, this holds true for MV distribution system where fixed/switching capacitor banks inject the reactive current. Therefore, in this case, the smart inverters are given the Q-priority over active power (P) to control the voltage. However, for case (iii), the opposite happens as in LV grid, P-priority is necessary to correct the voltage deviation for the resistive nature of the line. Case (ii) requires both to control the voltage and is very rare.

In traditional droop based hierarchal control architecture, primary layer controls the power injections from multiple DERs according to the voltage magnitude and frequency of the connection point. The electrical constraint here is to control the voltage within a specified allowable standard $V_{min} \leq V \leq V_{max}$. ANSI C84.1-2011 standard is 0.95 pu -1.05 pu for each phase throughout the network. Secondary control layer corrects the steady-state error induced by the primary control. Here, again, the electrical constraint is $Q_{min} \leq Q \leq Q_{max}$ where Q_{min} and Q_{max} are the reactive power generation capabilities for each inverter. The tertiary control layer provides the operating point reference to the secondary control layer that has a specific objective function that needs to be satisfied by the network. The exact reference for Q is unknown for each inverter and therefore precise coordination is a challenge.

2.4.2 Volt-Var capability of smart inverter

The purpose of the Volt-Var capability of the PV inverter is to inject and/or absorb reactive power in response to PCC voltage deviation from the nominal value following a predefined characteristics curve as shown in Figure 2-11. Voltage change from V_2 to V_3 requires no Q regulation from the solar PV inverter. This is called the dead band which is adjustable in the inverter local controller. V_1 and V_4 correspond to the V_{min} and V_{max} of the voltage standard respectively. Beyond V_2 and V_3, the reactive power gradient can also be set or updated via communication. Q_1 and Q_4 are equivalent to Q_{max} and Q_{min}=-Q_{max} of the inverter characteristics curve as shown in Figure 2-12(a).

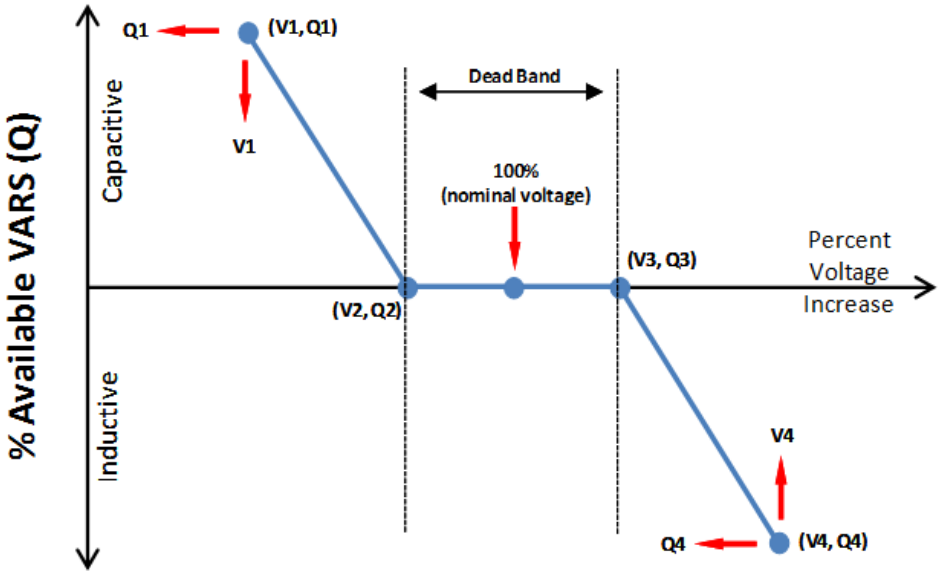

Figure 2-11: Volt-Var capability of an inverter

A different variation is also possible for giving Q-priority in the inverter settings. As PV inverters are used as a controlled current source, it is possible to extend the reactive power support capability with the expense of making the inverter slightly oversized. This is shown in Figure 2-12(b) where the inverter overcurrent limit is extended for an additional Q support. This does not require any P curtailment at times of peak solar irradiance which is

the case in Figure 2-12(a). It is worth mentioning that the maximum Q reserve of an inverter is not fixed. It depends on the apparent power (S) rating and active power generation of the inverter which are governed by the following equations-

$$Q_{RES} = \sqrt{S^2 - P^2_{PCC}} \ . \qquad (2.12)$$

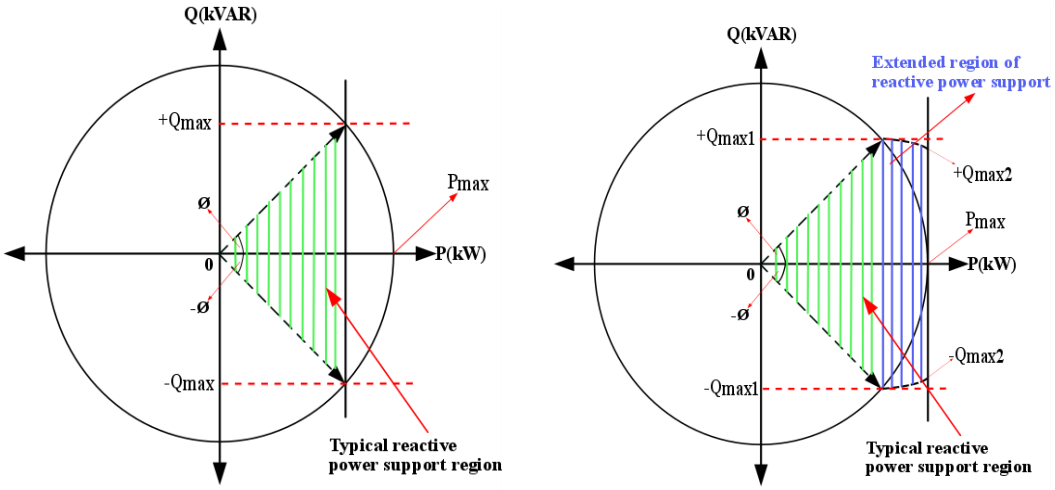

a. Conventional b. Extended Q-reserve

Figure 2-12: Inverter characteristics curve

2.5 Proposed distributed voltage control scheme

In case of high PV penetration, voltage control depends on the amount and direction of active power (P) and reactive power (Q) flow in the feeder. If PV inverters are connected at remote locations from the substation, voltage rise typically happens at the end of the line (EOL) which is difficult to control using the existing voltage control devices from the substation. The voltage also changes with light loading and heavy loading conditions throughout the day. Also, solar irradiance changes intermittently. So there exist four different combinations on any feeder. They are- (1) sunny day and light loading, (2) sunny day and heavy loading, (3) cloudy day and light loading and (4) cloudy day and heavy loading. High PV penetration is most likely to cause undesirable damage especially in the first condition, sunny day and light loading. This is because there are not enough loads to consume the peak generation from the PV panels and therefore back feed happens from the EOL to the substation. The power factor collected from the OLTC control panel located near the PV connection point is a good indication for the direction of the Var flow in the feeder as defined by the following equation-

$$PF = \cos\varphi = \cos\left(\tan^{-1}\frac{Q}{P}\right) \tag{2.13}$$

In case of moderate PV penetration and heavy loading condition, a lagging PF is observed in the OLTC control near the PCC. The var flows from the substation to the EOL. The smart inverter will inject reactive power to the PCC and operate as a capacitor bank. The Q reference for the inverter control system comes from the function as shown below-

$$Q_{ref} = Q_{max} + (V - V_{min})\frac{\Delta Q}{\Delta V} \tag{2.14}$$

Equation (2.14) corresponds to the operating range from (Q_1, V_1) to (Q_2, V_2) in Figure 2-11. For high PV penetration and light loading condition, a leading PF is observed in the OLTC

control near the PCC. The var flows from the EOL to the substation. If an OLTC is unavailable nearby, this information can also be gathered from the transformer that interconnects the PV to the grid. For leading PF, the smart inverter will absorb reactive power from the PCC and work as an inductive load. For this case, the governing equation is given as-

$$Q_{ref} = Q_{min} + (V - V_{max})\frac{\Delta Q}{\Delta V} \tag{2.15}$$

For (2.15), this operating range is from (Q_3, V_3) to (Q_4, V_4) in Figure 2-11. The setting in the inverter control panel changes with respect to seasonal variation as the loading changes in summer and winter. Updating the inverter settings, the PF information from the OLTC control is passed on. Thus, minimal communication is needed among the nearest OLTC or cap bank and the smart inverter. The proposed technique is shown in Figure 2-13.

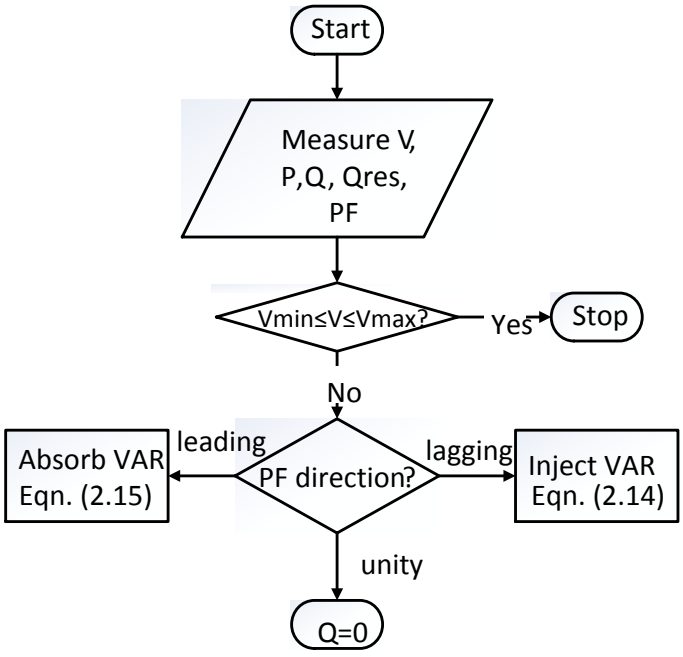

Figure 2-13: Proposed distributed voltage control

It is important to mention that the OLTC does not change the tap for the voltage deviation caused by reactive power. In Figure 2-11, if the voltage is within the dead band, the power factor will be near unity at the PCC. In this case, if the voltage changes slightly from the nominal values, the OLTC issues a tap change. For a smart inverter, this operation is equivalent to regulate the active power generation from the panels. As this is not always possible because of the weather dependency, active power curtailment occurs which is implemented by disabling the Maximum Power Point Tracking (MPPT) in the inverter control loop. This is not considered in this case.

2.6 Simulation results and analysis

A modified version of the IEEE- 13 bus test feeder is used to verify the proposed scheme as shown in Figure 2-14.

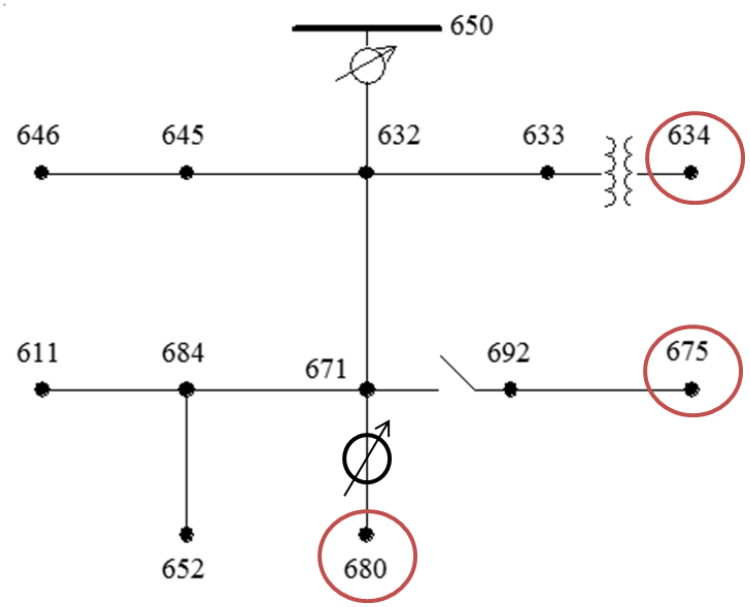

Figure 2-14: Modified IEEE-13 bus test system

This test system is 4.16 kV unbalanced MV distribution network with a total load of 3.46+j1.40 MVA. It has three phases at bus no 634, 675 and 680. Bus 675 is equipped with a 200 kVar fixed capacitor bank. Three 3-phase inverters, modelled with DC link voltage control technique are placed in bus 634, 675 and 680 (marked in red circles). Without any PV penetration from the inverters, a typical unbalanced power flow program converges which is shown in Figure 2-15. As seen, phase B voltages of buses 671, 675, 680 and 692 go beyond 1.05 p.u., even when no PV is injected. This can be attributed to the capacitor bank installed at bus 675. Also, note that buses 675 and 680 are the most two remote locations for this radial feeder.

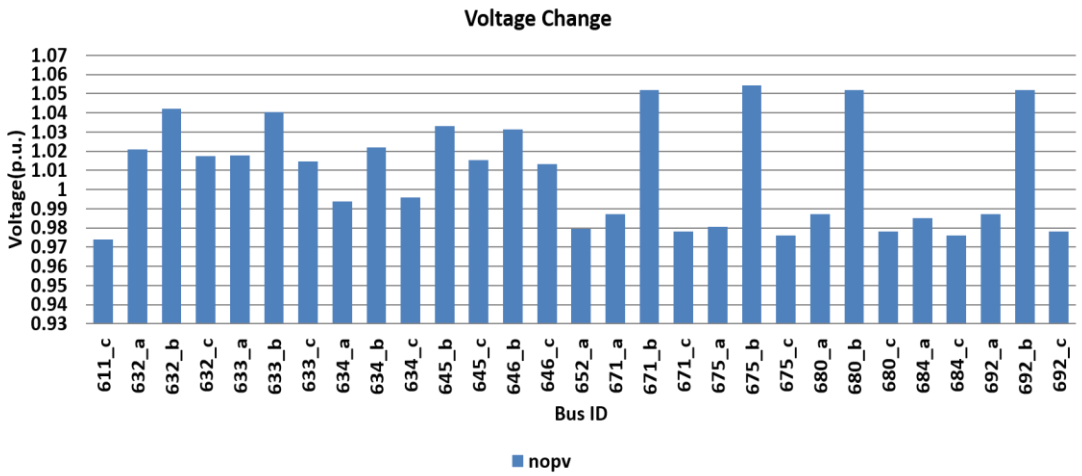

Figure 2-15: Bus voltages with no PV penetration

Therefore, if a 3-phase inverter is used which injects 3-phase balanced current in each phase, phase B of buses 675 and 680 will be mostly affected and suffer from voltage rise. For this high penetration (3MW), inverters need to absorb a large amount of reactive power to control the voltage and simultaneously inject P. With no Q constraint in the power flow program, this amounts to 1643.18 kVar. Phase wise var distribution is shown in Table 2-4.

Table 2-4: VAR requirement for high penetration

	Q (kVar)			
Bus	**Phase A**	**Phase B**	**Phase C**	**Total**
634	144.7	325.94	159.35	629.99
675	131.98	657.5	-159.2	630.28
680	138.69	105.37	138.85	382.91

From Table 2-4, each phase has different var requirements which cannot be satisfied using 3-phase inverter that injects balanced currents. In this context, using 1-phase inverters for each phase would be an expensive solution. Also, 1-phase inverter has limited power rating

which is not suitable for high penetration. An alternative approach is to control the 3-phase inverter current on per phase basis which is beyond the scope of this work. So, it is assumed that there is not much voltage difference across phases which holds true for most radial feeders.

As high penetration is considered, the solar irradiance is high also, thus producing the maximum PV generation, as shown in Figure 2-16. Solar irradiance data recorded at 1-min intervals are obtained from the National Renewable Energy Laboratory Measurement and Instrumentation Data Center (MIDC) database [49], cloud effects are ignored, and all PV panels are assumed to receive the same amount of solar irradiance.

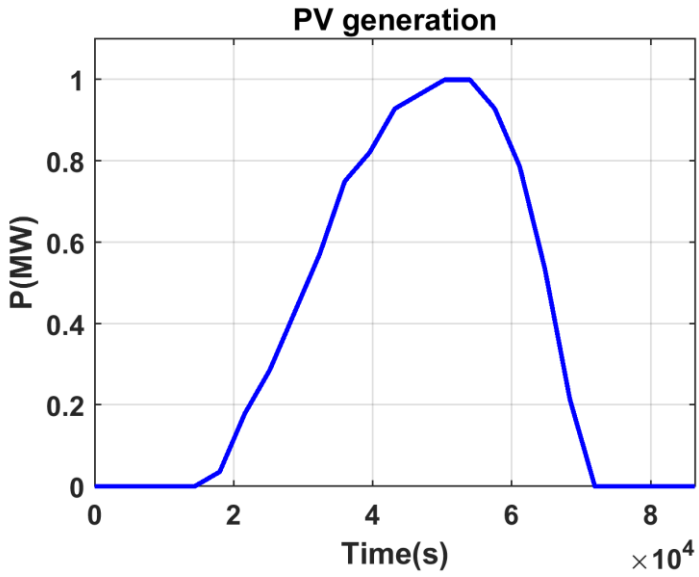

Figure 2-16: PV generation profile

2.6.1 Case I: Voltage at bus 680

Bus 680 is the most remote bus in this test system and has no load connected to it. A 1.11 MVA extended Q-reserve PV inverter is connected through an OLTC. The voltage profile for this bus is shown in Figure 2-17(a). It is shown that the voltage at phase B remained

the same whereas phases A and C voltages increased. To achieve this, reactive power (Q) is absorbed from the network. The inverter output is also shown in Figure 2-17(b). The figure shows that 1 MW active power injection has been made into the network by successfully regulating the reactive power reserve from the inverter connected at bus 680.

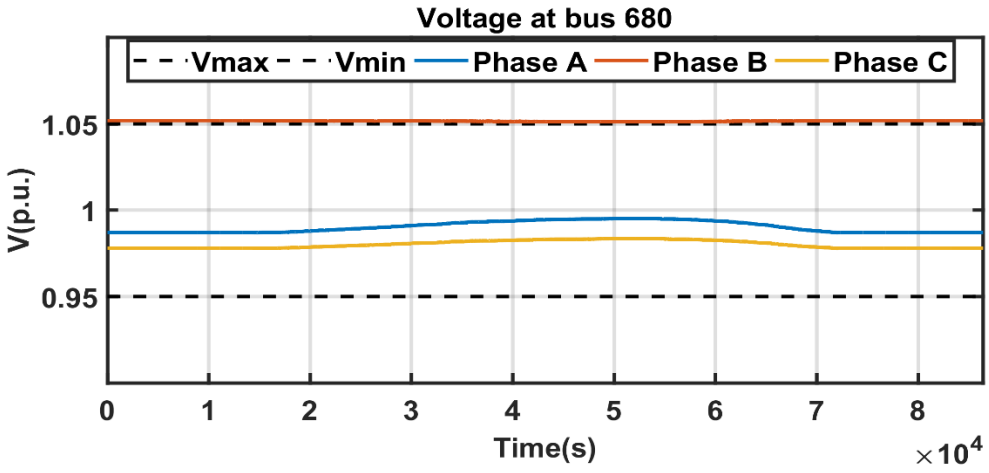

(a) Voltage at bus 680

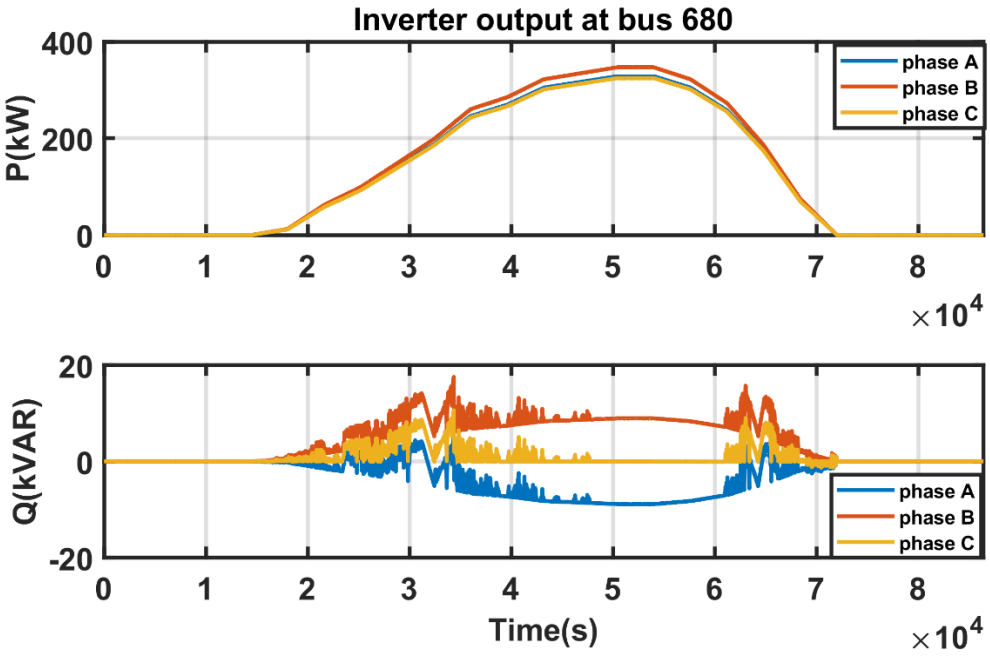

(b) P and Q from the inverter at bus 680

Figure 2-17: Voltage control at bus 680

2.6.2 Case II: Voltage at bus 675

Bus 675 is also in a remote location in this test system and has a 200 kVar three-phase capacitor bank connected across it. So, the voltage at phase B is already boosted up to 1.05 p.u. As a 1 MVA conventional PV inverter is connected, there is a chance of voltage rise on phase B. To tackle this problem, Q is again absorbed from bus 675 in coordination with the 200 kVar capacitor bank. The voltage profile for this bus is shown in Figure 2-18(a). The inverter output is also shown in Figure 2-18(b).

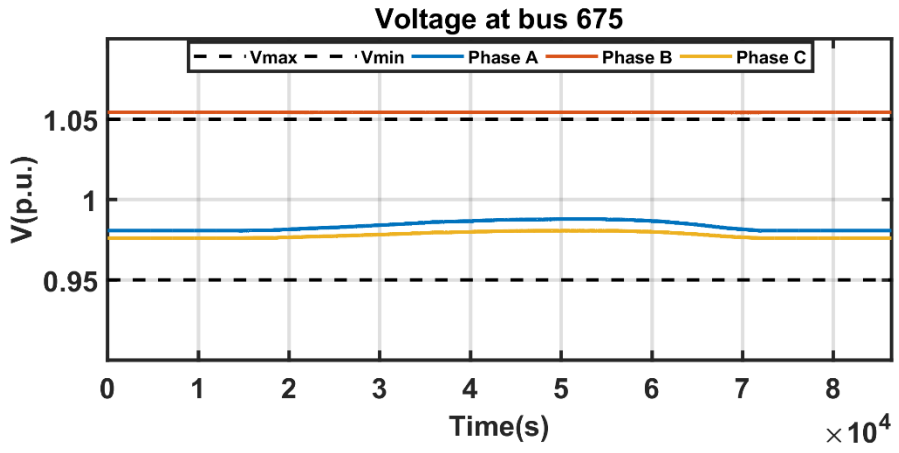

(a) Voltage at bus 675

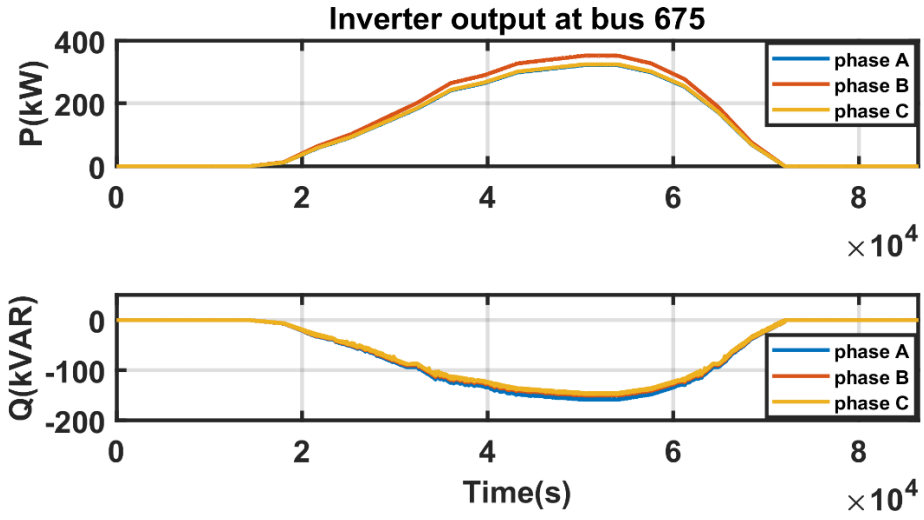

(b) P and Q from the inverter at bus 675

Figure 2-18: Voltage control at bus 675

2.6.3 Case III: Voltage at bus 634

Bus 634 is also in a remote location in this test system. A 1 MVA conventional PV inverter is connected after the transformer as shown in Figure 2-14. The voltage profile for this bus is shown in Figure 2-19(a). The inverter output is also shown in Figure 2-19(b).

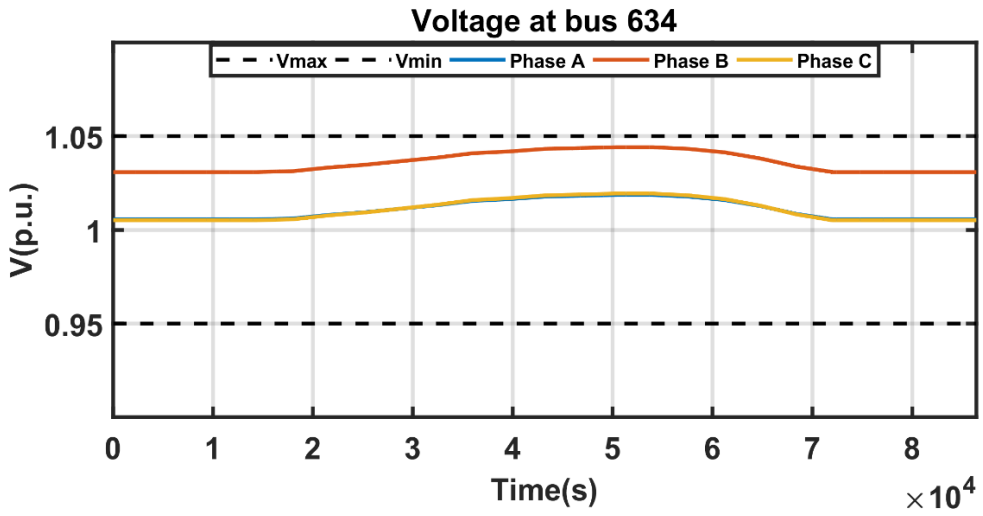

(a) Voltage at bus 634

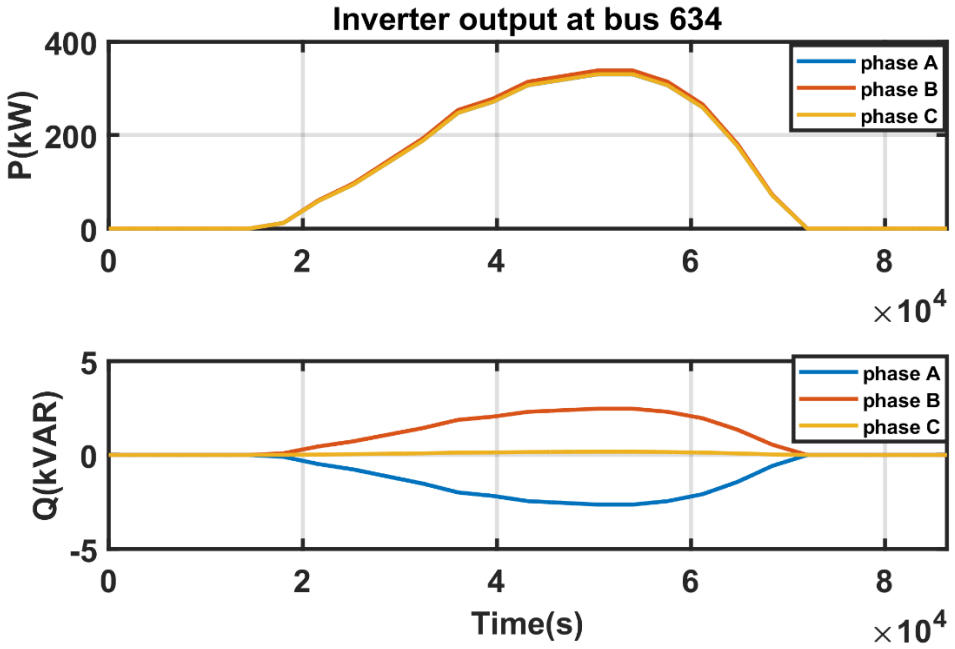

(b) P and Q from the inverter at bus 634

Figure 2-19: Voltage control at bus 634

As the voltage across all the phases are within limit, no voltage control measure has been taken. It is important to mention here that, power flow solution with no PV penetration already gave a hint for hosting PV at this location. All the phase voltages were within limit in the power flow solution.

2.7 Frequency regulation using smart inverters in high penetration distributed PV scenario

This section first discusses the Frequency-Watt Control (FWC) mechanism. Then, a coordinated FWC scheme for multiple inverters is proposed which mimics the principle of Inverse Definite Minimum Time (IDMT) characteristics. The proposed strategy is tested on a modified IEEE-13 bus test system. Dynamic analysis is carried out and results are discussed. Finally, the findings of the section are summarized. The main contribution of this work is in proposing a low-cost coordinated regulation scheme to mitigate over-frequency events, using advanced frequency-watt feature of smart inverters that does not require costly communication infrastructure, and assists in high PV penetration scenario.

2.7.1 Frequency-Watt control

The FWC settings curve is shown in Figure 2-20 which can be programmed inside the inverter control architecture.

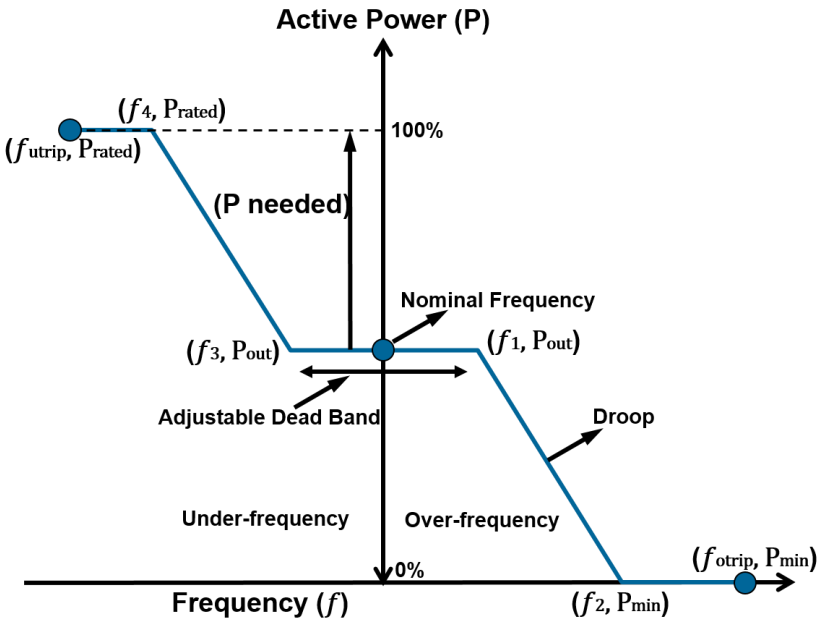

Figure 2-20: Frequency-Watt Control (FWC) curve of inverter

Most of the time, PV plants operate below their full rated capacity. Consequently, smart inverters also operate below 100% nameplate capacity (P_{rated}). The inverters can be set to respond to abnormal frequency event when it reaches a certain threshold defined as f_1 and f_3 in Figure 2-20. The difference between these two values is called the dead band which is adjustable. Beyond f_1, the output power (P_{out}) decreases to minimum (P_{min}) using a droop characteristic with the increase in frequency up to f_2. In Figure 2-20, P_{min} is shown to be at 0%. It can be adjusted if needed. The droop coefficient i.e. the slope per Hz is also fully adjustable. For under-frequency events i.e. below f_3, the P_{out} can be set to increase up to P_{rated} using a similar droop curve. The gradient of the line can also be adjusted which is effective until f_4. However, increasing the active power from P_{out} to P_{rated} physically means that there is additional solar energy to shine on the panels which is not always controllable due to weather and seasonal variation. In synchronous generator, this is equivalent to increasing the prime mover's fuel consumption which is possible to control for a wide range of frequency variation. The BESS solves this issue by discharging its stored energy to the DC link. But, as mentioned before, it is a costly solution. Therefore, most inverter manufacturers focus on the over-frequency region shown in Figure 2-20. Finally, the over-frequency trip and under-frequency trip threshold values are denoted as f_{otrip} and f_{utrip} respectively. These threshold values can be set locally or updated remotely via proper communication schemes. The optimum inverter settings depend on the knowledge of the system operation, historical frequency data and different control goals like profit maximization, loss reduction etc. In the over-frequency region, two cases can be considered as discussed below.

2.7.2 Case I: Instantaneous active power curtailment

The first case is shown in Figure 2-21. In this case, the active power curtailment happens instantaneously with the increase in frequency when it crosses the threshold value f_1.

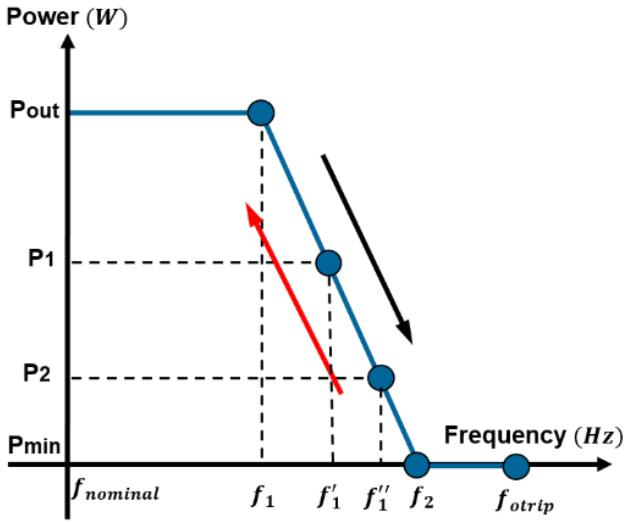

Figure 2-21: Over-frequency control with instantaneous active power curtailment

For example, when the frequency reaches f_1' exceeding f_1, the output power stands at P_1. Similarly, at frequency f_1", the output power is P_2. If solar energy is available, it goes back to the pre-disturbed output power (P_{out}) following the same droop curve. For f_2, the output power drops to the minimum value and finally the inverter trips when the grid frequency reaches f_{otrip}.

2.7.3 Case II: Active power freeze

The second case is shown in Figure 2-22. The power curtailment happens immediately for over-frequency events following the black arrow which is like case I.

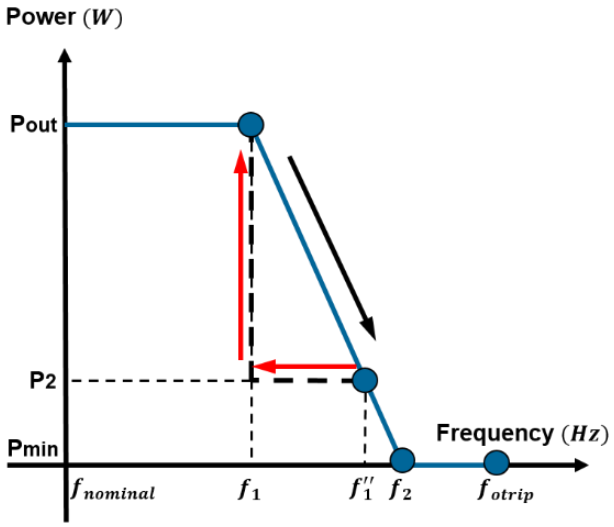

Figure 2-22: Over-frequency control with active power freeze

When the frequency restores from f_1" to f_1, the inverter active power may freeze to P_2 instead of going back to the output power (P_{out}) as shown by red arrow. This is possible because an inverter is primarily a current controlled device. f_2 and f_{otrip} have the same meaning as before.

2.8 Proposed coordination strategy

In case of high PV penetration in a distribution network, multiple inverters equipped with FWC need a coordination scheme among them to be able to mitigate the over-frequency event effectively. In most cases, there is no control signal exchange through communication channels between dispersedly populated smart PV inverters and DSO. Although this type of communication provides better controllability and observability in terms of system operation, it also requires additional cost for ultra-fast and reliable infrastructure. In FWC, active power curtailment is a function of grid frequency. There exists a simple solution to regulate the frequency without the communication scheme- a fixed active power curtailment, which can be implemented after the over-frequency threshold f_1 as in Figure 2-21. Doing this does not require any coordination at all because the inverter can be programmed to curtail a fixed amount of active power by observing any frequency deviation beyond f_1 seen at the point of common coupling (PCC). However, this is not a very good approach to the fix the frequency deviation and can lead to another frequency problem. If a fixed active power is curtailed, suddenly the load demand might exceed the generation which translates to an under-frequency event right after over-frequency recovery. As already mentioned, active power regulation is needed to fix an under-frequency event, therefore, this scheme is not usually deployed in practice. Considering all the above, a low-cost coordination strategy among multiple inverters is proposed in this section.

2.8.1 Inverter settings

To coordinate multiple inverters, first, it is important to set the required settings inside the inverter control architecture. The governing equations can be given as in Table 2-5. For this

purpose and as per discussion in section 2.7, FWC settings can be defined using the concept of instantaneous frequency deviation (Δf) and recalling Figure 2-21.

Table 2-5: Frequency-Watt Control settings of an inverter

Set $f_1, f_2, f_{nominal}, f_{otrip}, P_{min}, \frac{\Delta P}{\Delta f}\,(droop\ coefficient)$

Measure $f_{measured}$, P_{out}

Calculate $\Delta f = f_{measured} - f_{nominal}$

If $\Delta f < f_1 - f_{nominal}$

Then $P_{set} = P_{out}$

Else if $f_1 - f_{nominal} \leq \Delta f < f_2 - f_{nominal}$

Then $P_{set} = P_{out} - P_{out} * \frac{\Delta P}{\Delta f}$ (2.16)

Else if $f_2 - f_{nominal} \leq \Delta f < f_{otrip} - f_{nominal}$

Then $P_{set} = P_{min}$

Else $\Delta f \geq f_{otrip}$

Then *inverter trips*

2.8.2 Inverse Definite Minimum Time (IDMT) coordination

In power system protection theory, the relay and circuit breaker coordination issues have been solved using an IDMT characteristics. This type of coordination scheme has been studied for many years and is now a well-established practice in industry grade protection devices. The relay senses the actuating current and based on the minimum time settings, trips the circuit breaker. The same principle can be used to coordinate multiple inverters connected in a distributed network. The difference between the circuit breaker and the inverter coordination is that the first one trips, and the inverter responds to an abnormal

event. In the latter case, the actuating quantity depends on the length of the dead band in over-frequency region (Δk) in Figure 2-21 which is defined in (2.17).

$$\Delta k = f_1 - f_{nominal} \tag{2.17}$$

For the same frequency deviation, Δf, all the inverters will respond together if similar Δk is used for all the inverters which can be fixed using an additional time delay in commanding the inverters. To set the response time for different inverters, inverter ratings and droop settings can be considered. The highest rated inverter is set to respond first to an abnormal over-frequency event. As soon as the inverter curtails its active power, a frequency regulation is expected. However, in the proposed strategy, the highest rated inverter with the steepest droop-coefficient i.e. $\frac{\Delta P}{\Delta f}$ in (2.16) is set to respond first in comparison with the inverter programmed for a shallow gradient. The rationale behind this is given as follows. For instance, in a 60 Hz system, setting a 50% droop means, a 1 Hz change in frequency will result in the inverter dropping its output power is halved. Likewise, for a 40% droop, a 1 Hz change in frequency will result in the inverter dropping power from P_{out} to 60% of its pre-disturbed power. Therefore, to reduce the frequency deviation in a fast manner, the highest rated inverter is set to the steepest slope and given the highest priority to respond first. In this way, the active power curtailment is maximized which directly affects the frequency regulation. The other inverters can be set by following a decreasing order to respond based on their ratings and droop coefficients. The proposed strategy is shown in Figure 2-23. In Figure 2-23, it is assumed that the ratings and the droop coefficients of the inverter from 1 to N are in the decreasing order. If multiple inverters have same ratings, then the droop coefficients will be the determining factor to enable first responder. In this case, the inverter with the steepest droop-coefficients will respond first to the over-frequency

event. In such events, if the irradiation profile varies frequently such as passing cloud moments, inverter's active power source cannot be regulated further. In that case, the active power freezes at P_2 as shown in Figure 2-22. This physically means that the inverter is injecting a constant power irrespective of the frequency change. When clouds clear, P_2 restores to the pre-disturbed active power output (P_{out}).

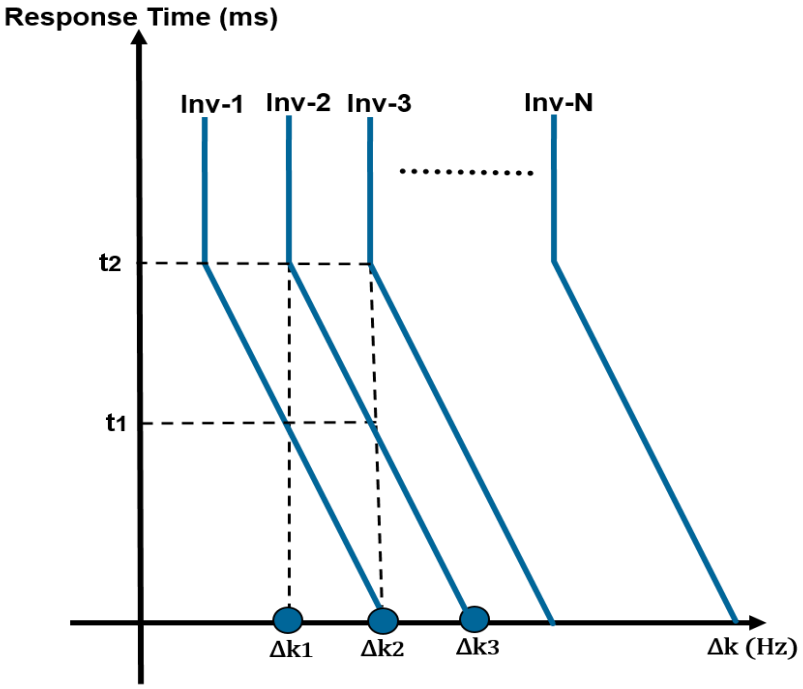

Figure 2-23: Coordinating multiple inverters using IDMT characteristics

2.9 Simulation results and analysis

A modified IEEE-13 bus test system with four inverters, as shown in Figure 2-24, is used to verify the proposed FWC coordination strategy. Three different cases are analyzed and discussed extensively.

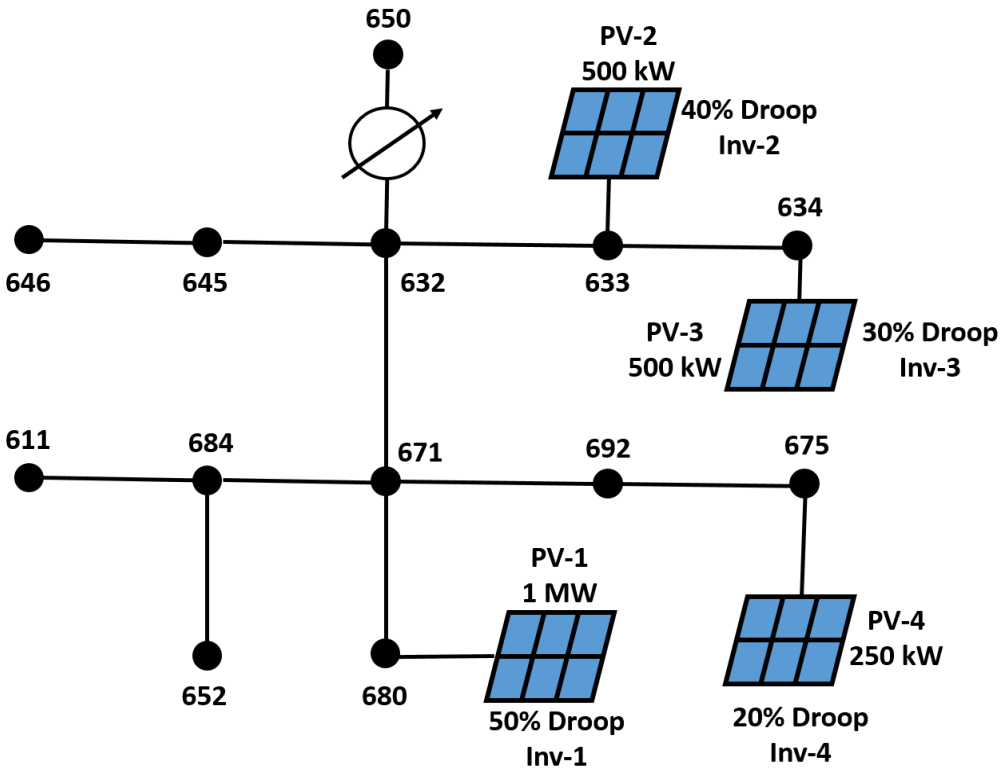

Figure 2-24: Modified IEEE-13 bus test system with multiple inverters

The inverter settings are presented in Table 2-6 as discussed in section 2.8.

Table 2-6: Inverter settings

Inverter No.	Location	P_{out} (kW)	f_1 (Hz)	Δk (mHz)	Droop coefficient
1	680	1000	60.05	50	50%
2	633	500	60.1	100	40%
3	634	500	60.2	200	30%
4	675	250	60.3	300	20%

The highest rated PV inverter, Inv-1, is located at bus 680 and given the priority to respond to an over-frequency event. The FWC control of this inverter activates when the grid frequency increases from 60 Hz to 60.05 Hz. As soon as the Δk value of inverter-1 crosses 50 mHz, Inv-1 is set to curtail its active power, dictated by the droop coefficient settings of 50%. Similarly, for a 100, 200 and 300 mHz deviation in grid frequency, Inv-2, 3 and 4 are given the priority to respond, respectively. For the same Δk, Inv-1, 2, 3 and 4 are set to respond within 1, 15, 45 and 75 cycles, respectively. The minimum output power (P_{min}) for all inverters are set at 0kW. Also, the value of f_2 and f_{otrip} are set to 60.4 Hz and 60.5 Hz respectively and are applied to each inverter. An example of the inverter FWC is given. A frequency sweep from 60 Hz to 60.5 Hz is used to test the frequency response of Inv-1 with the settings, as shown in Figure 2-25.

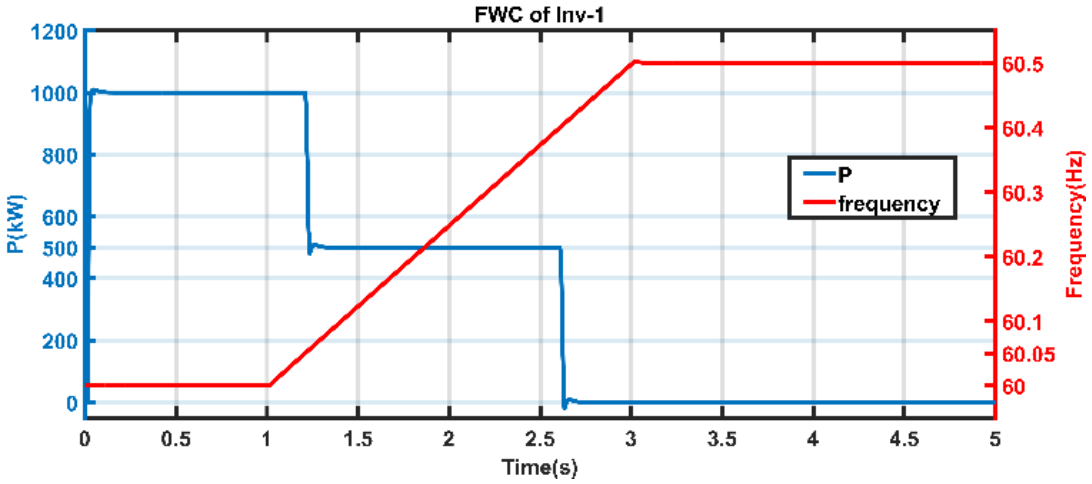

Figure 2-25: Frequency response of Inv-1

As expected, Inv-1 starts curtailing its active power at 60.05 Hz. It settles at a steady state curtailed value of 500kW until it reaches f_2 =60.4 Hz. At f_2, it curtails 100% of its nameplate power rating and goes to P_{min} which is set at zero. Finally, at f_{otrip} =60.5 Hz, the inverter trips due to over-frequency operational limit.

2.9.1 Case I: Coordination using different Δk

In the first case, a similar frequency sweep ranging from 60 Hz to 60.5 Hz is set in the synchronous generator located at bus 650 of Figure 2-24. The proposed coordination scheme is shown in Figure 2-26.

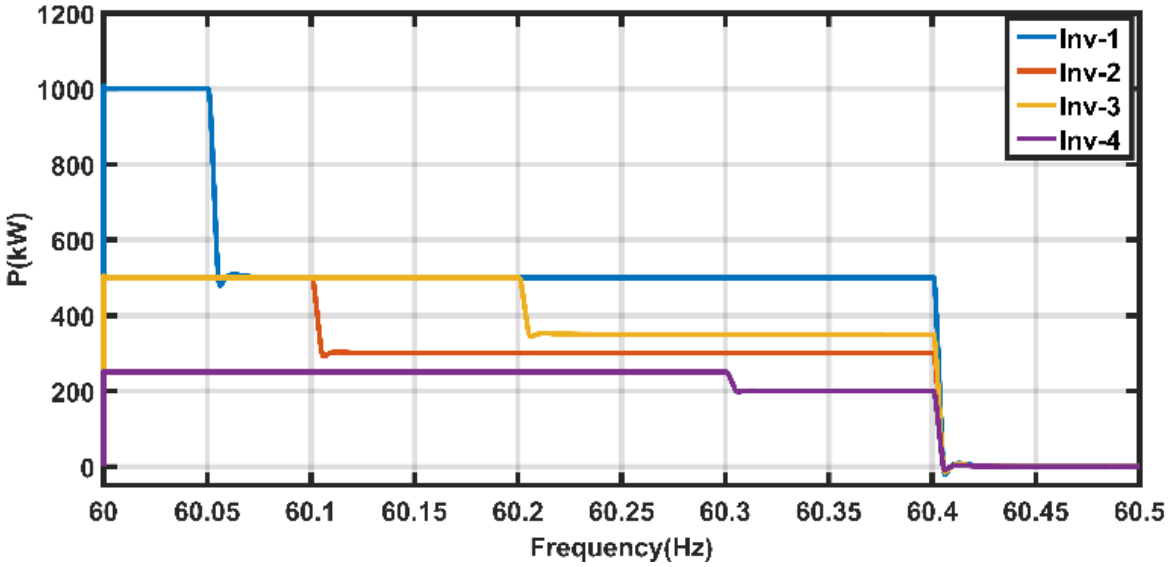

Figure 2-26: Coordination using different Δk

All the PV inverters are set to inject the rated power according to their nameplate rating. As expected, Inv-1 responds at 60.05 Hz and curtails its active power. Inv-2 and Inv-3 both are rated as 500kW but with 40% and 30% droop coefficient respectively. Therefore, Inv-2 is given priority to respond before Inv-3. The priority is set using different Δk where Inv-2 responds at 60.1 Hz and Inv-3 curtails its power at 60.2 Hz. Inv-4 responds when Δk becomes 300 mHz. All the inverters go to P_{min} at 60.4 Hz and trip at 60.5Hz, as expected.

2.9.2 Case II: Coordination using same Δk

In the second case, a frequency step change from 60 Hz to 60.05 Hz is applied at t=1.25s. So, after t=1.25s, the Δk remained at 50 mHz for all inverters throughout the entire 5s

simulation time. For the same Δk, the coordination works using time delay as shown in Figure 2-27.

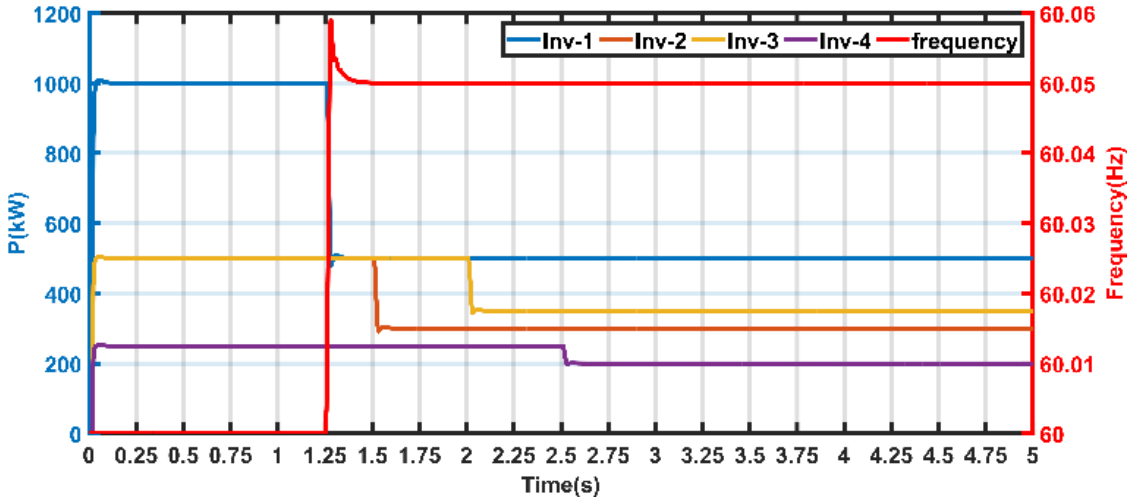

Figure 2-27: Coordination using same Δk

Inv-1 activates its FWC within 1-cycle and curtailed 50% of its power. Inv-2, 3 and 4 activated their FWC after 15, 45 and 75 cycles respectively as shown in Figure 2-27.

2.9.3 Case III: Dynamic frequency regulation

Dynamic frequency regulation can be obtained using the proposed FWC coordination strategy. The original load in the system is 3.5+j1.4 MVA. At t=1s, 1.5 MW of loads in the original test system are shed for 150ms and the frequency deviation of Inv-1 is measured as it is expected to respond first. This led to an over-frequency event with the peak frequency of 60.57 Hz and slow oscillation after that with around 60.4 Hz. This is shown in the top plot in Figure 2-28. With FWC disabled, this peak frequency is high enough to trip all the installed PV plants including Inv-1 which is shown in the bottom plot of Figure 2-28. The grid frequency crosses 60.5 Hz at around 1.05s and Inv-1 ceases its operation by disconnecting the inverter from the grid within 1 cycle.

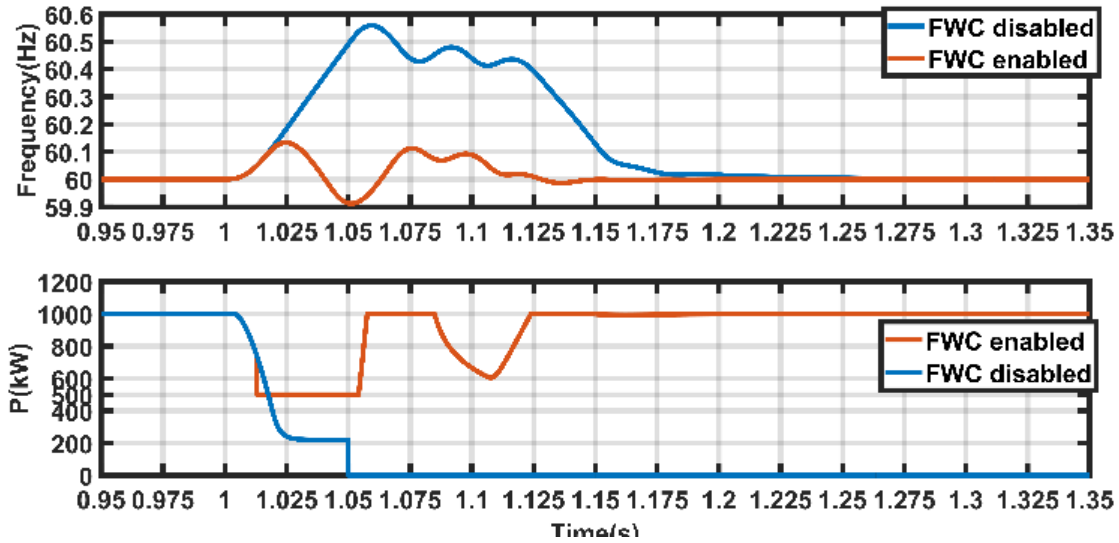

Figure 2-28: Frequency regulation using proposed coordination FWC strategy

With the proposed FWC coordination strategy, the over-frequency issue can be fixed which is shown in Figure 2-28. Considering Case I along with Table 2-6, at grid frequency of 60.05 Hz, Inv-1 responds within 1-cycle and curtailed 500kW which reduces the total PV generation from 2.25 MW to 1.75 MW. Curtailing 500 kW reduces the peak frequency to 60.13 Hz and creates an under-frequency event because at this point, load (2 MW) is greater than the net PV generation (1.75MW). However, as expected, a tight frequency control from the Inv-1 is achieved as the load and generation are now almost balancing each other. After t=1.05s, the grid frequency reaches at 59.9 Hz. As Inv-1 is assumed to operate on its 100% nameplate power, Inv-1 starts returning to its normal operation (P_{out}). Meanwhile, due to system dynamics, the frequency rises again and thus crosses the limit of Δk of Inv-1 one more time. Notice that from t=1.075 to 1.1 s, grid frequency is almost constant at around 60.1 Hz. Although the upper dead band of Inv-2 is set at 60.1 Hz, its response time is delayed by 15 cycles as discussed in Case II. Therefore, Inv-2 doesn't get activated and

within its response period, the grid frequency stabilizes at 60.02 Hz at 1.125s with the curtailment from Inv-1 only.

2.10 Conclusion

In this chapter, an autonomous control of smart inverter interface is presented. The designed controllers were effective in sharing the active and reactive power in grid connected and islanded modes. Then a droop control scheme is implemented for the BESS inverter. The proposed algorithms can extract the full potential from the smart inverters by utilizing the reactive power capability to its full extent. Also, it is recommended to disable the droop control in the transition period between two modes. This will help to activate the secondary control system to restore the voltage and frequency faster. Based on the findings, a directional power factor based distributed voltage control scheme is introduced. The algorithm supports minimal information exchange between the existing OLTC and installed smart inverter, and is therefore, distributed in nature. The proposed scheme utilizes the advanced Volt-Var characteristics of a smart inverter. An extended Q reserve inverter rather than a conventional inverter is shown to support the voltage more when the solar generation is at its peak. With a little additional cost for the DERMS, the proposed method mitigates the voltage rise problem in a high penetration scenario. Finally, Frequency-watt control is introduced with the focus on over-frequency operational region. A comparative discussion on the impact of FWC on under-frequency events and over-frequency are is presented. Then, mathematical formulation for the inverter settings is deduced. Dead band coordination is analyzed and IDMT coordination of multiple inverters with the same dead band is proposed. Finally, results are explained in accordance with the formulation.

CHAPTER 3: GRID SUPPORT APPLICATION OF SMART INVERTER AND BATTERY ENERGY STORAGE SYSTEM DURING GRID FAULTS

In this chapter, first, solar photovoltaic grid integration challenge during a three-phase balanced fault is addressed for string configuration. String configuration with miniature inverters attached to the panels is a recent trend. It is important to implement inverters capable of riding through various grid disturbances even in the miniature device level. A three-phase inverter and associated controllers are presented with a Fault Ride Through (FRT) capability also known as Low Voltage Ride Through (LVRT) to control the reactive power support in case of a balanced fault. The solar panel uses the incremental conductance algorithm for Maximum Power Point Tracking (MPPT) which is connected to the DC link throughout the fault duration on the grid side. The approach shows better results over the no-FRT case. EMTDC/PSCAD software package is used to simulate and validate the effectiveness of the controller design.

Secondly, an improved methodology for selective harmonic detection and compensation is proposed for smart inverters used as a Shunt Active Power Filter (SAPF). It is equally applicable in abnormal operating conditions such as in the event of an asymmetrical grid fault. A Multiple-Complex-Coefficient-Filter (MCCF) based Phase Locked Loop (PLL) is designed and tested for 5^{th} and 7^{th} harmonic compensation. Associated harmonic as well as fundamental current controllers in Synchronous Reference Frame (SRF) are designed and verified through simulation. Multiple linear rotating Proportional-Integral (PI) controllers are deployed for regulating the line current. MATLAB-SimPowerSystems package is used as a software platform for the demonstration of controllers' transient and steady-state

performances. The proposed approach can selectively detect and effectively reduce harmonics to meet IEEE standards. This approach can also be extended to *n* number of harmonic compensations in a fast and accurate manner.

3.1 Integration of solar energy in distribution system through smart inverter functionality and battery energy storage system

In this section, a single 650W solar panel is initially modeled in PSCAD. It is then scaled up to a 260kW solar PV facility. The PV system is connected to a buck converter and finally connected to a Thévenin equivalent of a grid through a three-phase inverter. Decoupled PQ control is deployed in the inverter. A battery model of 120V 6.5Ah is developed in PSCAD and scaled accordingly. Several simulations are carried out and presented.

3.1.1 System configuration

A two-stage converter architecture is used. The first stage is a DC/DC Buck converter that drives the PV installation on the maximum power point trajectory. The second stage is a DC/AC inverter that interconnects the DC side to the AC grid which is represented as a Thévenin equivalent. A BESS is connected to the input dc link of the inverter via a bi-directional DC/DC converter. The charging and discharging processes are fulfilled by regulating the current by adjusting the associated DC/DC converter of the BESS. The system diagram is shown in Figure 3-1.

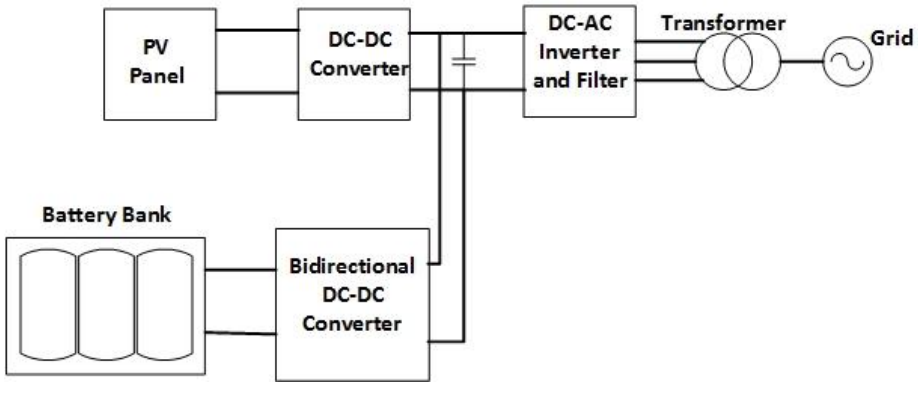

Figure 3-1: System configuration

3.2 PSCAD modeling of the system components

This section is divided into two sub-sections. The first section deals with the modeling of the solar cell and the second section presents the battery model.

3.2.1 Solar PV modeling

The solar panel is modeled and developed in PSCAD as described in [50]. The equivalent circuit of a solar cell can be represented as shown in Figure 3-2. The solar cell is composed of a current source, single diode and two resistors R_s and R_{sh}. The value of R_s is usually very low compared to R_{sh}.

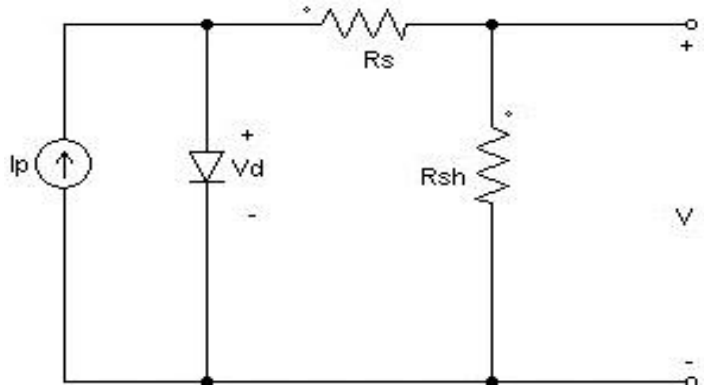

Figure 3-2: Equivalent circuit of a solar cell

3.2.2 Battery energy storage system

A battery model is developed as described in [51] and shown in Figure 3-3. The model works as a single unit (120V 6.5Ah) and depending on the capacity needed, it can be scaled up through series parallel combinations. The model represents a short-term discharge equivalent. Usually, when a fault occurs, voltage sag appears and lasts less than 5s [52]. As a result, this model is used without any problem. Other models can be used as well [53].

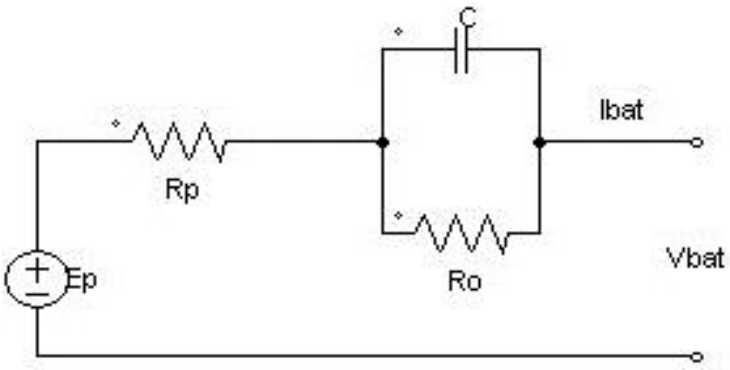

Figure 3-3: Equivalent circuit of a battery

3.2.3 Controller design

Three different controllers are designed - MPPT controller, bi-directional DC/DC controller and DC/AC inverter controller.

3.2.3.1 MPPT controller

The solar irradiance is intermittent in nature. Therefore, the PV cell doesn't always operate on the maximum power point. An algorithm called the incremental conductance algorithm [54] and based on the calculation of the instantaneous slope of the P-V curve is implemented to track the maximum power. The maximum power point decision is made based on the following three equations:

$$\frac{dP}{dV} = 0 \; if \; \frac{dI}{dV} = -\frac{I}{V}, at \; MPP$$

$$\frac{dP}{dV} > 0 \; if \frac{dI}{dV} > -\frac{I}{V}, left \; of \; MPP$$

$$\frac{dP}{dV} < 0 \; if \frac{dI}{dV} < -\frac{I}{V}, right \; of \; MPP$$

The DC/DC buck converter is shown in Figure 3-4. The control system is given in Figure 3-5.

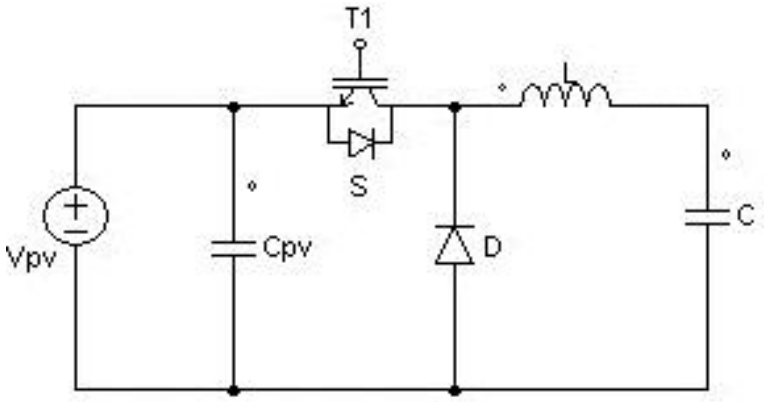

Figure 3-4: DC/DC buck converter

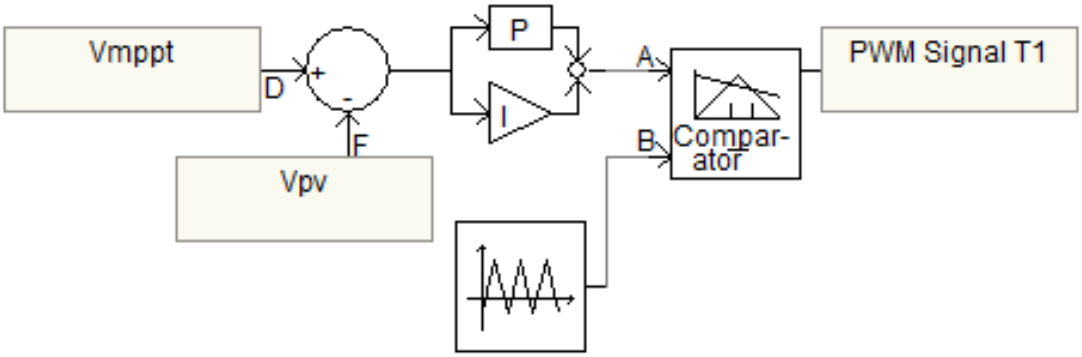

Figure 3-5: Control system of buck converter for MPPT

3.2.3.2 Bi-directional DC/DC controller

A simple bi-directional converter is implemented as a battery charge controller. The control is like a Current Controlled Voltage Source Converter (CCVSC) type [55]. The battery charger circuit is shown in Figure 3-6.

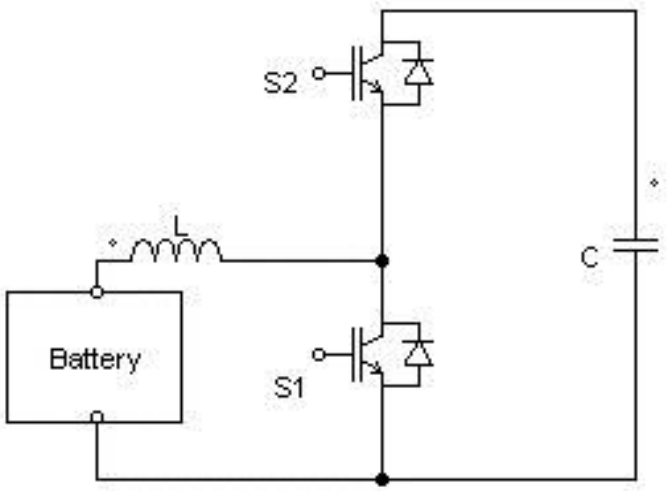

Figure 3-6: Bi-directional buck-boost converter

The controlling equation for a bi-directional converter can be given as (3.1) and (3.2):

$$\frac{V_{bat}}{V_c} = D;\ 0 \leq D \leq 1 \tag{3.1}$$

$$\frac{V_{bat}}{V_c} = \frac{1}{1-D};\ 0 \leq D \leq 1 \tag{3.2}$$

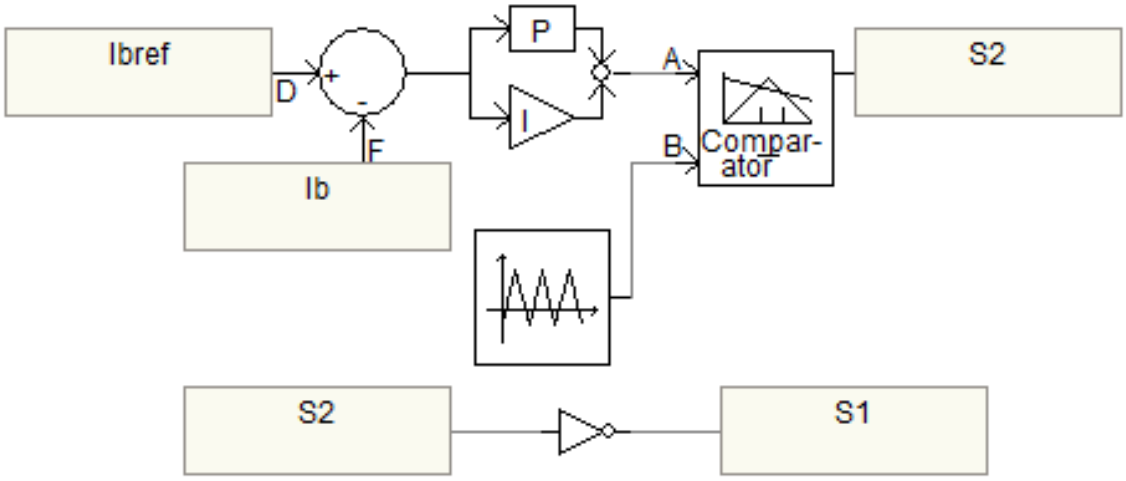

Figure 3-7: Battery charge controller

3.2.3.3 DC/AC inverter controller

The DC/AC inverter control is shown in Figure 3-8. The control system is developed based on the instantaneous reactive power theorem. Grid quantities are converted to the decouple Direct (D) and Quadrature (Q) axes.

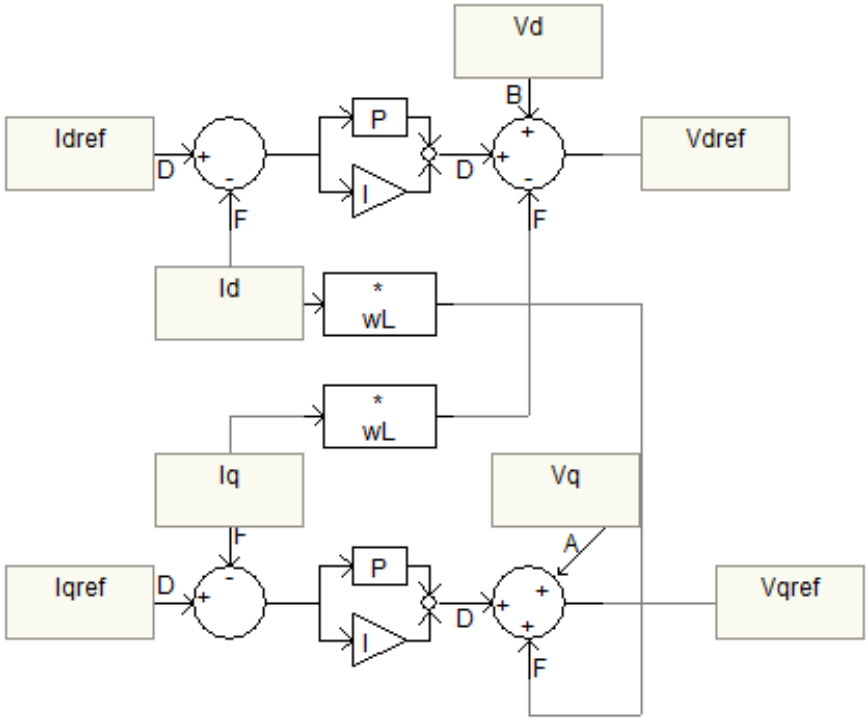

Figure 3-8: Decoupled DQ axis control

Bifurcating these two cases can be used to control the real and reactive power almost independently. Here the reference signals I_{dref} and I_{qref} are generated from the active and reactive power injection respectively. A PLL system tracks the phase and frequency of the grid and supplies the reference for the inverter control. The system relies heavily on this PLL tracking system. The reactive power injection is controlled by the grid-side voltage fluctuation. The active power injection here determines the real power flow in the system. Active power injection gets reduced during the grid fault. As the system is always operated

at the MPPT condition, the generated power from the solar panel can be successfully stored in batteries. In this way, the efficiency of the solar generation is maintained. The inverter control provides the voltage support by injection of reactive current into the PCC and thus providing dynamic grid support.

3.3 Simulation results and analysis

The simulation results show the comparison between FRT capability case and the no FRT capability case. The solar panel is disconnected from the grid in case of the fault which is the no FRT case. The capability of fault ride through is implemented here by connecting the PV and battery throughout the fault duration. A transformer rated 0.208/12.47 kV is connected to the grid which is at 12.47 kV. A three-phase balanced fault has been initiated at 6s which lasts for 1s. In the graphs shown below, the *x* axis represents the time in seconds. The DC link voltage, the inverter voltage and the grid voltage without any FRT capability are shown in Figure 3-9, Figure 3-10, and Figure 3-11 respectively.

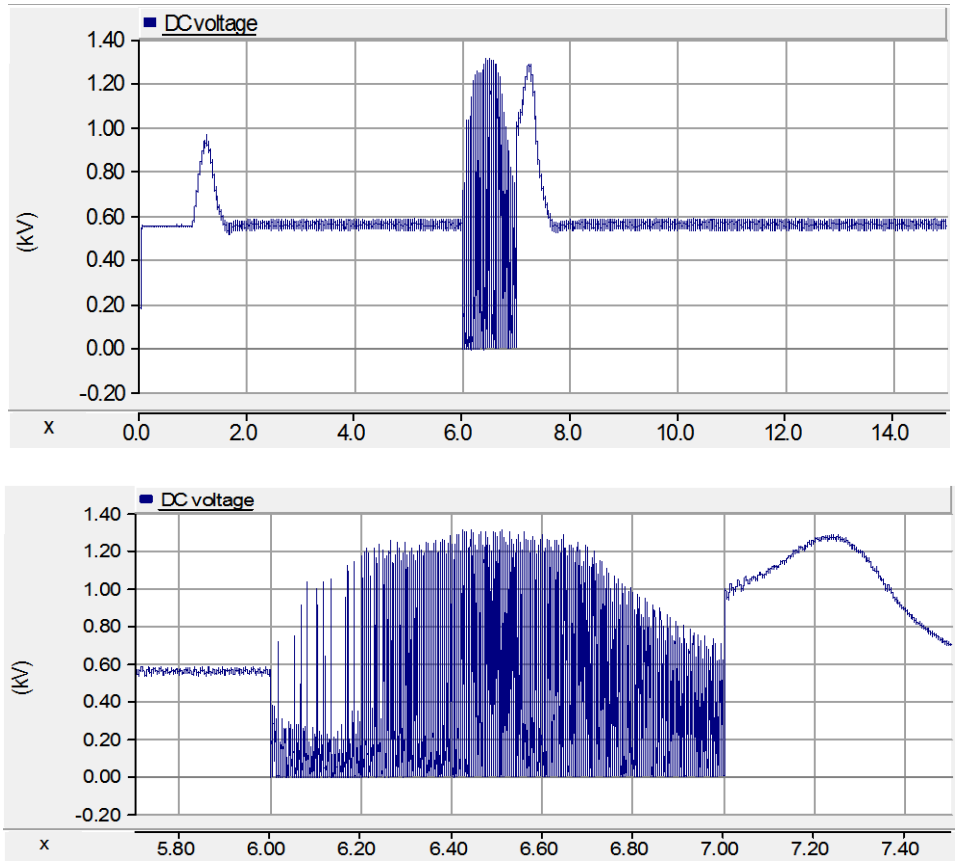

Figure 3-9: DC link voltage-No FRT (Zoomed 6-7s)

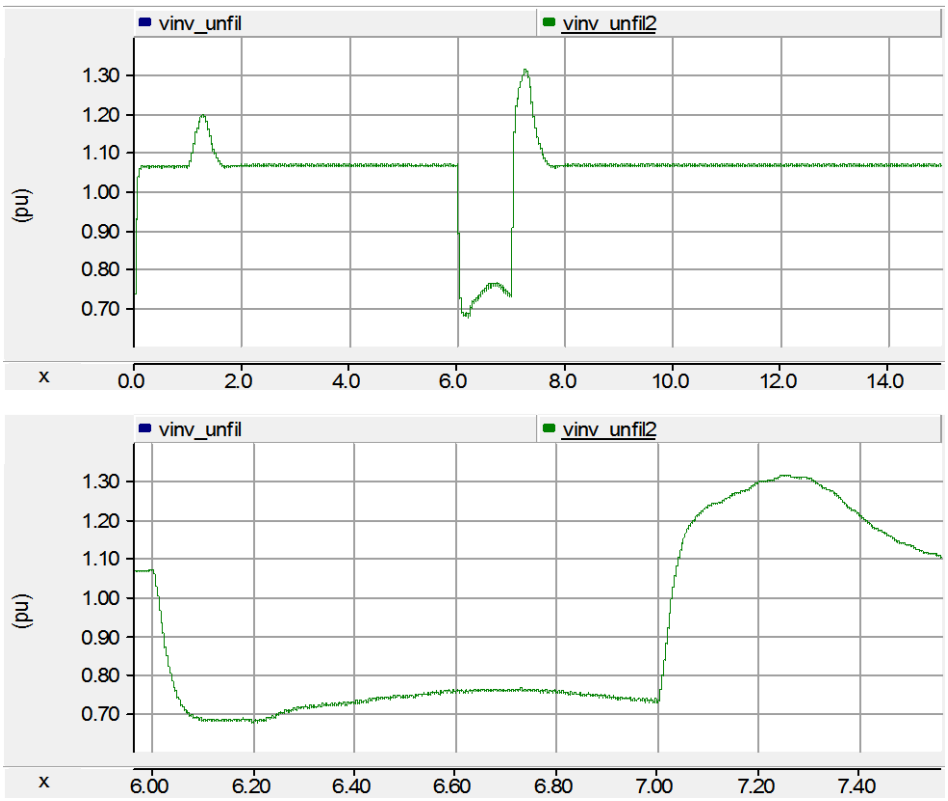

Figure 3-10: Inverter voltage-No FRT (Zoomed 6-7s)

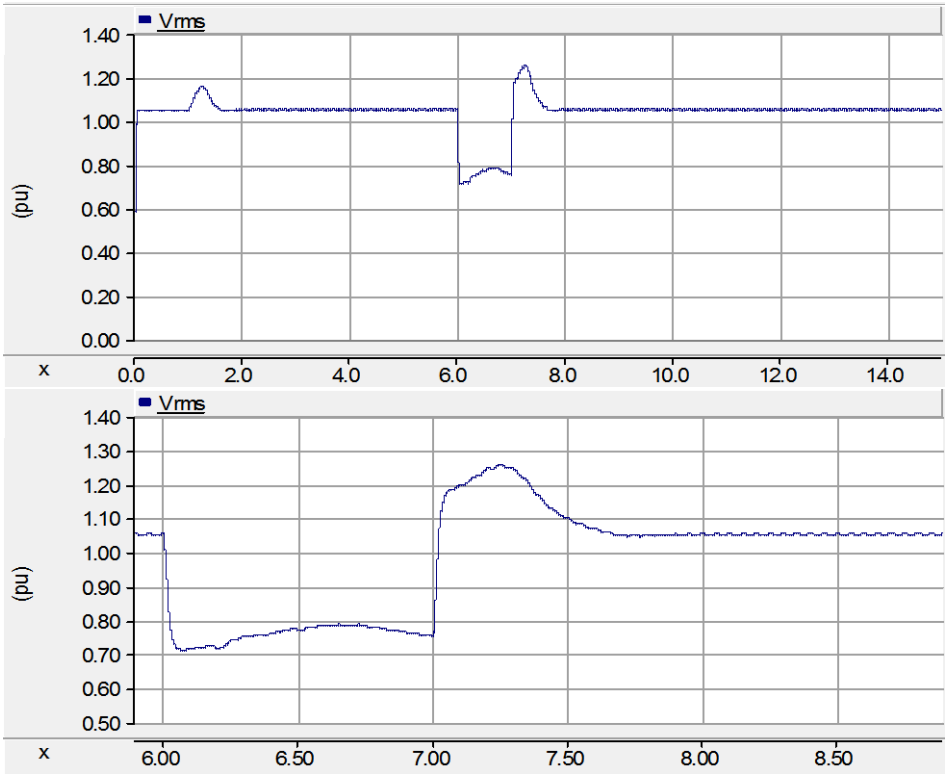

Figure 3-11: Grid voltage-No FRT (Zoomed 6-7s)

With the implementation of the battery and with the MPPT enabled throughout the entire fault, the DC link voltage rises to around 0.65 kV compared to 1.3 kV from the previous case. Figure 3-12 shows the result. From Figure 3-13 and Figure 3-14, it can be inferred that with the FRT capability; the grid and the inverter voltage experience sag of 20% which is an improvement over the previous case, i.e., the case without FRT.

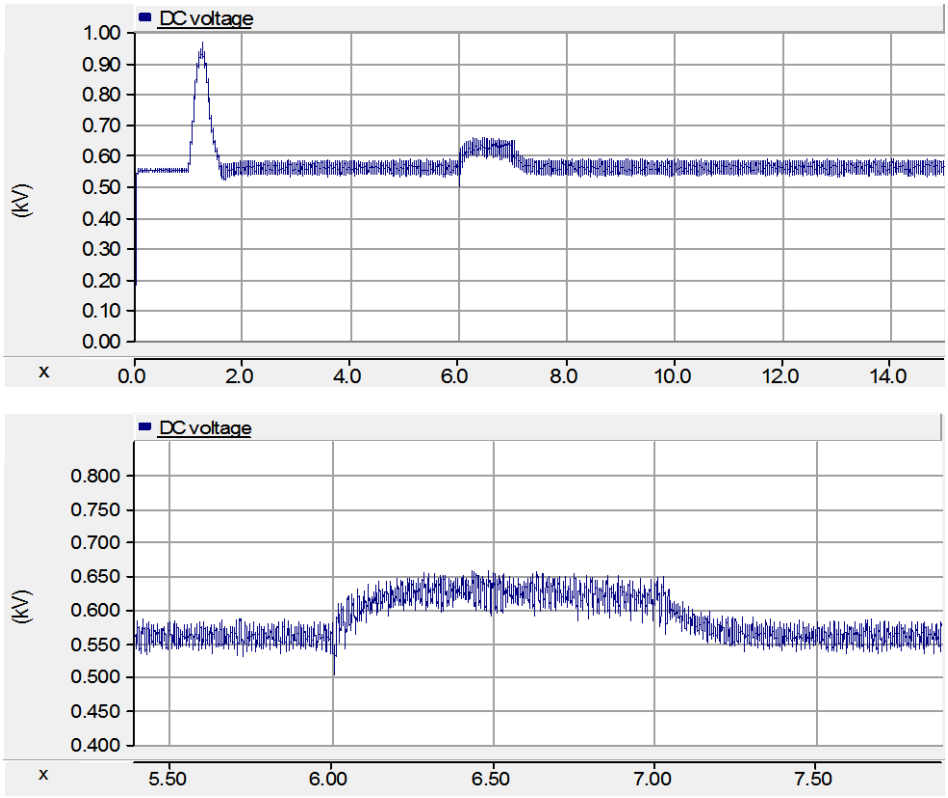

Figure 3-12: DC link voltage- with FRT (Zoomed 6-7s)

It can be seen from Figure 3-14 that the grid voltage regains its pre-fault value within 0.2s after the fault. This is made possible because the BESS discharges energy immediately after the fault, thereby restoring the voltage in a much shorter time. It is fair to say that without the BESS, this wouldn't be possible. The improvement of the grid sag voltage is 10% which seems minimal, but recovery time gets shorter. Voltage sag depends on whether

the grid is ‘strong’ or ‘weak.’ A weak system with high source impedance may not work the same way as a strong interconnection.

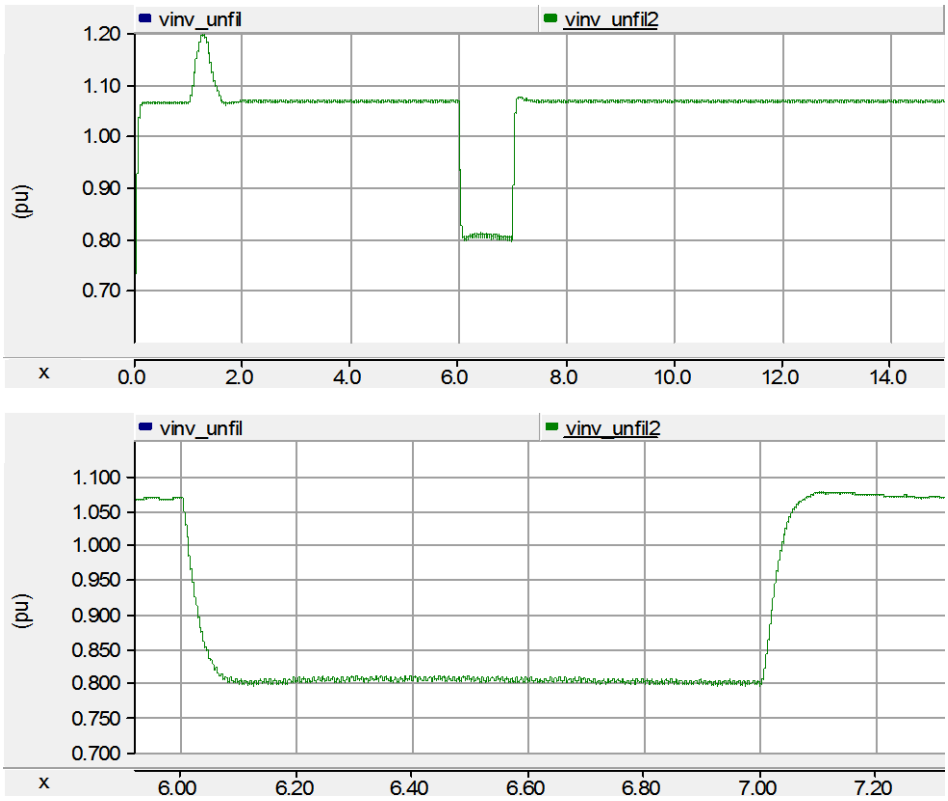

Figure 3-13: Inverter voltage-FRT (Zoomed 6-7s)

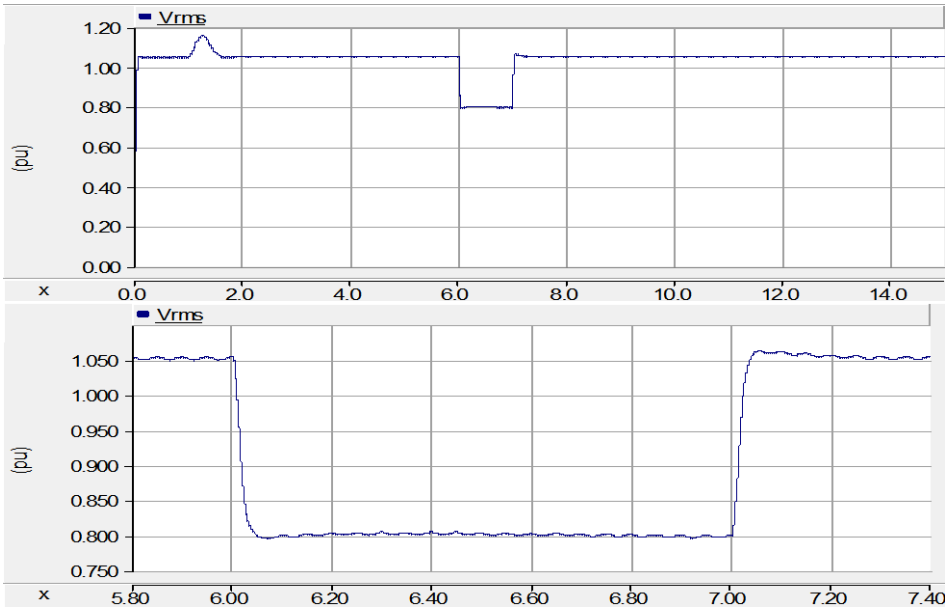

Figure 3-14: Grid voltage-FRT (Zoomed 6-7s)

Figure 3-15 and Figure 3-16 show the battery characteristics. For the no FRT case the battery tries to maintain the DC link voltage. Initially, it maintains around 270 V. When the fault occurs, the BESS starts discharging, but without the PV support, it fails to maintain the DC link voltage. Consequently, the reactive power support from the inverter is lost and the grid voltage experiences a 30% sag. Voltage measurement is shown to be inverted in this case.

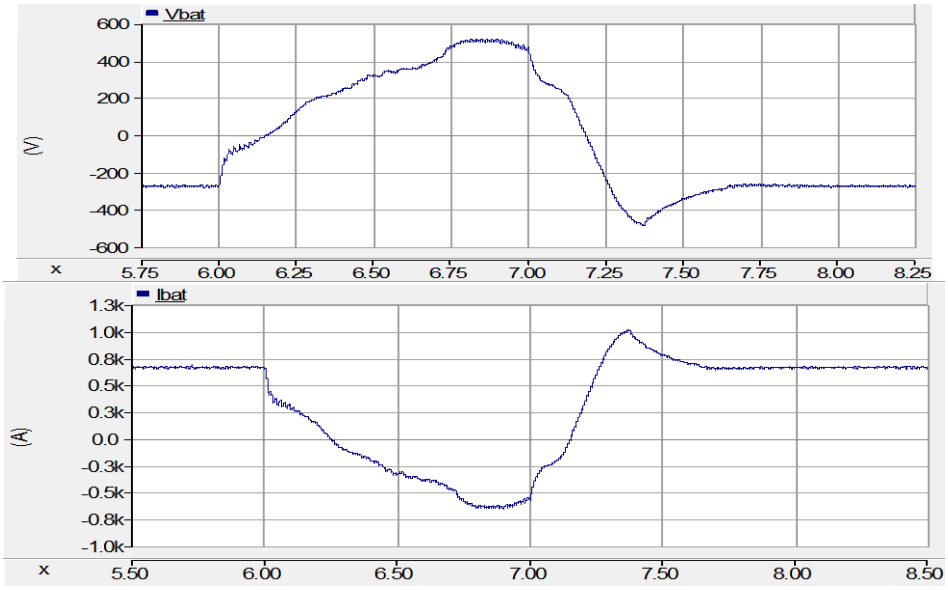

Figure 3-15: Battery voltage and current- no FRT (Zoomed 6-7s)

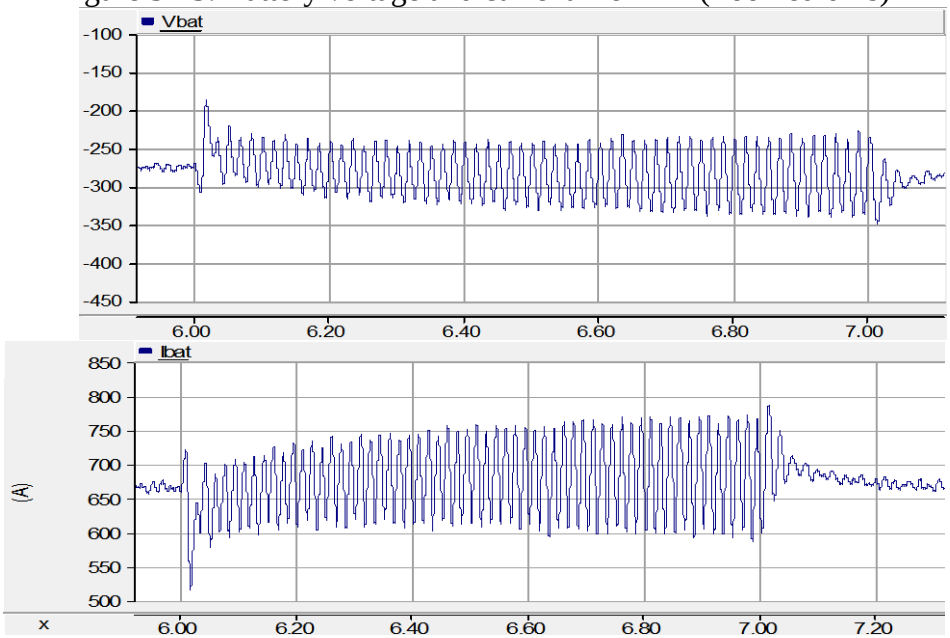

Figure 3-16: Battery voltage and current- FRT (Zoomed 6-7s)

3.4 Selective Harmonic Compensation by Smart Inverters using Multiple-Complex-Coefficient-Filter (MCCF) during Unbalanced Fault Condition

In this section, we propose an improved harmonic detection and compensation strategy for smart inverters used as a SAPF with the aim of compensating 5^{th} and 7^{th} harmonic currents. Moreover, this method can also be extended to any number of harmonics. The contributions of this section are as follows- a) detection of selected lower order harmonics and reducing the targeted ones, even under asymmetrical grid fault situation, can be achieved by using the proposed technique. The robust approach accurately identifies and rapidly extracts the fundamental positive sequence component, within a few millisecond ranges, to remain synchronized with the grid which is fast compared to other technologies, and b) a new and expandable Phase Locked Loop (PLL) based on Multiple-Complex Coefficient-Filters (MCCF) is designed and tested through simulation. With this improved PLL, smart inverters can respond to the grid fault situation quickly and effectively maintain the power quality if used as a Shunt Active Power Filter (SAPF). The simulation results and analysis done by MATLAB-Sim Scape Power Systems package.

3.4.1 Multiple-Complex-Coefficient-Filter

To synchronize the operation of the inverter with the grid, a PLL is deployed which works well for high Bandwidth (BW) during normal conditions. A typical PLL has three fundamental components as shown in Figure 3-17.

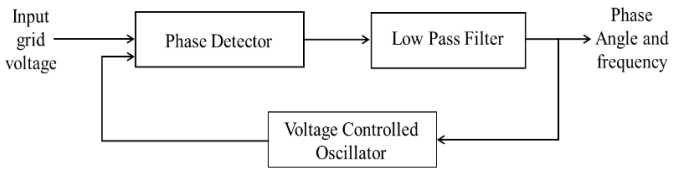

Figure 3-17: Conventional PLL structure

For the phase detector block, its output is governed by (3.3) where *G* is the phase detector gain, θ_i and θ_o are phase angles of grid voltage and voltage-controlled oscillator's output voltage respectively. So, the instantaneous frequency of the PLL is adjusted through multiplicative feedback and low-pass filtering. A conventional PLL can track only the fundamental positive sequence component of voltage vector. It also does not provide any harmonic sequence information.

$$x = G\sin(\theta_i - \theta_0) \tag{3.3}$$

When a fault happens in the network, the voltage vector gets highly distorted by harmonics and there is a phase jump in θ_i. Followed by the low-pass filter, the PLL then attempts to extract the fundamental sequence component but fails due to improper BW. In this case, changing the filter BW dynamically extracts the fundamental positive sequence component. Governing equations of the voltage vector in case of a fault are-

$$|v| = \sqrt{\frac{3}{2}\left[(V^{+1})^2 + (V^n)^2 + 2V^{+1}V^n\cos\big((n-1)\omega t\big)\right]} \tag{3.4}$$

$$\theta = \omega t + \tan^{-1}\left[\frac{V^n\sin\big((n-1)\omega t\big)}{V^{+1}+V^n\cos\big((n-1)\omega t\big)}\right] \tag{3.5}$$

Where, V^{+1} is the fundamental positive sequence RMS voltage and V^n is the magnitude of the n-th harmonic voltage which could be positive or negative sequence. In stationary reference (αβ0) frame, quantities in (3.4) and (3.5) become sinusoidal using Clarke's transformation. For better clarity and visualization, the locus of the voltage vector using (3.4) with 75% fundamental positive and 25% fundamental negative sequence component is shown in Figure 3-18, where n=-1 and ω=377 rad/sec. Theoretically, introducing a Band

Pass Filter (BPF) should give immunity to the fundamental voltage from other harmonics but unfortunately it doesn't.

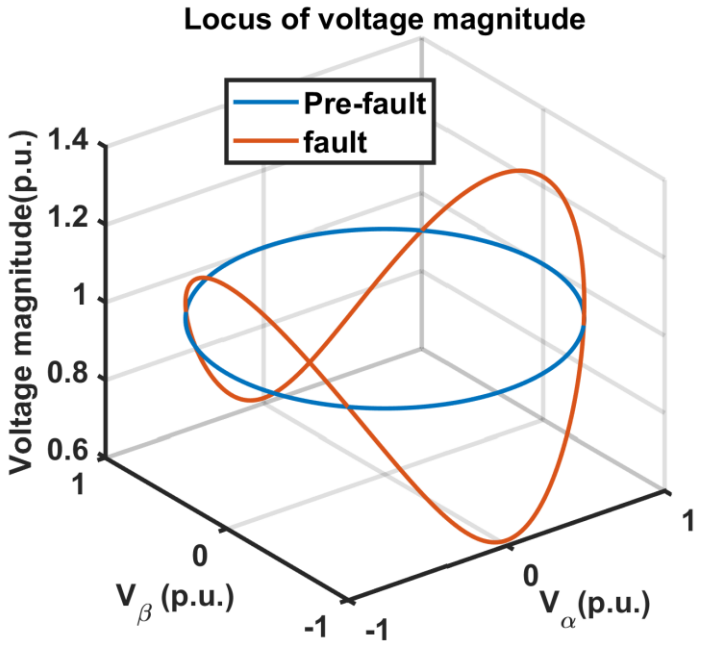

Figure 3-18: Locus of voltage magnitude

The transfer function for a second order BPF with real coefficients is shown in (3.6) below-

$$H_{RCF}(s) = \frac{H_0\omega_c^2}{s^2 \mp \frac{\omega_c}{Q}s + \omega_c^2}. \tag{3.6}$$

Where H_0 is the gain, ω_c is the cut-off frequency and Q is the quality factor. From Figure 3-18, it is evident that the fundamental positive sequence component of the voltage vector during fault condition is not constant and cannot be extracted by just filtering [45]. Plotting frequency response of (3.6) in Figure 3-19, the BPF does not attenuate the same positive and negative frequencies because the filter gain for ±60Hz is the same. Also, using a filter directly affects the control system performance such as bandwidth reduction. The damping factor of these filters also plays a vital role. Moreover, these filters should be frequency adaptive that makes the filter design complicated.

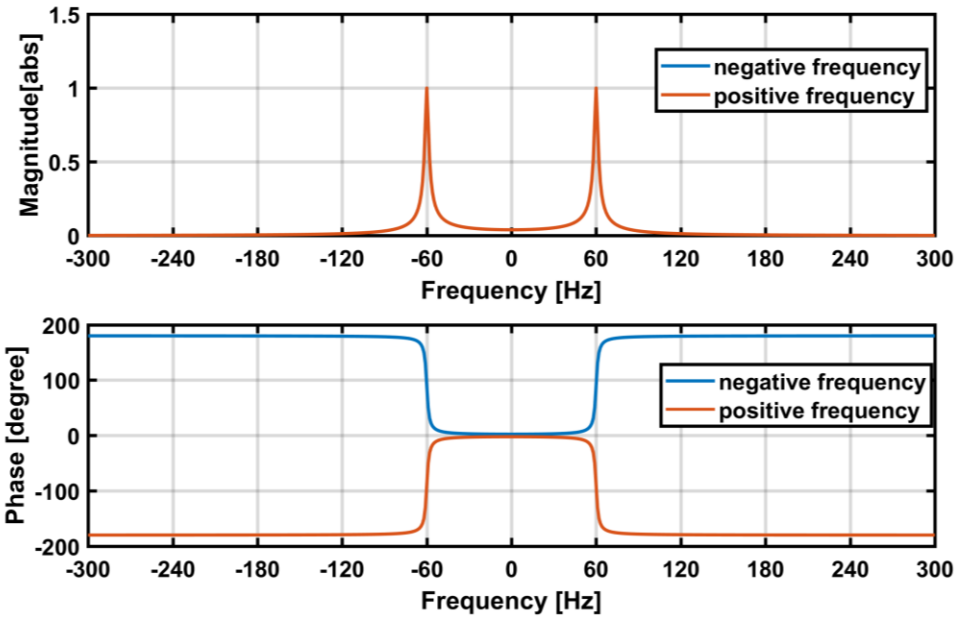

Figure 3-19: Frequency response of a second order Band Pass Filter (BPF)

To solve the problem, a synchronous reference frame PLL (SRF-PLL) is deployed in [56]. The idea is to extract all sequence information by using adaptive filtering in the synchronous rotating frame. This makes the SRF-PLL response slow, which is not acceptable during faults. Some of the advanced PLLs are fast PLL [57], DSOGI [58], Enhanced PLL [59] based on Adaptive Notch Filtering (ANF) technique, and Decoupled Double Synchronous Reference Frame PLL (DDSRF-PLL) [60]. All of these require complex transformations, and this makes the inverter control system complicated. In 2011, Guo *et al.* presented a Multiple-Complex-Coefficient-Filter (MCCF) based PLL [61] which does not need filter bandwidth reduction and complex transformations. The main idea comes from the fact that a Real-Coefficient Filter (RCF) is not polarity selective. On the other hand, Complex-Coefficient Filters (CCF) can distinguish between positive and negative frequency which is essential for sequence extraction during an asymmetrical grid fault condition. The transfer function of a first order CCF is shown in (3.7).

$$H_{CCF}(s) = \frac{\omega_c}{s \mp j\omega_0 + \omega_c} \tag{3.7}$$

Where ω_0 is the desired frequency to be extracted and ω_c is the cut-off frequency. It produces polarity selective frequency which gives it an edge over RCF as shown in Figure 3-20 where $f_0 = f_c = \pm 60$Hz. As shown, it produces different gains for the same positive and negative frequencies.

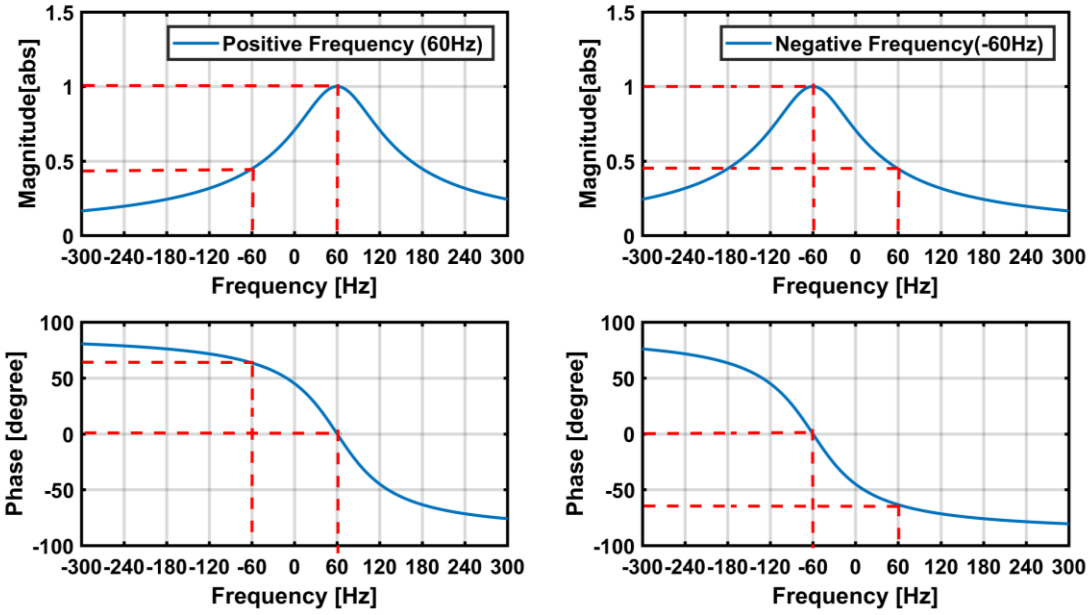

Figure 3-20: Frequency response of first order Complex-Coefficient Filters (CCF)

The transfer function in (3.7) can be used multiple times to extract selective harmonic components and sequence at the same time. Such a structure is shown in Figure 3-21 keeping in mind only to extract the 5th and 7th harmonic voltage components in αβ0 frame. There are total of six filters corresponding to ±60Hz, ±300Hz and ±420Hz.

The fundamental frequency positive sequence voltage component can still be used for synchronization and designing the control structure. Using this effectively detects the harmonic components even under a large disturbance. This case is different if there are

non-linear loads connected to the PCC. Generally, these loads generate harmonics that are deterministic in nature and can be controlled. On the other hand, in case of an unbalanced fault condition, generated voltage harmonics depend on the fault type and other variables that influence the voltage wave shape. Then, it is required to detect some selective distortion elements such as 5^{th} and 7^{th} harmonics as fast as possible and with proper sequence information. By adding more CCFs, this concept can be extended to any order, magnitude or sequence as needed.

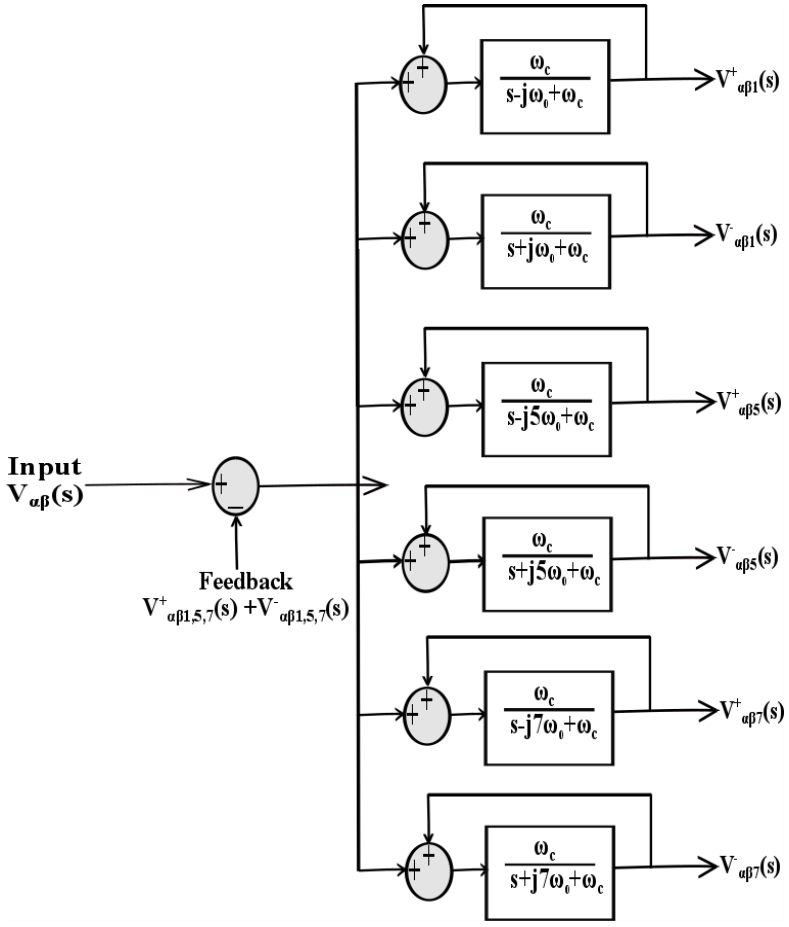

Figure 3-21: Multiple-Complex-Coefficient-Filter (MCCF) based PLL

3.5 Control architecture

Consider a simple system with measured signals to test the proposed idea as shown in Figure 3-22(a). The quantities in αβ0 frame obtained from MCCF PLL are transformed to dq0 frame quantities as in Figure 3-22(b).

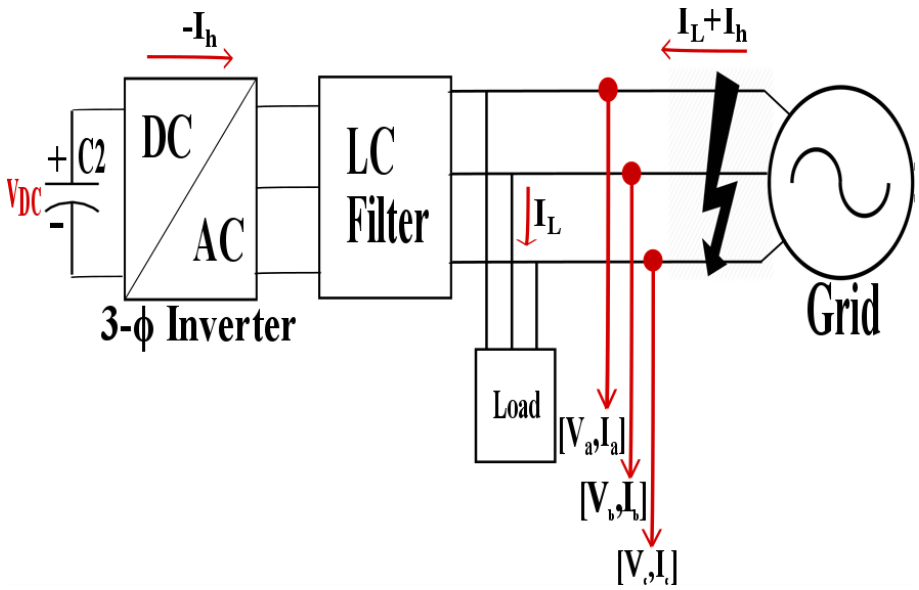

(a) Schematic diagram of the test system

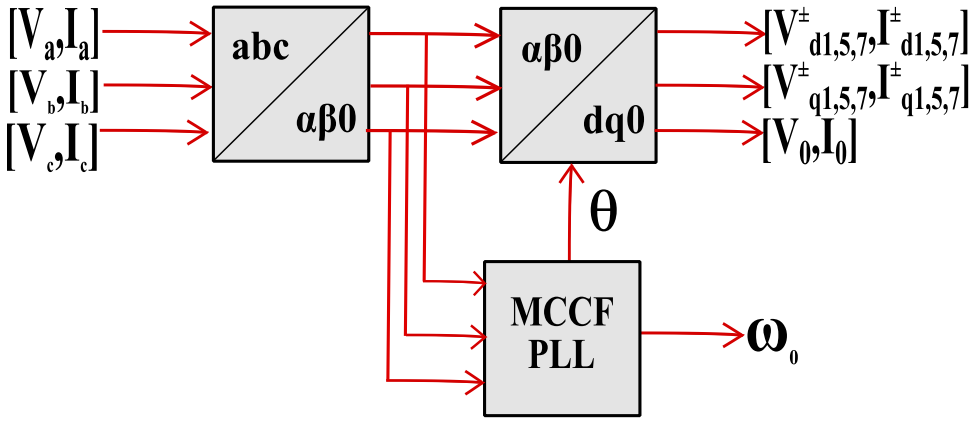

(b) Voltage and current measurement

Figure 3-22: Schematic diagram of harmonic compensation-based system

As this research focuses on SHC using smart inverter technology, the load connected is considered aggregated and linear in nature, and it is assumed that the selective harmonics

get generated during the fault condition. The input of the inverter can be a Renewable Energy Source (RES) like solar PV or a storage system such as a Battery Energy Storage System (BESS). Once the selective harmonics (5^{th} and 7^{th} in this research) are detected using MCCF, the next step is to reduce it. To do that, a Multiple Rotating Integrator (MRI) based current control approach with non-zero proportional term [62] is selected because of its simplicity. In this approach, voltage and current quantities are transformed into dc quantities in the synchronous reference frame (dq0). Therefore, active and reactive current components can be controlled independently by I_d and I_q respectively. Also, the control structure is decoupled in nature i.e. regulating active and reactive current does not affect each other. Figure 3-23 shows a step-by-step visualization of the proposed SHC. For the current harmonics that are desired to be eliminated, the references are set to zero ($I_{ref,\pm5}$=0, $I_{ref,\pm7}$=0). This reduces the harmonics and the smart inverter must deal with only the fundamental components.

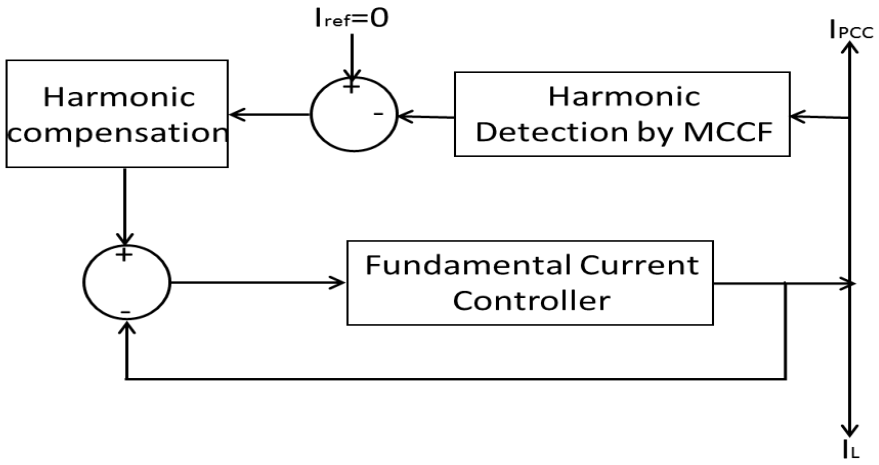

Figure 3-23: Selective harmonic compensation-based inverter control scheme

Figure 3-24(a) shows the controller structure for 5^{th} harmonic compensation. In this case, positive and negative sequence components can be compensated with the same scheme i.e.

PI1 and PI2 gains remain the same. Similarly, Figure 3-24(b) shows the controller structure to reduce both sequences of the 7th harmonic. The PI controllers (PI1 and PI2) tuned for 5th harmonic elimination can also be used for 7th harmonic elimination. This is true because the current control dynamics depends on the line parameters, which are the same for both.

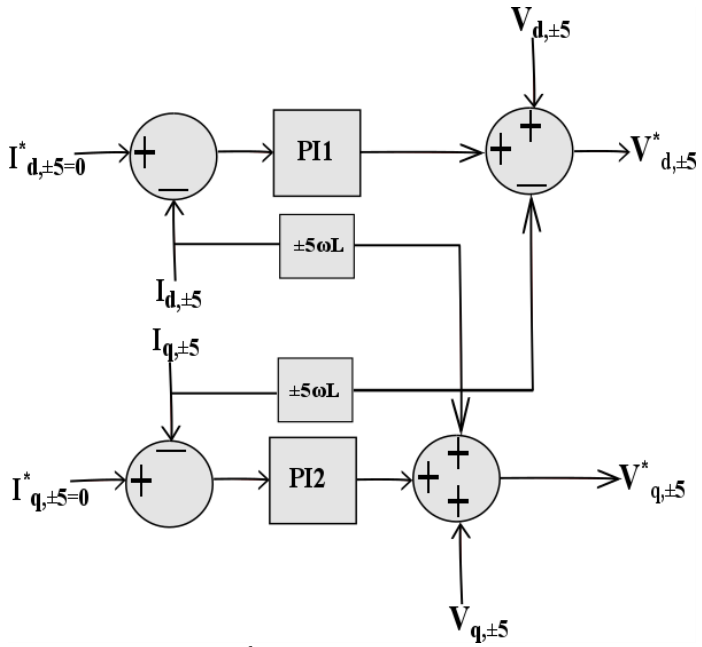

(a) 5th harmonic controller

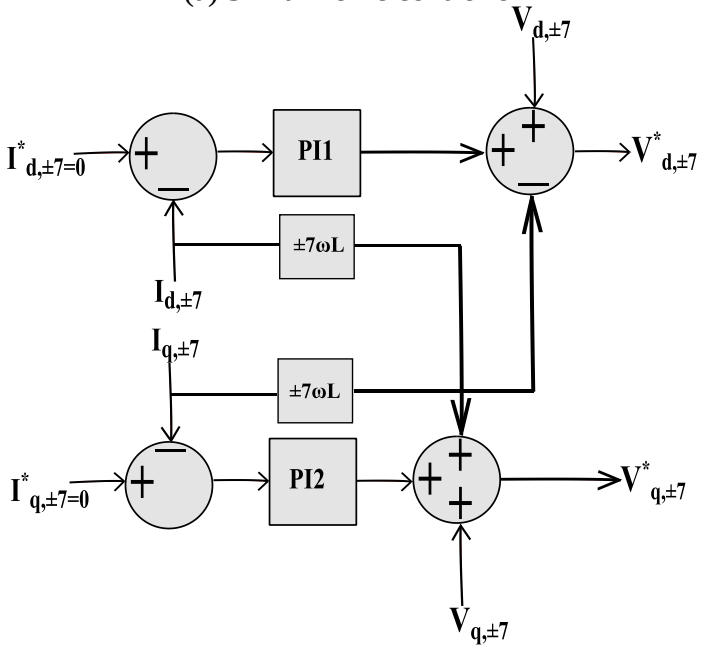

(b) 7th harmonic controller

Figure 3-24: Selective harmonic controller

The current controllers in Figure 3-24 generate a reference value for the voltage of that harmonic for the PWM scheme of the inverter. This is shown as $V^*_{dq,\pm5}$ and $V^*_{dq,\pm7}$. These values are made equal to zero using the proposed scheme during the fault period and the PWM scheme is left with only the fundamental positive sequence voltage component as in the case of a conventional PLL. The fundamental current controller is shown in Figure 3-25 for unity power factor operation because $I^*_{q1}=0$ which makes Q=0.

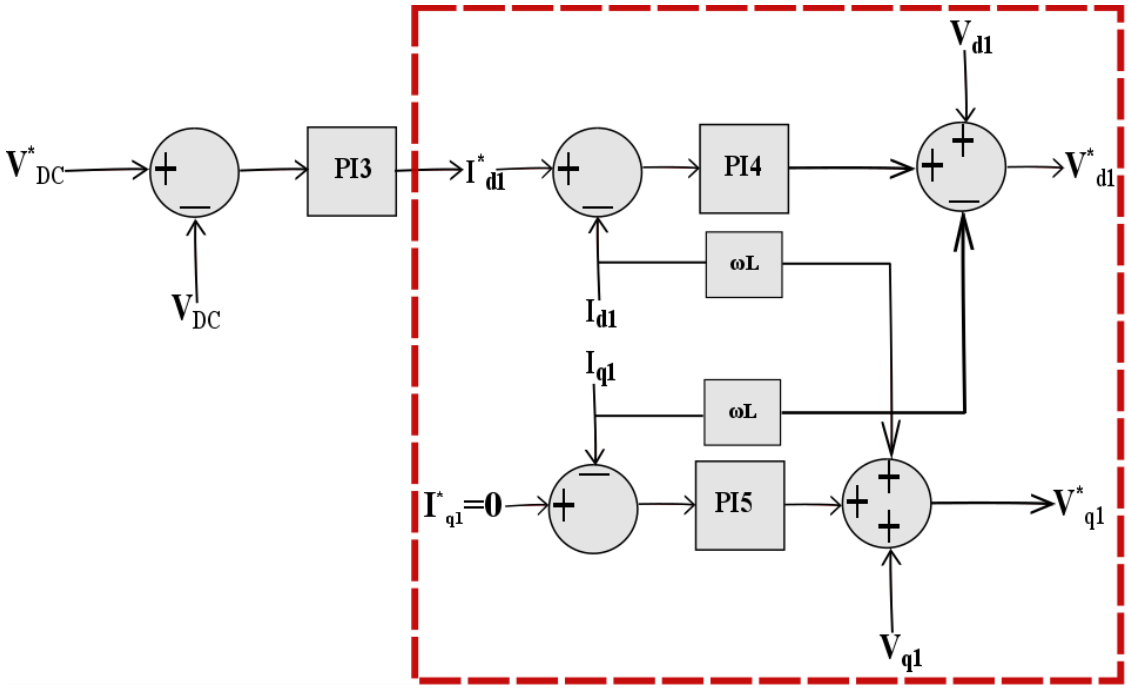

Figure 3-25: Fundamental current controller structure (unity power factor)

The same current controller enclosed in dotted red square is used for fundamental positive sequence component to generate the reference V^*_{dq1} that feeds the inverter PWM scheme. The outer loop takes care of the dc link voltage across the input capacitor connected to the inverter input port. The dc link voltage reference is set as V^*_{DC} and the error between the measured and the desired dc link voltage is regulated by another PI controller (PI3). The output of PI3 controller is the current reference I^*_{d1} that drives the active current of the

inverter. Figure 3-26(a) shows the arrangement of semiconductor switches inside the inverter. Transforming V^*_{dq1} to V^*_{abc} creates the voltage reference that in turn produces the gate pulses T1-T6 inside the inverter as shown in Figure 3-26(b).

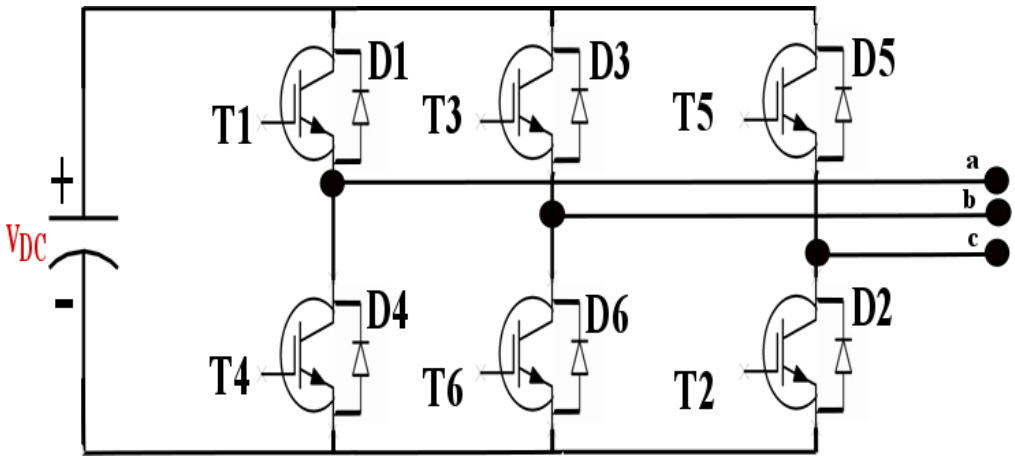

(a) 3-Ø VSI

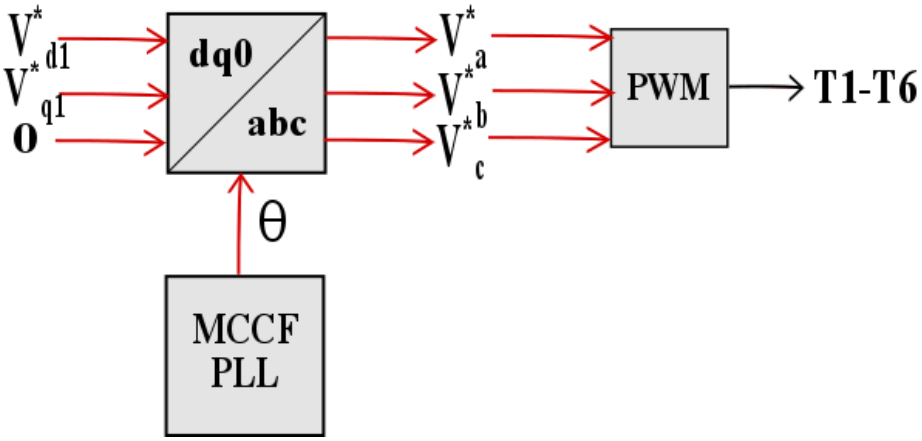

(b) Gate pulse generation

Figure 3-26: Inverter topology and gate pulse generation

3.6 Simulation results and analysis

Based on the system shown in Figure 3-22, a single line to ground fault is considered where phase A is the faulty phase. Table 3-1 shows the system configuration and PI values. Fault start time is at t=2s and the duration is 200 ms. This short duration is chosen intentionally to validate the transient and steady-state performance of the designed controllers.

Table 3-1: System parameters

Key components	**Parameters**
Line parameters	R=0.8 Ω, L=30 mH
Rated grid voltage	12.47 kV, 60 Hz
PI1	K_p=300, K_i=133.33
PI2	K_p=300, K_i=26.67
DC link voltage	800 V
PI3	K_p=7, K_i=800
PI4 and PI5	K_p=0.3, K_i=20

Immediately after the grid fault, the grid voltage and consequently, the line current get distorted by unknown harmonics as shown in Figure 3-27. However, for the proposed SHC technique, only the 5th and 7th harmonics are monitored and evaluated.

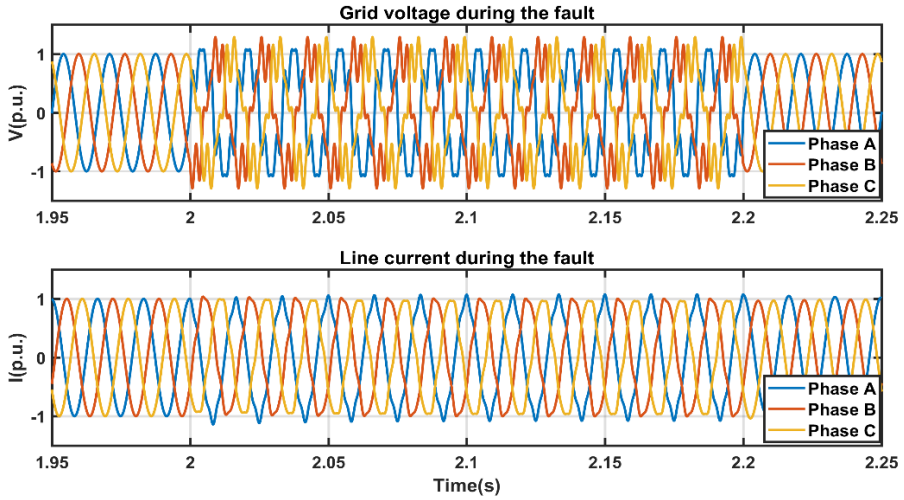

Figure 3-27: Voltage and line current during fault

As expected, MCCF tracks the harmonic sequence and magnitude within 5 ms of the fault. It is seen from Figure 3-28 that the grid voltage has a positive sequence 5th harmonic with 0.25 per unit magnitude. A detailed observation reveals that it also contains a negative sequence 7th harmonic component whose magnitude is 0.20 per unit. Therefore, it is evident that the MCCF successfully detected the voltage harmonics and associated sequence information.

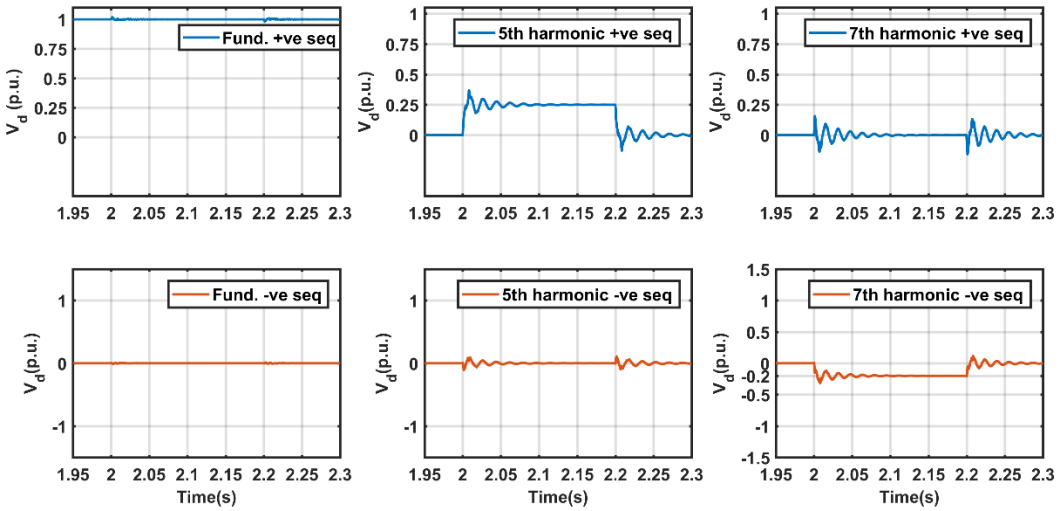

Figure 3-28: MCCF output during fault

The next step is to eliminate the harmonics already discussed in section 3.5. Using the harmonic controllers shown in Figure 3-24, the voltage references for the selected harmonics are nullified i.e. $V^*_{d,\pm5}=0$ and $V^*_{d,\pm7}=0$. This is demonstrated in Figure 3-29 where $V^*_{d,+5}$ and $V^*_{d,-7}$ becomes reduced as compared to Figure 3-28. It takes 50 ms for the controller to compensate and reach steady-state condition. So, its transient performance is quite fast and reliable. Initially, the load current (I_L) was supplied by the grid. During fault, as soon as the voltage reference for the inverter gets generated, the inverter injects the compensating current at the PCC. This alleviates the distorted line current as 5th and 7th

harmonics are nullified. The inverter behaves as a controlled voltage source that compensates the harmonic current as seen from Figure 3-30. It may be seen in the figure that the inverter injects the compensating current for the entire grid fault event.

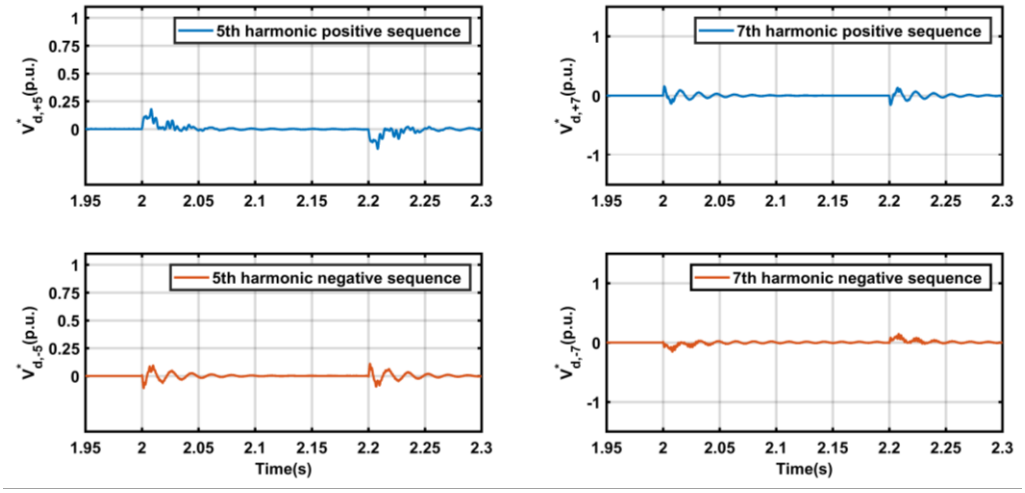

Figure 3-29: Compensated voltage reference ($V^*_{d,\pm5}$, $V^*_{d,\pm7}$)

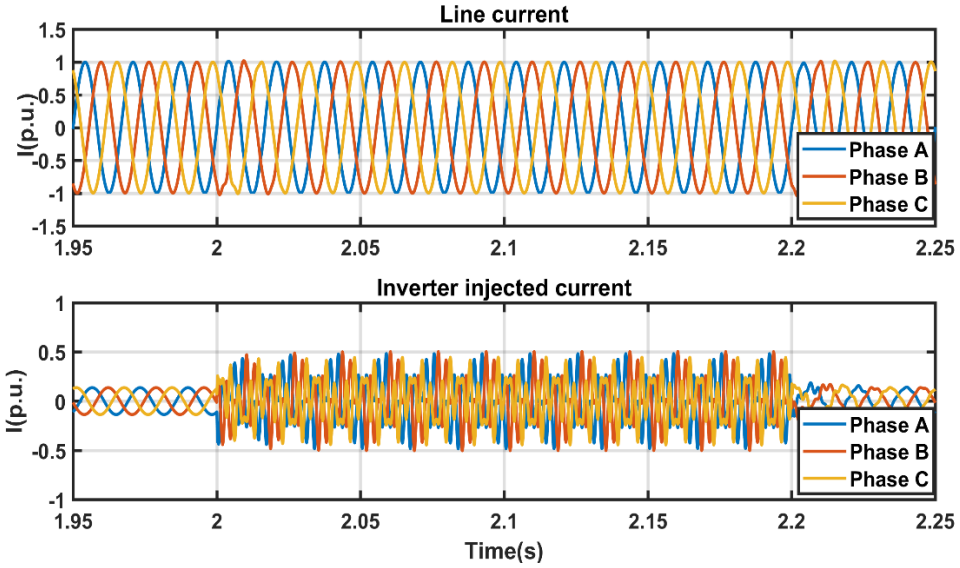

Figure 3-30: Compensated line current and inverter injected current

Figure 3-31 is obtained after analyzing the current harmonics using Fast Fourier Transformation (FFT). In the uncompensated case, the 5^{th} and 7^{th} harmonics were 4.30% and 2.45% of the fundamental frequency component respectively.

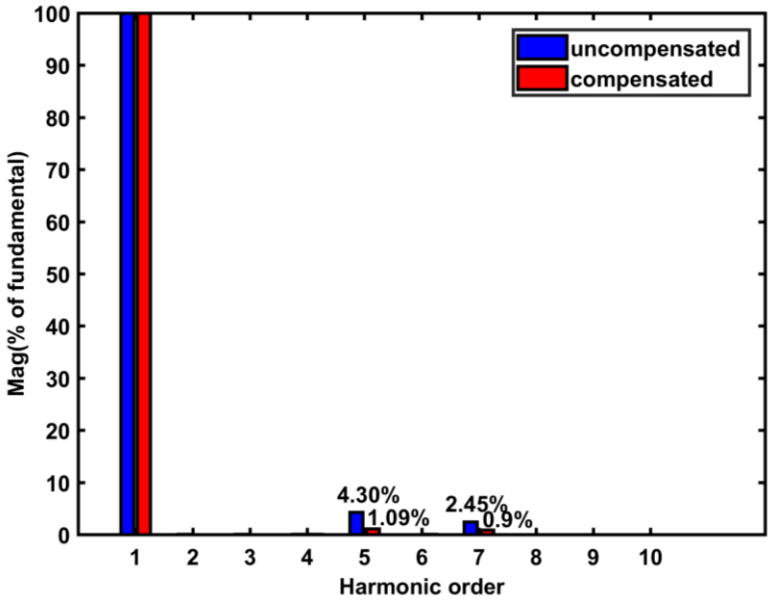

Figure 3-31: Harmonic order for uncompensated and compensated line current

The Total Harmonic Distortion (THD_I) and other frequency components for both the uncompensated and the compensated line current are shown in Table 3-2.

Table 3-2: THD_I and other harmonic components

Harmonic order	Uncompensated	Compensated
1	100.00%	100.00%
2	0.07%	0.02%
3	0.05%	0.01%
4	0.04%	0.03%
5	**4.30%**	**1.09%**
6	0.02%	0.07%
7	**2.45%**	**0.90%**
8	0.02%	0.02%
9	0.01%	0.01%
10	0.01%	0.01%
THD_I	5.43%	1.46%

3.7 Conclusion

In this chapter, at first, it is shown that through the proposed FRT scheme, the BESS stores energy generated by the PV plant enabling it to continue operation in MPP condition for the duration of the fault. At the same time, the spare capacity of the grid side inverter can be used to support the system operation by providing additional reactive power injection to the grid up to the maximum current carrying capability of the power switches, if needed. The importance of the energy storage system is evident from the simulation results. Decoupled control provides acceptable results. PI control of the system shows satisfactory performance during the grid faults. A three-phase balanced fault is created. The performance of the system depends on the phase and frequency tracking capability of the PLL system. For unbalanced faults on the grid side, it is important to design an adaptive PLL system. Based on the findings, a value proposition for smart inverters is proposed and therefore, a harmonic current detection and compensation technique was introduced. Using this strategy, voltage source inverters may become more powerful and versatile. The technique can compensate selective line current harmonics within a few milliseconds. Using the proposed approach, it is possible to push the boundary of maintaining power quality measures even during asymmetrical grid fault conditions. The limitation of a conventional PLL scheme during fault condition was discussed first. Then a CCF-based detection scheme was introduced and compared with the performance of an RCF. Also, multiple CCF-based PLL structure and a detailed inverter control scheme were discussed. Harmonic controllers for reducing 5^{th} and 7^{th} harmonics were presented which can easily be extended to other higher order harmonics. The results found are quite satisfactory and agrees with the theory.

CHAPTER 4: A RECONFIGURABLE AND FLEXIBLE VOLTAGE CONTROL STRATEGY WITH INTEGRATED ENERGY STORAGE FOR ADVANCED DISTRIBUTION SYSTEMS

4.1 Overview

A novel circuit topology is proposed for utility-owned PV inverters with integrated Battery Energy Storage System (BESS) and compared to two state-of-the-art configurations. The proposed topology offers flexibility and can be applied to a range of distribution networks for tight voltage regulation. During BESS maintenance, the solar-storage system reconfigures itself for self-run mode of operation, and actively compensates high penetration induced voltage fluctuation without activating overcurrent protection of the inverter, which is an added advantage of this strategy. This advantage is achieved by slightly increasing the inverter size to reserve a portion of inverter's current-carrying capability. A dynamic model of the new configuration is also developed to analyse its performance in providing fast response for high ramp up/down solar irradiance variation. As the proposed control strategy is implemented at the device level, the local voltage regulation is quite guaranteed to be in the permissible range. Results from the analysis performed on a modified IEEE 33 bus Medium Voltage (MV) distribution network with multiple inverters show evidence that the proposed strategy has the potential to mitigate voltage fluctuation in several extreme cases.

4.2 Introduction

High penetration of solar PV energy in any feeder has the potential to change the voltage profile. Injection of active power from these DGs may increase the voltage to unacceptable levels, especially at the End of the Line (EOL) in a low voltage, weak radial distribution

system [63]. For medium and high voltage distribution systems, it depends on the Hosting Capacity (HC) at different locations of the network [64]. On a cloudy day or during peak load period, the voltage fluctuates, and without proper control, the system could experience voltage instability. Furthermore, managing voltage fluctuations caused by roof-top single-phase PV inverters, which are mostly connected to low-voltage networks, requires significant investment and a complex infrastructure. This issue has been reported as the main concern for utilities in the face of high penetration of photovoltaic power [65], [66]. Therefore, in contrast, utilities are now becoming more interested in investing in their own MW level PV generation connected to medium voltage distribution networks [67].

Voltage regulation issue has been extensively studied in the literature. Volt-Var control [68]–[70], active power curtailment [71]–[73] are thoroughly investigated. These methods often do not take the PV inverter dynamics into account. Also, utility-owned conventional assets for voltage regulation such as On Load Tap Changers (OLTC), Step Voltage Regulators (SVR) and capacitor banks are shown to be properly coordinated with the newly installed smart PV inverters [74]–[76]. Battery Energy Storage Systems (BESS) have become an integral part in this architecture because of its various grid supporting features. BESS may be connected on the AC side, or it could be integrated with the PV on the DC side, which is a less expensive solution [77]. A dedicated Power Conditioning System (PCS) for the BESS operation is also not uncommon which adds more costs to the investment.

Today, Distributed Network Operator (DNO) is responsible for voltage regulation in their networks. Until now, PV inverters have been forced to operate at zero reactive power output. This has been modified in IEEE standard 1547a-2014 and now included in IEEE

standard 1547a-2018. By this modification, IEEE aims at putting DGs to control the bus voltage. This is possible because the advanced capabilities of a smart inverter now include automatic voltage control. For proper coordination among different inverters, broadly two approaches have been proposed - 1) centralized and 2) decentralized/distributed. The centralized approach offers wide area voltage control but requires a reliable communication scheme [78], [79]. A decentralized approach provides autonomy but suffers from limitation on voltage control range [20], [80], [81]. Multi-agent-based schemes have also been investigated in the literature which again requires reliable cyber communication protocols to transmit point-to-point messages among neighbors [82], [83]. Moreover, voltage control depends on R/X ratio at the Point of Common Coupling (PCC). For different voltage levels, voltage control mechanisms are different [84]. This is shown in Table 4-1.

Table 4-1: Typical line parameters

Type of line	$\frac{\mathbf{R}}{\mathbf{X}}$	**Voltage level (kV)**	**Voltage control mechanism**
Low voltage	7.7	< 1	Active power (P)
Medium voltage	0.85	1-34.5	Reactive power (Q) and/or Active power (P)
High voltage	0.31	34.5-above	Reactive power (Q)

It is clear from Table 4-1 that voltage control by injecting or absorbing reactive power only applies to a high voltage line, and, in some cases, to a medium voltage line. Low and medium voltage distribution networks require active power to correct a voltage issue, which is not considered in [68]–[70]. Moreover, PV panels connected to the far end of the distribution network create a weak grid, where voltage control depends mostly on local inverter control. OLTC and SVR respond slowly (within minutes) and sometimes require

longer time due to communication latency. On the other hand, the nodes which are closer to the substation end, create a stronger grid. In this case, voltage control of these nodes depends on the voltage sensitivity with respect to active and reactive power [85]. Voltage Source Converters (VSC) are typically used as interface for solar PV systems for forward and reverse power flows in the feeder. The key to controlling the power flow is to control the dc-link voltage of these inverters as they operate only for a stable range of dc link voltage. Therefore, dc link voltage dynamics should be a key concern when injecting or absorbing active/reactive power which is often not considered in the existing solutions.

Considering all the above factors, this section first proposes a new topology for integrating BESS with the utility-owned PV. Secondly, a reconfigurable control strategy comparing the conventional and proposed two-stage solutions is outlined in detail. This strategy offers wide voltage control range for weak or strong grid locations. At the same time, it drives the inverter in such a way that its capability can be harnessed effectively. Flexible voltage control is achieved by changing reactive power (Q) as a function of a sensitivity index or active power (P) injection. This is decoupled in nature and can be done independently. In summary, the contribution of this work is in the introduction of a distributed voltage control strategy in a reconfigurable and flexible manner based on the capacity of PV inverter and BESS.

4.3 Proposed control strategy

4.3.1 Background on voltage control strategy

Most distribution systems are radial in nature. However, when a DG is connected, the system is no longer radial. A simple single line model of such a distribution system is shown in Figure 4-1.

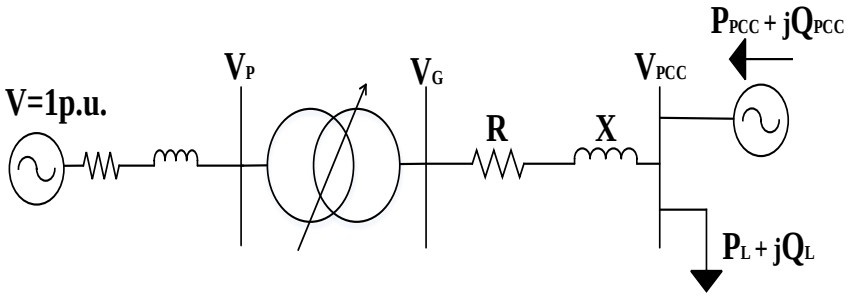

Figure 4-1: Single-line diagram of two generating stations

The upstream network with respect to the PCC is generally a bulk power system. Here, the transformer shown is an OLTC which regulates the voltage (±5%) at the feeder end which response time is in minutes. The voltage at the PCC can be approximated as follows [48]-

$$V_{PCC} \approx V_G + \frac{RP+XQ}{V_{PCC}^*}. \tag{4.1}$$

Where, V_G is the substation bus voltage, $P=P_{PCC}-P_L$ and $Q= Q_{PCC}-Q_L$ are the net active and reactive powers injected at the PCC respectively, and R and X are the feeder resistance and reactance respectively. To compensate for the voltage, rise/drop caused by P, i.e. to make $V_{PCC} \approx V_G$, the required Q is given by-

$$\frac{Q}{P} \approx -\frac{R}{X}. \tag{4.2}$$

Substituting the values from Table 4-1 in (4.2) shows that the Q demand is high for low voltage distribution systems. For other voltage levels, this requirement is relatively low.

The negative sign indicates that net injection of active power (P) from the PV panels requires reactive power absorption to keep the PCC voltage at nominal value. Until now, a fixed power factor operation of the inverter is required by DNOs. This is equivalent to keeping the Q/P ratio constant. With the modification of IEEE 1547a-2014, this is going to be a challenge as DGs are now required to contribute toward correcting voltage issues by controlling both P and Q. However, as (4.2) shows, voltage support by only reactive power exchange greatly depends on the R/X ratio of that bus. Therefore, reactive power control capability of the inverter must be considered. The Q reserve of an inverter depends on the maximum allowable current rating. The reserve can be shrunk or released based on the active power utilization of the inverter. From (4.2), for a medium voltage distribution system, the R/X ratio can be such that it may be able to compensate the voltage by only regulating Q. In most of the cases, this is not true as heavy loading draws reactive power from the line.

Therefore, the second-best choice is to curtail P to control the voltage rise which needs an integrated storage solution to store the curtailed power. A BESS provides this support here. The alternative approach is to find a value for Q_{PCC} that minimizes the voltage rise caused by $P_{PCC.}$ The PV injected current at the PCC can be calculated as follows-

$$I_{PCC} = \left(\frac{P_{PCC}+jQ_{PCC}}{V_{PCC}}\right)^{*} = \left(\frac{P_{PCC}-jQ_{PCC}}{V_{PCC}cos\delta - jV_{PCC}sin\delta}\right). \quad (4.3)$$

In (4.3), δ is the angle between the voltage vector V_{PCC} and V_G. Using the real and imaginary part of the calculated current and taking the voltage and impedance into consideration, a zero voltage drop equation can be derived as follows-

$$V_G V_{PCC} \cos\delta = V_G^2 - RP_{PCC} - XQ_{PCC} \tag{4.4}$$

$$V_G V_{PCC} \sin\delta = RQ_{PCC} - XP_{PCC} \tag{4.5}$$

Solving (4.4) and (4.5) to keep the voltage V_{PCC} at 1 p.u., the required Q is obtained by (4.6).

$$Q^*_{PCC} \approx \frac{X}{R^2+X^2} - \sqrt{\left(\frac{X}{R^2+X^2}\right)^2 - P^2_{PCC} + 2\frac{RP_{PCC}}{R^2+X^2}}. \tag{4.6}$$

If a load is connected to the generator bus as shown in Figure 4-1, then setting the inverter reactive power reference, $Q_{ref} \approx Q^*_{PCC}$ as per Eq. (4.6) guarantees a stable voltage profile. On the other hand, Q_{ref} can be set based on the inverter rating derived from the reserved Q as follows-

$$Q_{RES} = \sqrt{S^2 - P^2_{PCC}}. \tag{4.7}$$

$$Q_{RES} = P_{PCC} \tan Ø \tag{4.8}$$

Where, S is the inverter rating and Ø is the power factor angle. Considering variable power factor control, (4.7) provides the total reserved Q capacity. If a fixed power factor control is desired, then (4.8) provides the Q reserve. In either case, Q_{RES} calculated from the above two equations may not be able to fulfill the requirement as calculated by (4.6), i.e. $Q_{RES} \neq Q^*_{PCC}$. In a worst-case situation like this, active power curtailment is needed. In a conventional case without BESS, the OLTC/SVR changes its tap to correct any voltage issue. In this work, the assumption is that the inverter is the primary asset to fix the voltage and faster than OLTC in operation.

4.3.2 Voltage sensitivity calculation

From (4.1), the sensitivities of voltage at PCC with respect to the net injected active and reactive power are calculated by (4.9) and (4.10).

$$\frac{\partial \mathrm{V_{PCC}}}{\partial \mathrm{P}} = \frac{R}{V_{PCC}^{*}} \tag{4.9}$$

$$\frac{\partial \mathrm{V_{PCC}}}{\partial \mathrm{Q}} = \frac{X}{V_{PCC}^{*}} \tag{4.10}$$

Dividing (4.9) by (4.10), sensitivity index, SI can be defined as in (4.11).

$$S_I = \frac{\partial Q}{\partial P} = -\frac{R}{X} \tag{4.11}$$

Partially differentiating (4.6) with respect to P_{PCC} we get (4.12).

$$S_I = \frac{\frac{R}{R^2+X^2} - P_{PCC}}{Q_{PCC} - \frac{X}{R^2+X^2}} \tag{4.12}$$

At initial operating point, PV doesn't inject any active or reactive power i.e. $P_{PCC} = 0$ and $Q_{PCC}=0$. So, (4.12) becomes (4.11) which is the easiest computation and usually enough for a wide range of loading conditions if static loading operation is assumed. For time-varying loads, the same sensitivity index can be used as the impact of loading on sensitivity has been found to be very small in all cases studied to date [85].

4.3.3 Reconfigurable control strategy

For a two-stage power conversion, the VSC is typically followed by a dc/dc boost converter which generates the duty cycle needed for the Maximum Power Point Tracking (MPPT). This is shown in Figure 4-2(a). This scheme injects or absorbs active current component according to the user defined dc link voltage reference (V^{*}_{DC}). In this way, the dc link voltage is preserved by using the inverter as a current controlled device. This mode will be

referred to as configuration 1 throughout the chapter. However, this configuration lacks the ability to directly control active power. As mentioned earlier, if the dc link voltage is within operational limits, active power (P) and reactive power (Q) can be controlled in a flexible manner. Therefore, to make configuration 1 more robust and achieve greater virtual inertia, the BESS is integrated with the dc link using a bi-directional dc/dc buck-boost converter as shown in Figure 4-2(b).

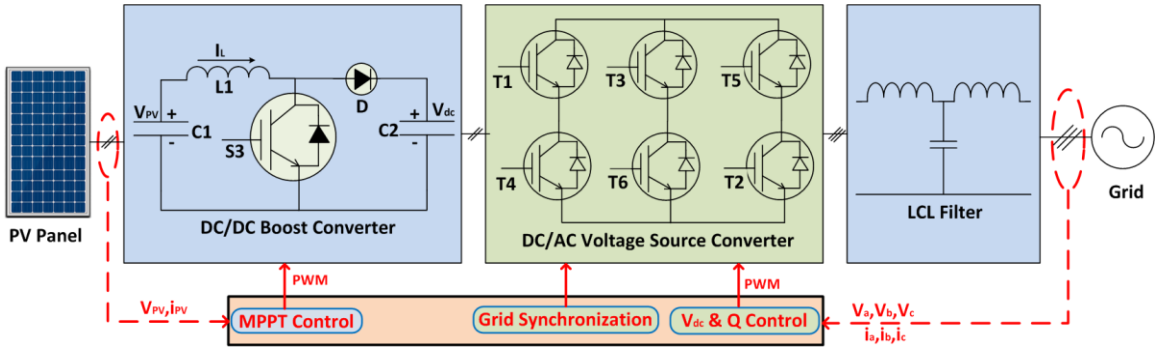

(a) Configuration 1: two-stage power conversion for PV integration (conventional)

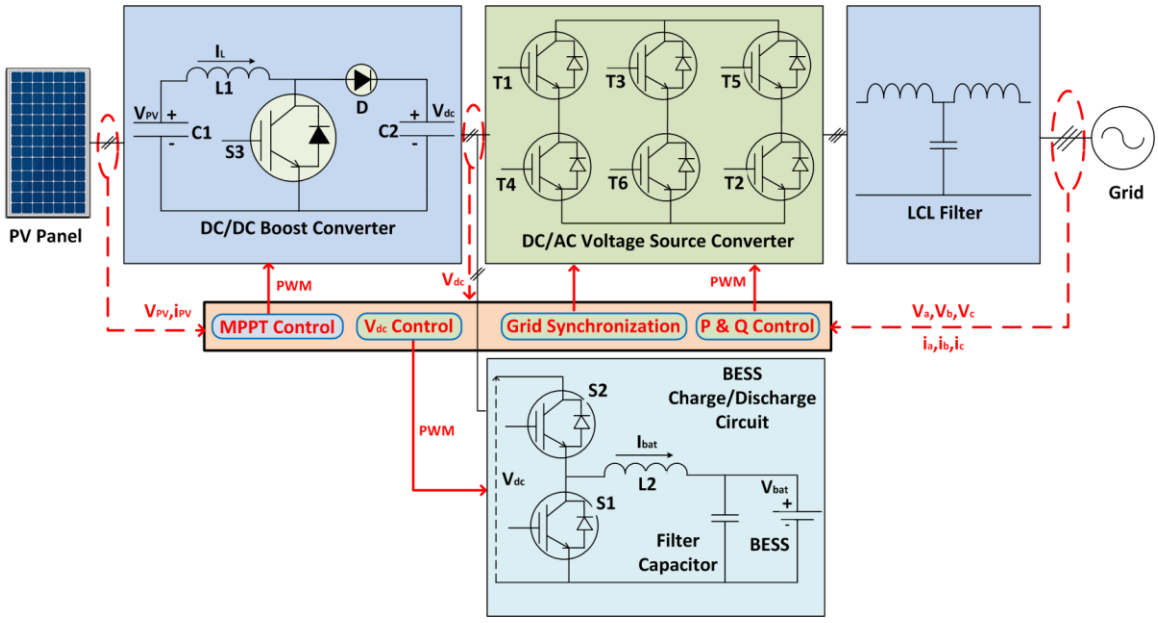

(b) Configuration 2: BESS integrated with inverter input side capacitor C2 (conventional)

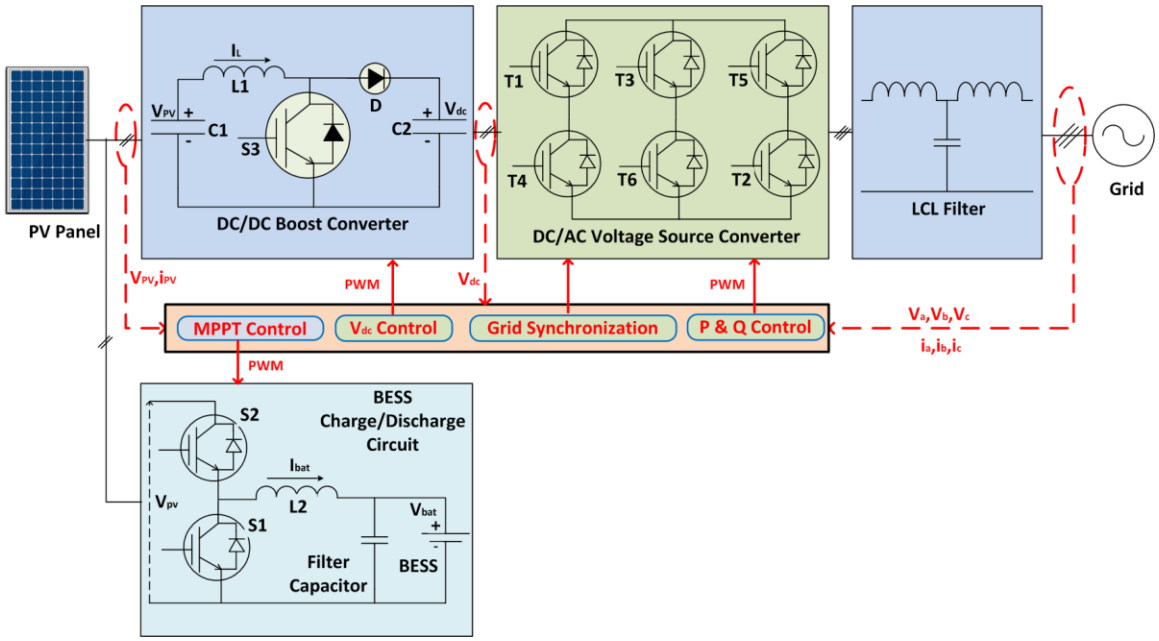

(c) Configuration 3: BESS integrated with the PV output side capacitor C1 (proposed)

Figure 4-2: Comparison between conventional and proposed topology

This opens a new dimension allowing one to use the PV source as a dispatch-able generator. This is referred to as configuration 2. In this configuration, however, the control objectives of the boost and bi-directional buck-boost converter overlap. Moreover, this topology has several drawbacks. For instance, changing the load creates large transients in the dc link that might damage the BESS. It also requires a high voltage compatible charge balancing circuit which makes the control system more complicated. Moreover, it is difficult to ensure safety measures for the high voltage level of BESS.

To design a dedicated controller for each specific task and avoid overlap in this dynamic environment, the BESS is proposed to be integrated with the PV output capacitor C1 as shown in Figure 4-2(c). This will be called configuration 3 henceforth. The proposed topology ensures low voltage operation of the batteries with the scope of flexible design and proper safety. On top of that, it offers a reconfigurable control strategy with or without

BESS that requires minimum modification in the controller design as discussed in section 4.4. From MW-scale utility-owned PV standpoint, this is clearly an advantage for the Battery Management System (BMS). If the BESS needs overhauling and regular maintenance, the PV system can still be operated without any problem through automatic transitioning to configuration 1. The control objectives are listed in Table 4-2.

Table 4-2: Control philosophy in two-stage PV inverter technology

Converter	**Configuration**		
	1	2	3
Boost	MPPT	MPPT	V_{dc} control
Bi-directional buck-boost	N/A	V_{dc} control	MPPT
VSC	V_{dc} and Q Control	P and Q Control	P and Q Control

4.3.4 Flexible control strategy

The logic behind the reconfiguring decision can be implemented based on the BESS status. Transition from configuration-2/3 to configuration-1 depends on the battery State-of-Charge (SOC). There is a standard operating range of the BESS SOC for every utility. This range ($SOC_{min} \leq SOC \leq SOC_{max}$) can be set considering the life-span and functionality of the BESS. For this work, this range is set to 50% ~ 90% as longevity of Li-ion batteries are considered [86]. Violating this constraint results in transition to configuration-1. The algorithm is shown in Figure 4-3. After the BESS status becomes known, the algorithm takes the PV production and load demand as inputs and checks the voltage status. There is an upper (V_{upth}) and a lower voltage threshold (V_{loth}), for which the inverter starts correcting the voltage. The constraints on this threshold are- $V_{upth} < V_{max}$ and $V_{min} < V_{loth}$. Once the voltage reaches any of these thresholds, the proposed control strategy then automatically takes the voltage deviation into consideration and first attempts to regulate

the reactive power (Q) to mitigate the problem. The rationale behind this action is that the reactive power regulation is typically the most cost-effective way to fix a voltage problem caused by P. To do this, Q_{ref} is calculated by (4.6) and available Q reserve is calculated by (4.7) or (4.8) based on the utility practice. To understand Figure 4-3, a step-by-step configuration wise approach is required. In configuration-1, when $V>V_{upth}$, when Q reserve is found to be not enough, the controller starts by disabling the MPPT operation, which is not desired for PV systems. In such a case, configuration-2 and 3 is desirable as it can charge the BESS with the excess solar energy. When $V<V_{loth}$, in case of configuration-2 or configuration-3, the BESS discharges. For configuration-1, this voltage condition means Q support has become limited.

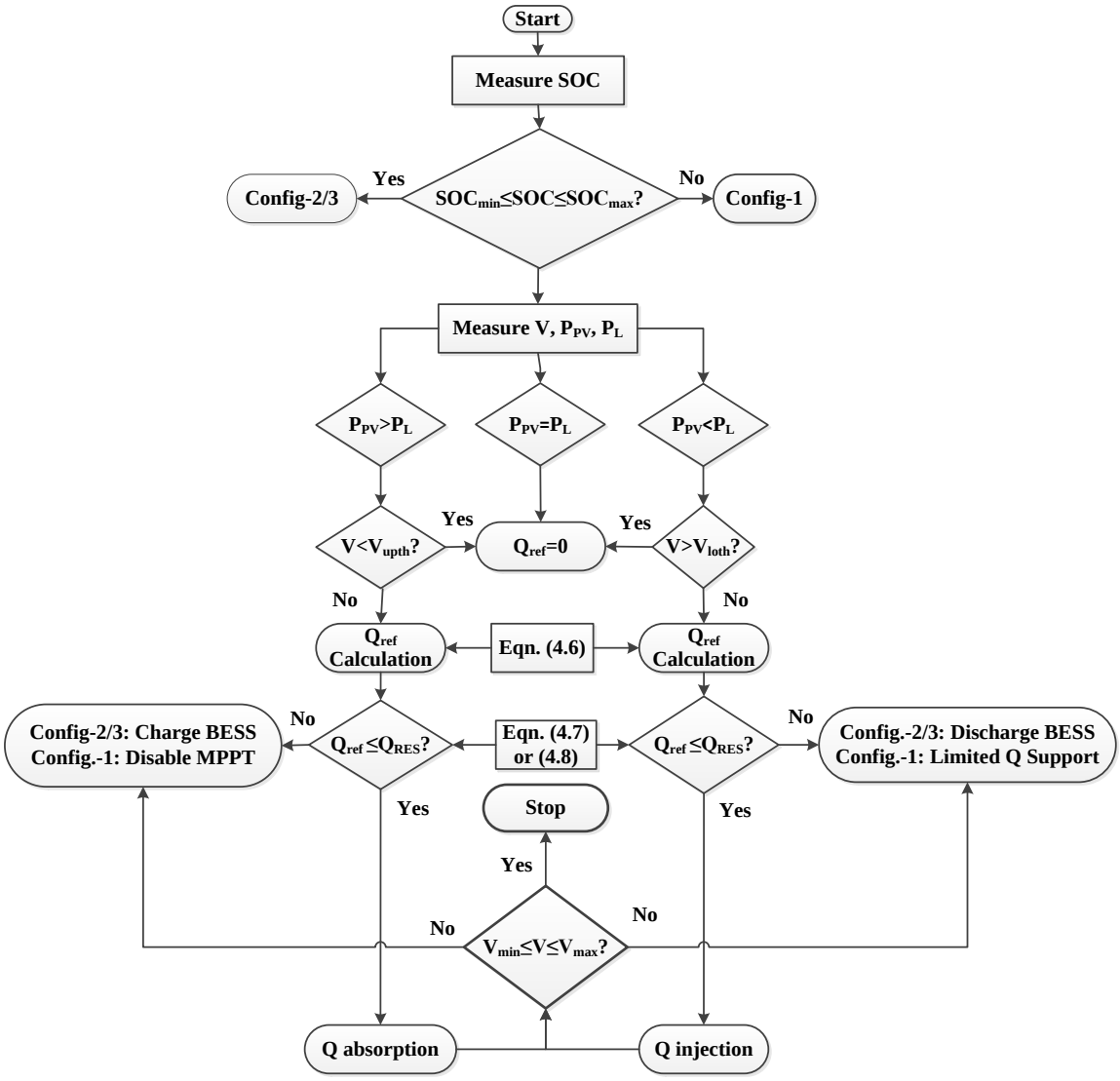

Figure 4-3: Proposed control strategy of PV inverter

This is a regular case for PV without having a BESS and the inverter is essentially set to output maximum active power obtained by the MPPT algorithm used. However, the VAR control range can be broadened without activating the overcurrent protection, even while the inverter supplies maximum P, by using a current reserved inverter as discussed in section 4.3.5. In this work, P curtailment amount is calculated by multiplying the inverter's active power reference (P_{ref}) with the ratio of the nominal voltage to the measured voltage at the PCC. At the same time, Q control is used according to (4.6) in collaboration with P

by calculating the sensitivity using (4.11-4.12). In other words, the proposed control strategy is decoupled in nature to compensate the voltage change based on the need for either active power (P) or reactive power (Q) or both. This is possible because the inverter can control P and Q independently up to the maximum current limit. Theoretically, an inverter can inject Q on a cycle-by-cycle basis. In practice, it has some time delay due to switching and communication latency. Therefore, voltage change is also not instantaneous, but this is still faster than OLTC operation.

4.3.5 Inverter operational limit

Conventional PV inverter capability curve is shown in Figure 4-4(a). There is a limit of reactive power that can be injected or absorbed at any time. This is denoted by $+Q_{max}$ and $-Q_{max}$. The maximum active power rating is P_{max} and Ø is the power factor angle. If the dc link voltage is kept at an operational range, for low PV period or night time operation, Q capacity can be released and controlled within the rated current limit. It is important to mention here that dc link capacitor requires active power to store charge in its electrostatic field. So, it is not possible to control the dc link voltage without BESS at night time, or at any instant when the PV power is not enough. Similarly, for a user defined fixed leading/lagging power factor operation, the reactive power support suddenly vanishes when the PV panels produce the maximum active power P_{max} as shown in Figure 4-4(a). In other words, the maximum allowable current capacity is dedicated for active power. However, meeting the interconnection requirements as in IEEE 1547a-2018 is often not possible for this type of inverter.

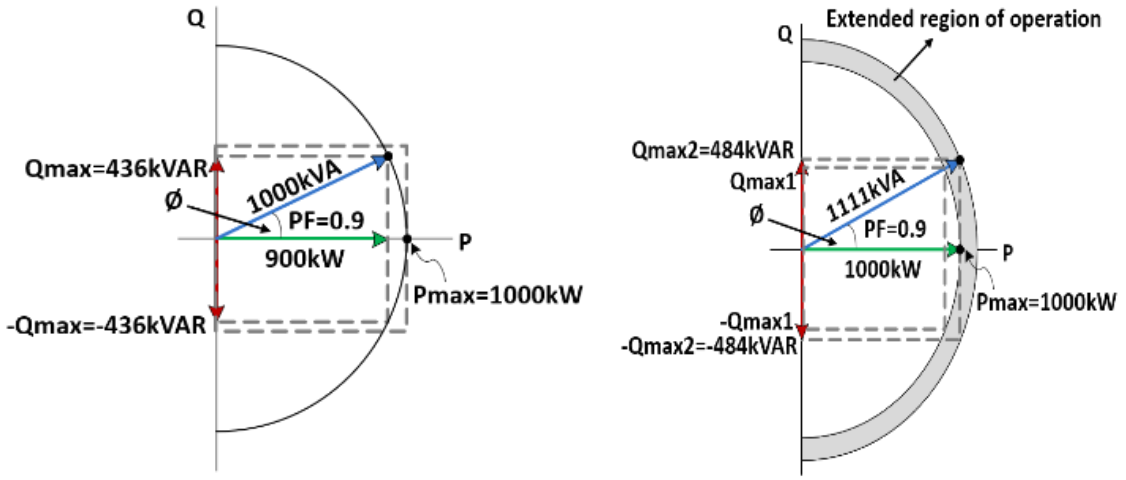

(a) Conventional (b) Current reserved

Figure 4-4: Inverter capability curve

An intelligent solution for better VAR support by using a slightly modified PV inverter is shown in Figure 4-4(b). Like the previous case, the limit of reactive power that can be injected or absorbed at a point of time is denoted by $+Q_{max1}$ and $-Q_{max1}$. But this time, a portion of current capacity is reserved for VAR support when the PV panels produce maximum power, P_{max}. This is possible because the inverter is usually operated as a current controlled device. This reserved portion is denoted by $+Q_{max2}$ and $-Q_{max2}$. For a fixed power factor operation, $+Q_{max2} > +Q_{max1}$ and $-Q_{max1} > -Q_{max2}$. Of course, this increases the rating of the inverter, but the cost is worth it in the context of supporting VAR. For example, at 100% loading, an 1111 kVA inverter can supply 1000kW and simultaneously 484 kVAR with a power factor of 0.9 lagging at the cost of current increase by only 11.1%. For the same power factor operation, a conventional 1000 kVA inverter provides 900kW and 436 kVAR. This can be calculated from (4.7) and (4.8). To summarize, the overcurrent protection of the inverter does not get activated for another 11.1% margin of current increase compared to a typical 1000 kVA inverter. For partial loading, both the inverters provide the same support. Although most of the time, PV does not provide peak generation,

but the capacity installed should be maximized. In case of seasonal and spatial variation, this would be a better strategy for the utility companies. The comparison of the VAR support capability of the two inverters (conventional vs. current reserved) is shown in Figure 4-5. Here, it is shown that the current-reserved PV inverter instantaneously provides maximum support (Q_{max2}) when it reaches P_{max}, whereas it vanishes for a conventional inverter. The extended region of reactive power support is marked in Figure 4-4(b).

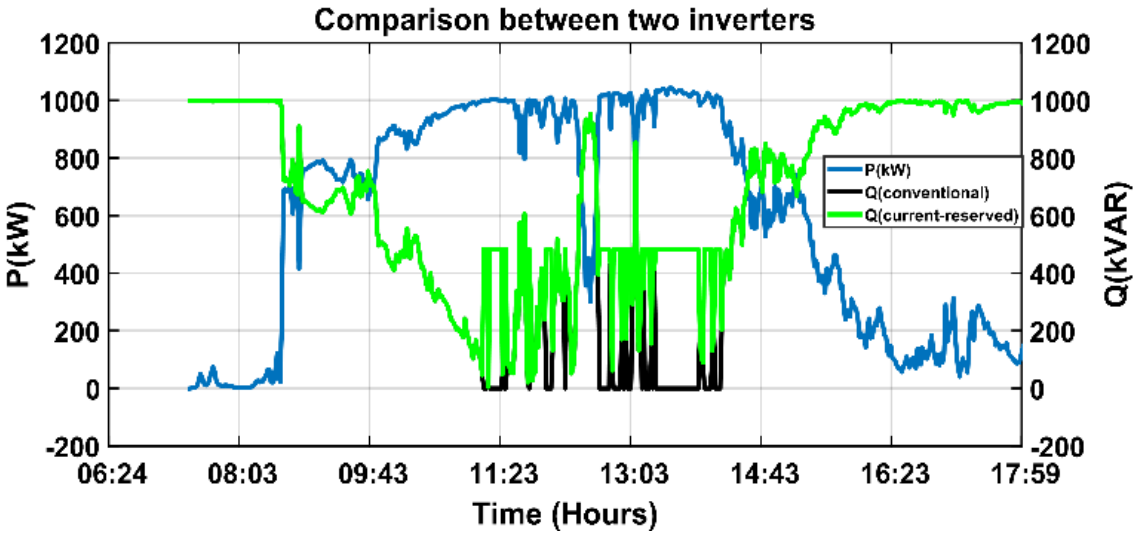

Figure 4-5: Comparison between two inverters' Q- reserve

4.4 Dynamic modelling and control system design

A dynamic model is necessary to fully understand the proposed control strategy. This section investigates control system design for all the configurations. Figure 4-6 shows the detailed converter topologies used in configuration-3.

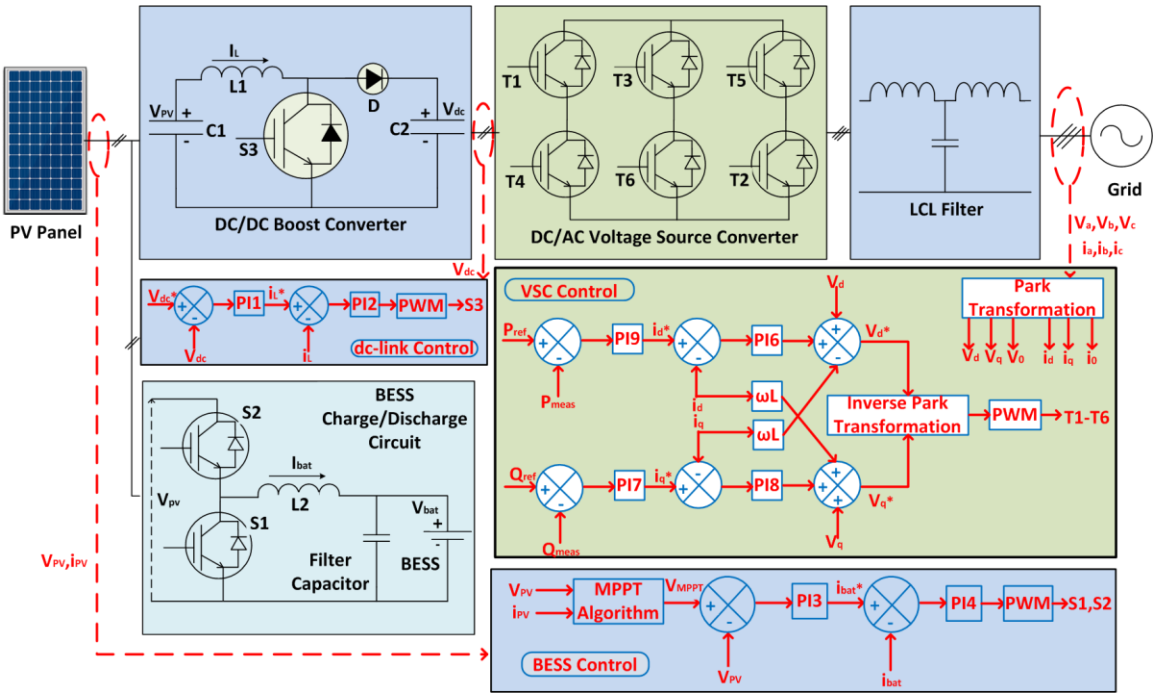

Figure 4-6: Detailed converter topology in configuration-3

The grid voltage and current are measured at the PCC. A Phase Locked Loop (PLL) tracks the voltage angle at the PCC, and thus synchronizes the operation of the inverter with the grid. The Incremental Conductance (IC) algorithm is deployed for MPPT operation. Measured three phase voltages and currents are then converted to voltage and current dq0 quantities respectively using Clark's and Park's transformation. The d-axis component controls the active power and the q-axis component controls the reactive power. Using the instantaneous power theory, per-unit active and reactive power can be computed as in (4.13) and (4.14).

$$P_{meas} = V_d I_d + V_q I_q \tag{4.13}$$

$$Q_{meas} = V_q I_d - V_d I_q \tag{4.14}$$

Here, V_d and I_d are the d-axis components of grid voltage and line current respectively. Similarly, V_q and I_q are the q-axis components of the same.

4.4.1 Boost converter design

As flexibility is the primary focus, the front-end dc/dc boost converter has two different functions as discussed in Table 4-2. For the boost converter, in Figure 4-6, the PWM pulses can be generated by a cascaded controller to trigger the switch S3. For configuration 1 and 2, the purpose of the boost converter is to track the MPPT voltage and control the current across the inductor L1. This is done by the outer voltage and inner current loop controllers. Configuration 3 has the same controller except the outer voltage control loop now fixes the voltage across C1. Eventually the Proportional-Integral (PI) controllers (PI1, PI2) tuned for configuration-1 and 2 can effectively be used for configuration-3 as the inductor current dynamics does not vary too much for the same amount of power as shown in Figure 4-7.

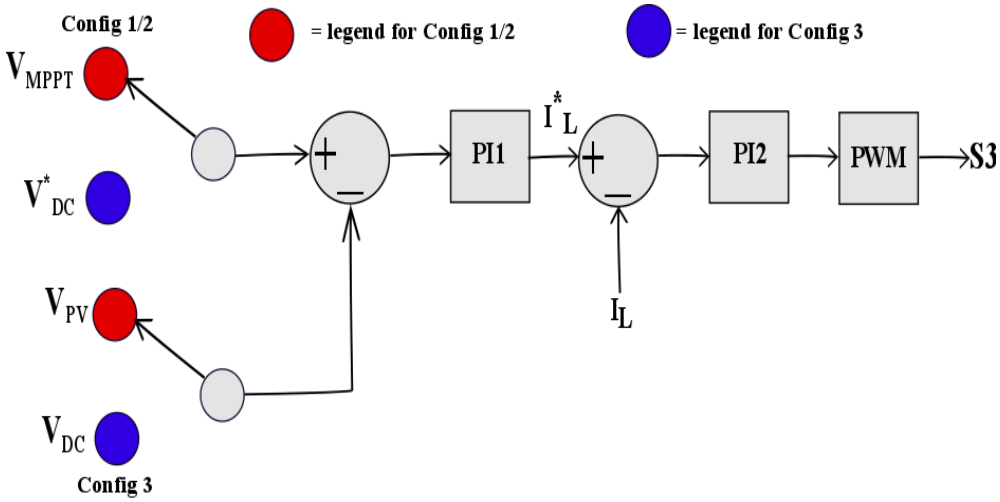

Figure 4-7: Boost converter control

4.4.2 Bi-directional buck-boost converter design

Configuration-1 does not have bi-directional buck-boost converter as this is required only for BESS. Figure 4-8 compares the controllers for the two configurations (without BESS and with BESS at inverter input). For the proposed configuration, MPPT is implemented in this converter. The input voltage is taken from capacitor C1. The same topology is applicable for configuration-2 which requires the input voltage to be taken from capacitor C2 as in Figure 4-2(b). But in configuration-2, this converter is responsible for maintaining the dc-link voltage by charging or discharging the BESS from the inverter input. The goal is to generate the PWM signals for switches S1 and S2. Also, notice that the same references (V_{MPPT} and V^*_{DC}) have been used alternately as in Figure 4-7.

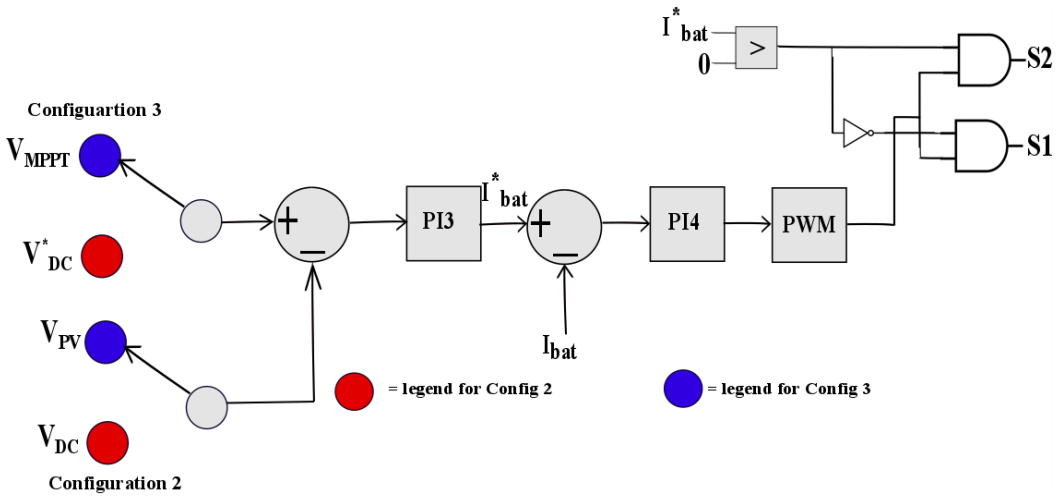

Figure 4-8: Bi-directional buck-boost converter control

4.4.3 VSC controller design

VSC controllers and its PWM generation scheme are shown in Figure 4-9(a) and Figure 4-9(b). Synchronous Reference Frame (SRF) transformation is used to decouple the voltage control. In SRF, the AC quantities is converted to DC and simple PI control can be used for compensation. In dq0 axis, the inverter voltage references can be generated using (4.15) as follows-

$$\begin{bmatrix} V_d^* \\ V_q^* \end{bmatrix} = R \begin{bmatrix} I_d \\ I_q \end{bmatrix} + L \frac{d}{dt} \begin{bmatrix} I_d \\ I_q \end{bmatrix} + \omega L \begin{bmatrix} -I_q \\ I_d \end{bmatrix} + \begin{bmatrix} V_d \\ V_q \end{bmatrix}. \quad (4.15)$$

Here, the first two terms represent the filter dynamics, ωL is the decoupling term and the last term in (4.15) is the feed forward voltage from the grid. Figure 4-9(b) shows the PWM pulse generation scheme for the proposed strategy using (4.15). Configuration-1 regulates the active power based on the dc link voltage reference (V^*_{DC}). It can indirectly control active power by changing the active current inverter processes; to maintain the dc link voltage following reference, set by user.

Based on the availability, reactive power (Q) can be controlled directly and independently. In configuration-2 and configuration-3, P and Q can directly be commanded to follow the reference (P_{ref} and Q_{ref}). To re-circuit these configurations, only one pre-tuned outer loop controller is required, namely, controller PI9 in configuration-2/3 which is different from PI5 in configuration-1 as shown in Figure 4-9(a).

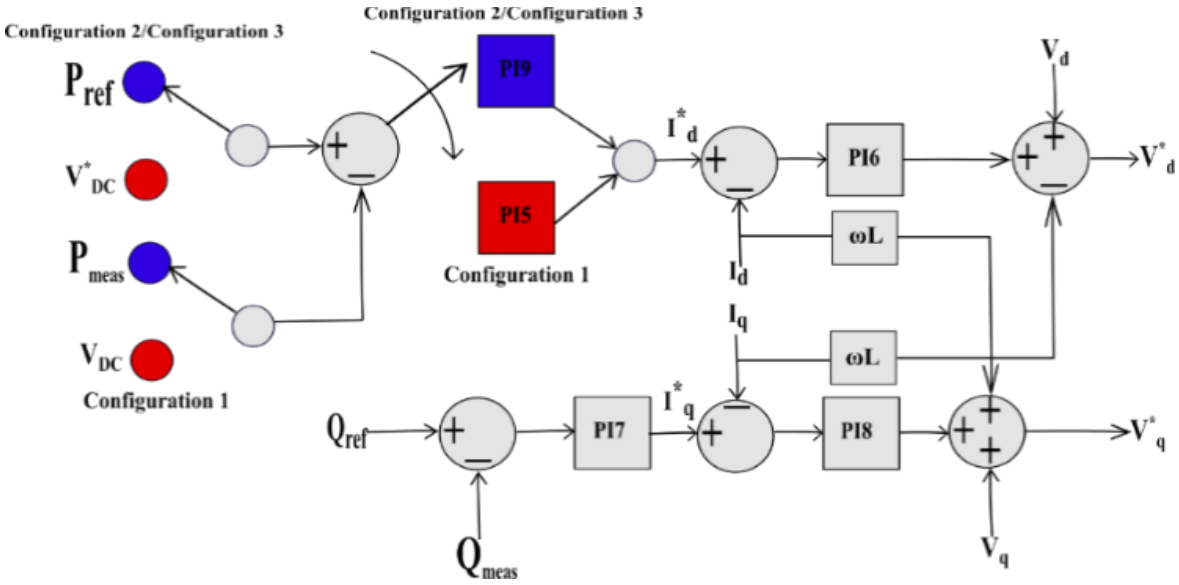

(a) VSC controller

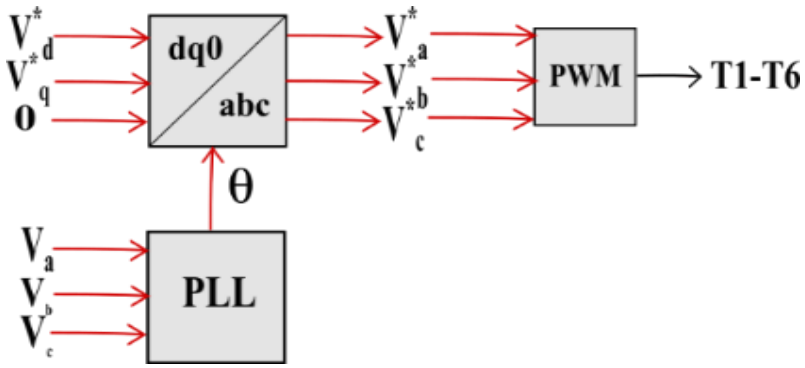

(b) PWM pulse generation for VSC

Figure 4-9: Detailed VSC controller design of configuration-2/3 with transition to configuration-1

4.5 Simulation results and analysis

The proposed control strategy has been tested in a modified IEEE 33 bus test system. It is a 12.66 kV medium voltage network. The total load of the system is 3.7+j2.3 MVA. Three PV generating stations, each rated at 1.11 MVA (P_{max}=1 MW) are connected to three different buses-18, 22 and 33 as shown in Figure 4-10. Please note, all the sites do not have to install solar-storage system to deploy the proposed strategy as discussed later in the section.

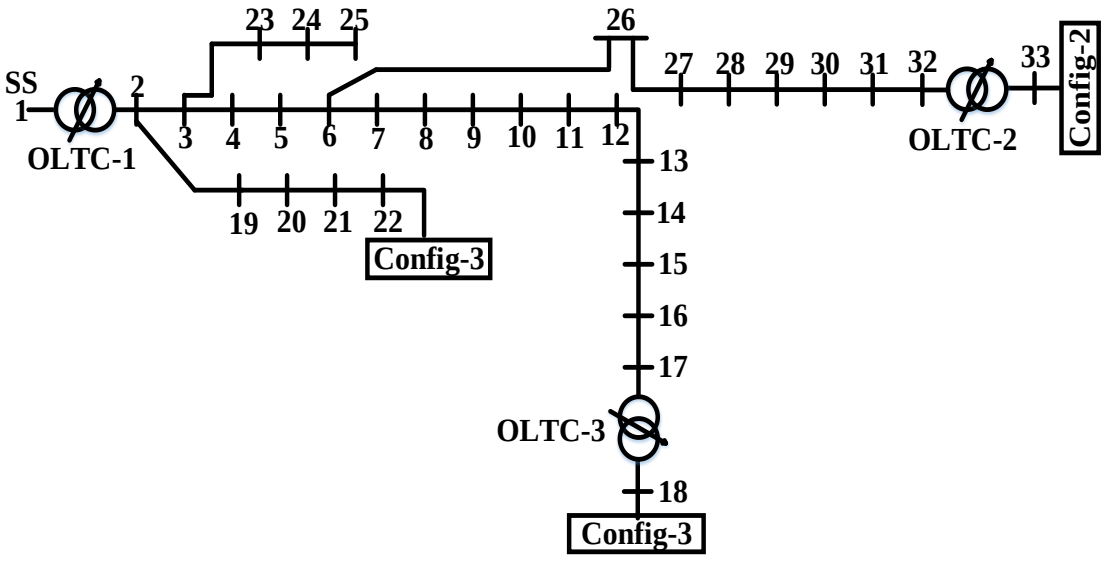

Figure 4-10: Modified IEEE 33 bus test case

These buses are chosen as they are at the EOL and therefore challenge the proposed control strategy the most. Based on different optimization goal, different location for the PV and BESS can be chosen as discussed in [86] which is out of the scope of this thesis. There are also two OLTCs newly installed between buses 32 and 33, and buses 17 and 18. OLTC-1 is already installed at the substation. These are the locations that are located far enough from the substation. Actual solar irradiation data has been used from [49] to simulate different cases. It has been assumed that these inverters, in any voltage violation, respond

first before the OLTC. Solar data is taken at every 1-minute interval. All system parameters are listed in Table 4-3.

Table 4-3: System parameters for PV and BESS

PV panels	Panel: V_{oc}=64.2V, I_{sc}=5.96A Series/parallel modules=15/219
Each inverter	1111kVA, 3-phase, 60Hz
BESS-configuration 2	800V, 1250 Ah, Li-ion
BESS-configuration 3	500V, 2000 Ah, Li-ion
[kp1, ki1]	[0.05,10]
[kp2, ki2]	[0.025,10]
[kp3, ki3]	[0.4,0.1]
[kp4, ki4]	[0.1,0.5]
[kp5, ki5]	[7,800]
[kp6, ki6]	[0.3,20]
[kp7, ki7]	[0.01,25]
[kp8, ki8]	[0.3,20]
[kp9, ki9]	[0.1,250]

4.5.1 Case I: Low PV period with high variability

In a highly variable low PV period, buses 18 and 33 suffer from voltage drop without any reactive power support. This is shown in Figure 4-11(a). Bus-18 and 33 both are at the far end of the network and have weak grid characteristics. This is a typical case for a weak grid condition if the bus is at the far end of the network. Voltage drop despite active power injection from the PV indicates that there is simply not enough reactive power flow in the feeder. Typically, utilities deploy capacitor banks to tackle this issue. Smart inverters can be controlled to work as a capacitive element to support the voltage. Figure 4-11(b) shows the voltage regulation using Q control from the inverter. Also, using an oversized inverter increases the Q reserve which provides additional support to mitigate voltage fluctuation. In this case, only regulating Q is enough to do the job. No active power regulation is needed.

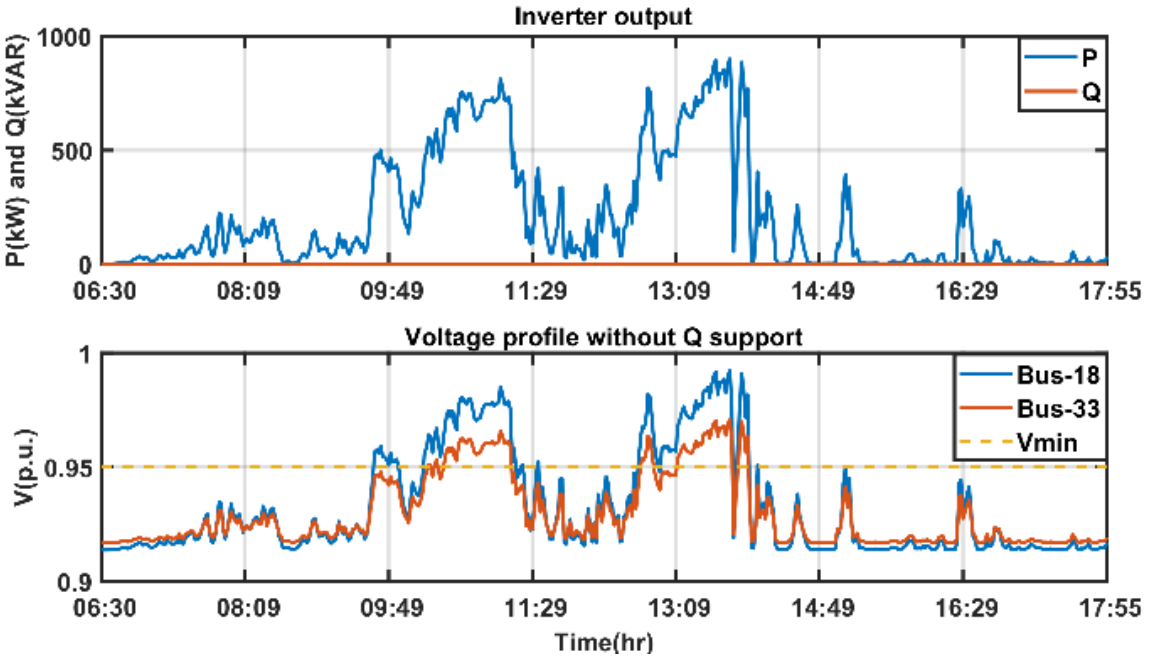

(a) without Q control

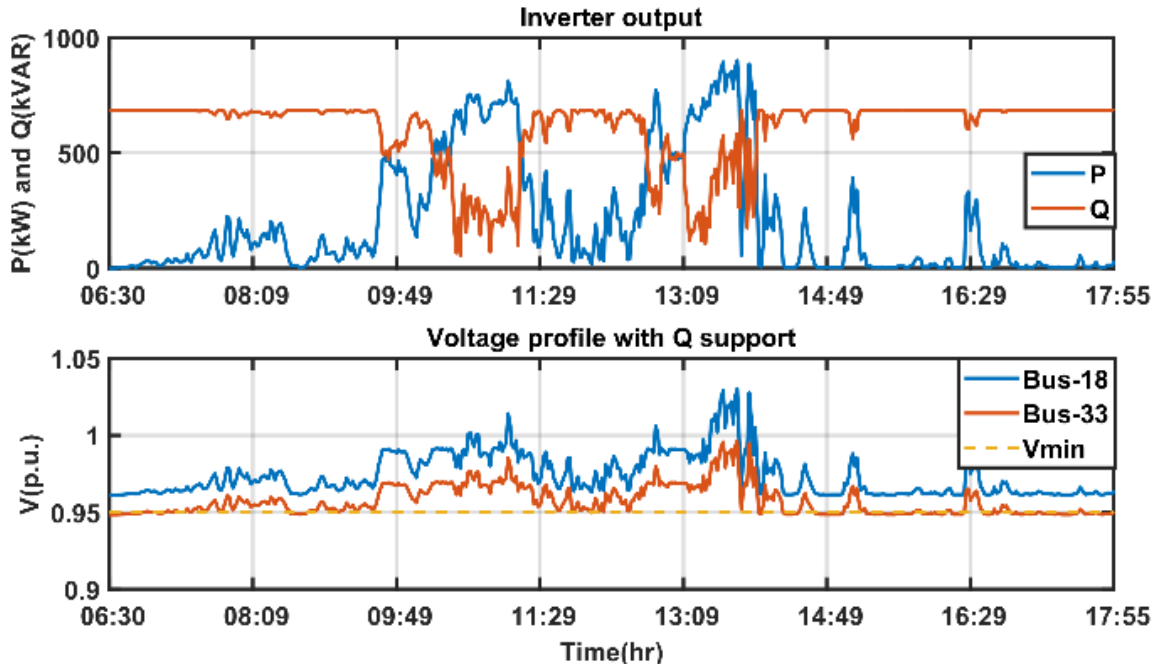

(b) with Q control

Figure 4-11: Voltage control during low PV period with high variability

4.5.2 Case II: High PV period with communication latency

In high PV period, a communication latency of 100ms inside the inverter control signal is considered. At bus 18, configuration-3 is installed. As expected, the injected power increases the voltage. Without activating the active power curtailment, first reactive power control is applied to fix the voltage. Interestingly, voltage remains within the limit for most of the time until there is a drastic reduction in active power production due to passing clouds, as shown in Figure 4-12(a). At this point, due to a 100ms communication latency, Q_{ref} calculated by (4.6) is greater than Q_{RES} of (4.7) which leads the voltage to go below V_{min}. This is a high rate ramp down situation which can be tackled by active power curtailment according to the proposed technique which is shown in Figure 4-12(b). Curtailed power is used to charge the BESS and it solves the voltage issue even for a sudden change is PV production. The voltage remains within the specified limit of 0.95 p.u.-1.05 p.u. during this event as indicated in Figure 4-12(b).

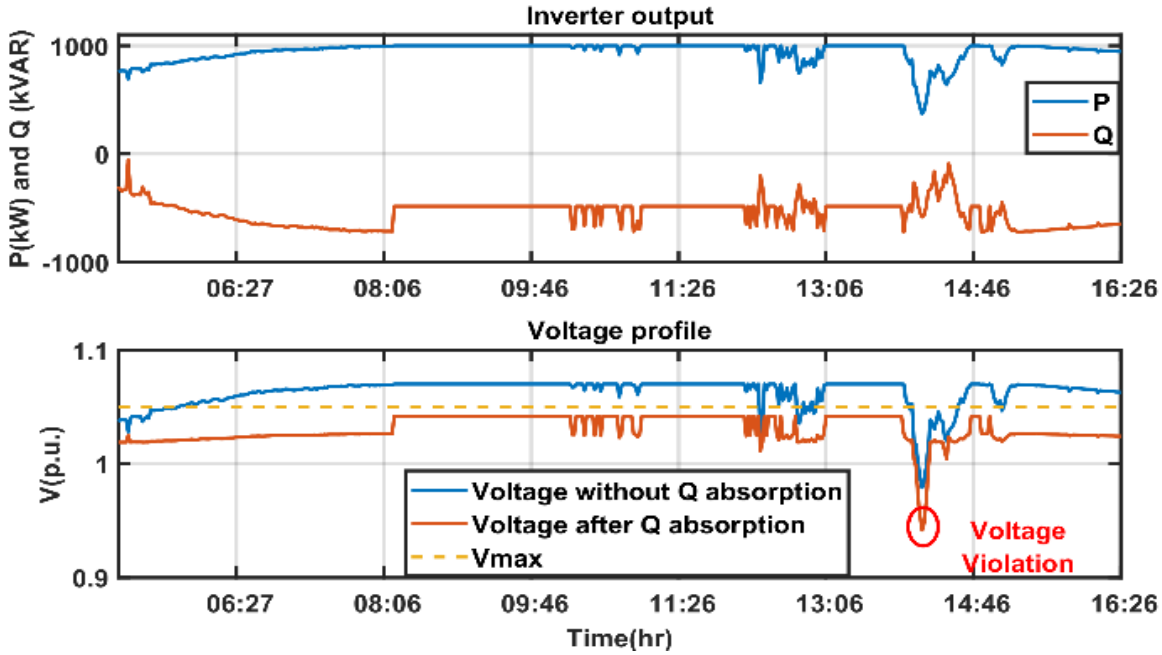

(a) with Q control

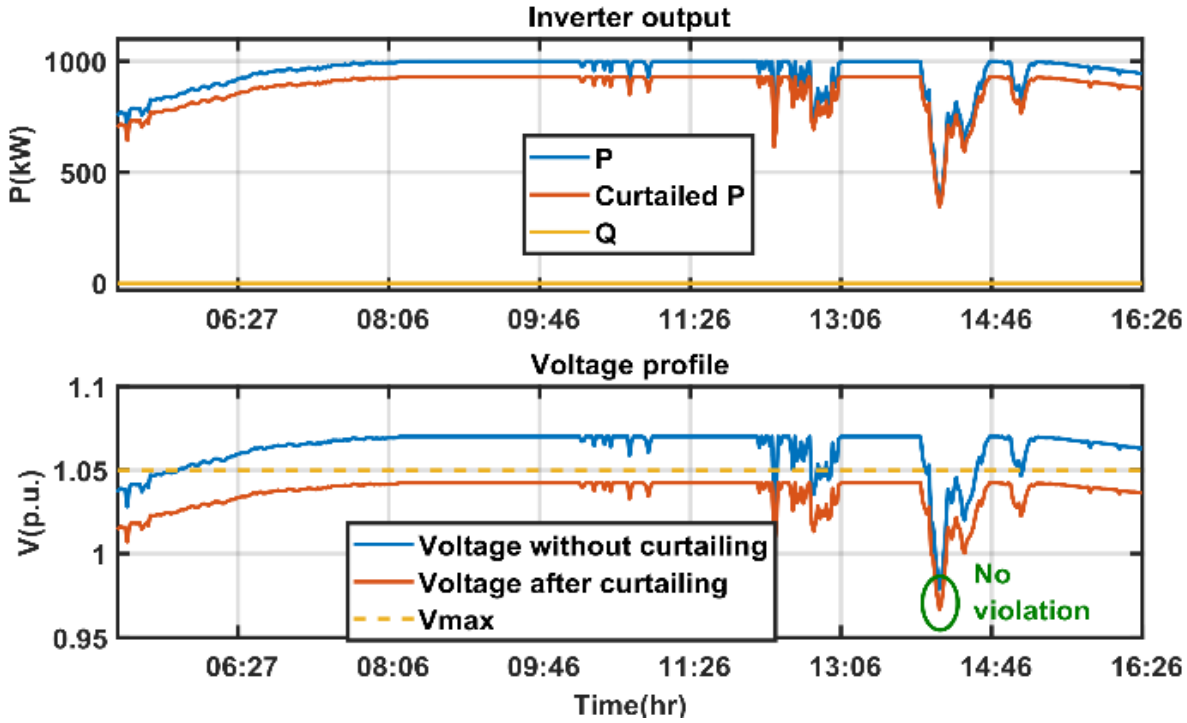

(b) with P curtailment

Figure 4-12: Voltage control during high PV period with communication latency

4.5.3 Case III: Effects of time-varying load

An aggregated time-varying load profile and a PV generation profile is shown in Figure 4-13(a). The voltage profile at bus 22 is shown in Figure 4-13(b). Regulating Q according to (4.6) is found to be not enough to support voltage in case of high peak load occurred in the evening. This can be attributed to the fact that bus-22 is closer to the substation and has a sensitivity index of 2 as calculated by (4.11). The inverter installed here has configuration-3. Therefore, proposed flexible control strategy uses the P regulation from the BESS. This is possible because it is assumed that BESS has enough SOC and therefore supported the evening peak load by injecting 800kW as shown in Figure 4-13(c). As shown in Figure 4-13(b), there is no significant voltage violation observed in this case. In section 4.3.2, it was discussed that the sensitivity change with respect to the loading condition is small. This case provides evidence that the proposed flexible voltage control strategy can be applied to a wide range of load profiles, imposing varying sensitivity index on the system, throughout the day. However, without the support from the BESS, this voltage regulation becomes limited specially in the evening.

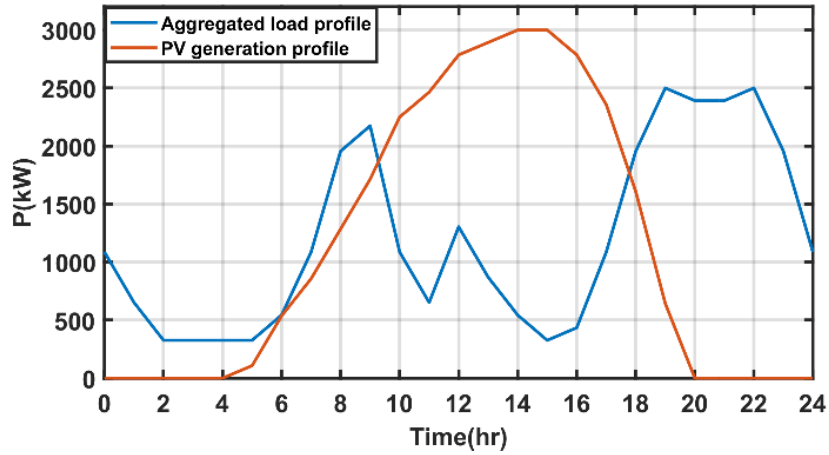

(a) PV generation and time-varying load profile (bus-22)

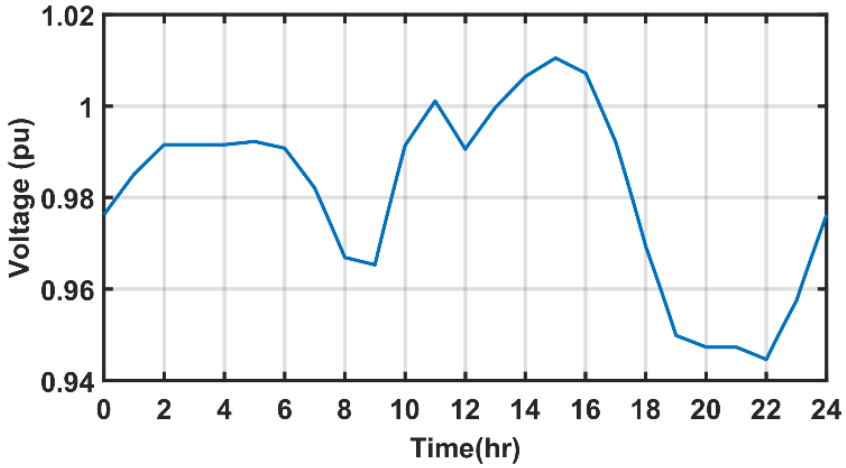

(b) Voltage profile for time-varying load (bus-22)

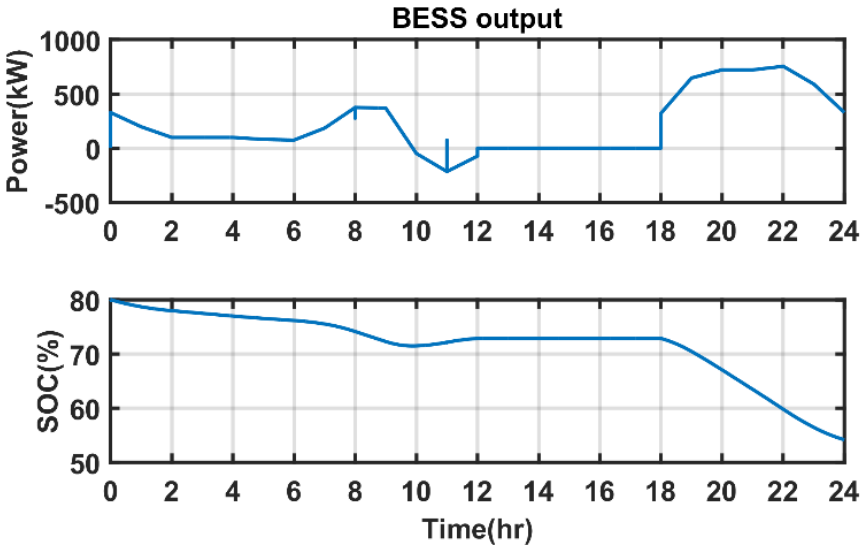

(c) BESS output for time-varying load profile (bus-22)

Figure 4-13: Effect of time varying load

4.5.4 Case IV: Transition from configuration-3 to configuration-1

A dynamic simulation for the proposed reconfigurable strategy at bus 18 is carried out. Figure 4-14 shows a case of transition from configuration-3 to configuration-1.

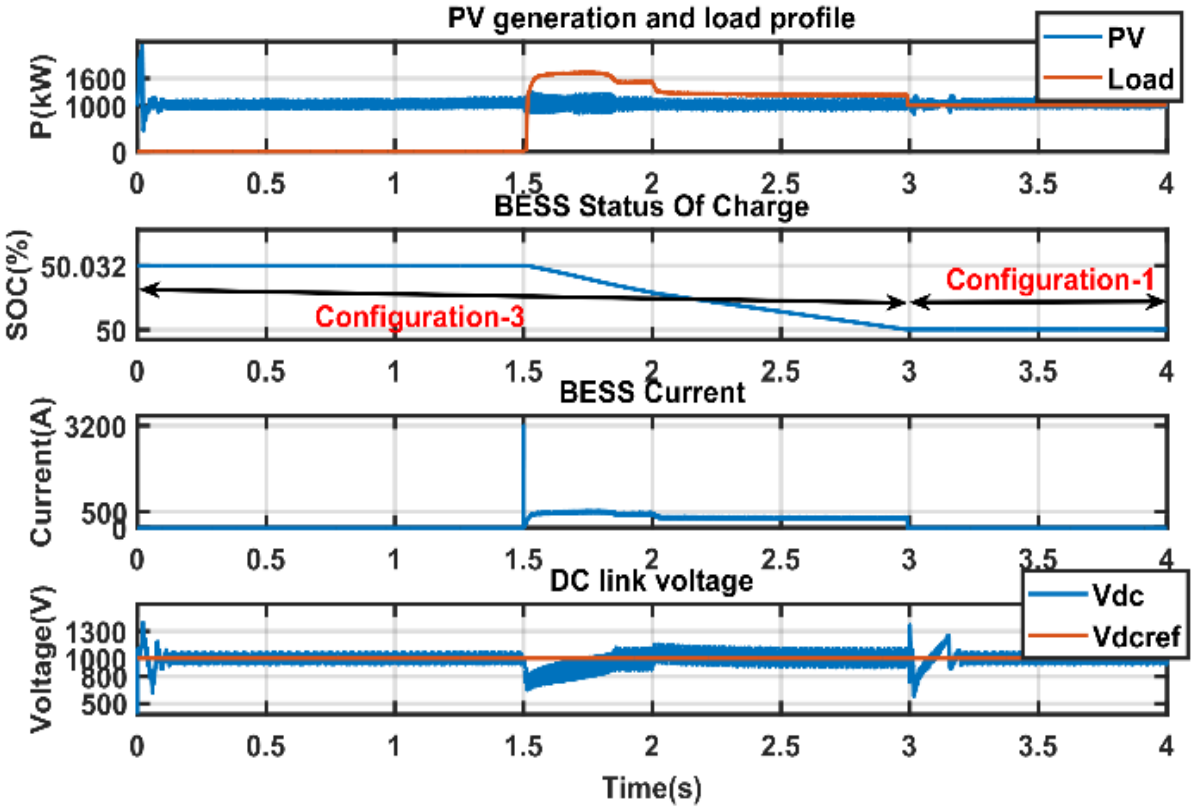

Figure 4-14: Transition from configuration-3 to configuration-1

PV generation is kept constant at 1000 kW while an aggregated variable load profile is considered. Initially, there was no load. At t=1.5s, load increases suddenly which creates a transient surge current of 3.2kA at the DC link. The load becomes 1.6MW almost instantaneously. In practice, this high current is enough to damage the BESS if configuration-2 is considered. Proposed configuration-3, however, avoids this issue as the BESS is now connected to the input of the boost converter. PV generation is not enough to meet this demand. Therefore, the BESS takes care of the remaining 600 kW load. Assume that the initial SOC of the BESS was 50.032% and the lowest operational threshold is at

50%. At t=3s, the BESS hits this limit. So, the discharging current from the BESS becomes zero and the system reconfigures itself to configuration-1. This can be observed by a transient in the dc link voltage at t=3s. After that, the PV continues to inject 1000 kW whereas the grid takes care of the remaining load demand. This transition shows that the BESS can be in standby mode of operation when it crosses its SOC operation limit without interrupting the operation of the PV inverter to compensate the voltage variation. This means a degree of flexibility can be achieved for the system operator.

4.5.5 Case V: OLTC tap changing operation

A comparison between the proposed control strategy with OLTC coordination vs an OLTC-only case is carried out. The performance index to evaluate the result is taken to be the total number of tap changes occurred during a voltage violation. The OLTC parameters are shown in Table 4-4.

Table 4-4: OLTC parameter settings

Parameters	**OLTC**
Reference voltage (p.u.)	1.0
Tap step width (p.u.)	0.625
Dead band (%)	0.625
Target nodes (OLTC-1, 2, 3)	2, 33,18
Time for each tap (s)	60

As shown in Table 4-5, the OLTC-only case suffered frequent voltage violations and higher number of tap operations in all three cases compared to the proposed control strategy with OLTC coordination. In case I, the simulation is carried out for the Q-control with PV-BESS-OLTC arrangement. Tap change count gets reduced eight-folds. A better result is shown for case II where the proposed strategy curtailed the active power to regulate the voltage profile. In a conventional case, it will require 29 tap changing operations to tackle the high ramp up/down rate. As can be seen from the result of solar-storage, no tap

changing operation was required. The reason behind it is that the active power curtailment is comparatively a better strategy for voltage regulation, however, it comes with a cost of reduction in net PV energy yield. BESS gets charged to avoid this loss. This result also shows that the assumption made earlier- inverter is faster compared to OLTC operation (one minute for each step change) and thus, capable of correcting the voltage issue within a few seconds, is justified for this case. In case III, the tap changing operation also reduces which justifies that the calculated sensitivity index in (4.12) for time varying loads works quite well as it does for static loading condition.

Table 4-5: Simulation results for tap changing operation

Case No.	**OLTC-only**	**Proposed strategy with OLTC coordination**
	No of tap changes	No of tap changes
Case I	23	3
Case II	29	0
Case III	14	1

4.5.6 Case VI: Feasibility and limitations of the proposed strategy

The size of battery and capacity of boost converter of configuration 3 tend to become larger than those of configuration 2. For this reason, the initial investment on equipment will increase as well. However, there is a trade-off between the ability to reconfigure and initial investment cost. The strategy proposed in this research is useful at times where BMS needs regular maintenance and/or unexpected outage. The proposed strategy also offers flexibility from the operational point of view as the proposed configuration-3 can still operate without the BESS with a slightly modified feedback control system. For the existing PV systems in the market, it seems unreasonable to utilize the proposed configuration due to the established physical structure. Therefore, transition between configuration-2 and configuration-3 is not feasible and not discussed in this work.

4.6 Conclusion

In this chapter, a reconfigurable solar-BESS topology is introduced and based on this, a flexible voltage control strategy is proposed. The reconfigurable topology is compared with two state-of-the-art topologies used in industry-grade operation today. The flexible control strategy is proposed and studied by taking consideration of BESS and PV inverters' capacity. The contribution of this chapter can be summarized as follows-

(1) A reconfigurable voltage control strategy is proposed for the two-stage utility owned PV and integrated BESS technology. Then, a novel topology is introduced to incorporate a BESS which is safe and easy to reconfigure from an operational standpoint.

(2) As an example of automatic voltage control, a modified IEEE 33 bus test system, with three current-reserved PV and integrated BESS inverters, has been investigated. Both dynamic and steady-state analysis have been carried out. It is worth mentioning that this control strategy and proposed algorithm is applicable to a weak or strong network where high PV penetration is desired.

(3) Voltage control using the proposed algorithm is done by device level controllers. As a result, local voltage control is guaranteed. This combines autonomous control with operational flexibility.

(4) To make automatic active power curtailment, ratio of the nominal voltage to the measured voltage at the PCC is used. As shown, this can mitigate voltage variations in critical ramp up/down operational scenario.

(5) OLTC tap changing operation can be minimized by coordinating it with proposed solar-BESS topology. This reduces the number of total tap changes compared to the case where OLTC is the only voltage regulating device as shown.

CHAPTER 5: DISTRIBUTED DYNAMIC GRID SUPPORT USING SMART PV INVERTERS DURING UNBALANCED GRID FAULTS

5.1 Overview

In this chapter, a dynamic voltage support strategy using smart PV inverters during unbalanced grid faults events is proposed. It uses Karush-Kuhn-Tucker (KKT) condition for finding optimal solutions to calculate the inverter's active and reactive current references. The proposed methodology also takes the X/R ratio into consideration which allows the inverter to differentiate weak or strong grid conditions and adjust its reference currents. Existing Multiple-Complex Coefficient-Filter (MCCF) based Phase Locked Loop (PLL) is used to extract the positive and negative sequence components. The proposed strategy deploys existing Dual Vector Current Control (DVCC) to ensure optimal current injection and Low Voltage Ride Through (LVRT). A distributed ride-through coordination approach among multiple inverters is also proposed based on different optimization goals- either fundamental positive or fundamental negative sequence voltage support. The strategy is simulated, and inverter's transient performance is experimentally verified on a modified IEEE-13 bus test feeder using Controller Hardware-in-the-Loop (C-HIL) approach. Results show substantial evidence that the proposed method can be successfully applied to support the grid during an unbalanced fault event.

5.2 Introduction

In recent years, high penetration of solar photovoltaic (PV) generation is becoming an issue of increasing concern to the bulk electric utility industry. There is a greater call for long-term grid reinforcement to accommodate high levels of PV generations. One of the key challenges is to make the PV power-plants intelligent enough to ride through momentary

voltage sags on the grid side, which is different from the anti-islanding condition [87]. In a low/medium voltage distribution network, unbalanced grid faults are more common compared to balanced three-phase faults. In case of a fault, one of the greatest challenges from the inverter's operational point of view is to remain synchronized with the grid [88], [89]. In other words, during momentary faults, the inverter overcurrent protection must not *trip* or *disconnect* the Voltage Source Inverter (VSI) from the Point of Common Coupling (PCC). According to the IEEE 1547a-2014 standard [21], PV plants are required to ride through the voltage disturbances for a specific period as shown in Table 5-1.

Table 5-1: Voltage ride-through requirement

Voltage range (p.u.)	**Clearing time (s)**
V<0.5	0.16
0.5≤V<0.88	2.00
1.1<V<1.2	1.00
V≥1.2	0.16

A two-stage PV inverter architecture, the most used topology in the industry, is shown in Figure 5-1. In Figure 5-1, the role of the boost converter is to (1) boost up and match the voltage required for the inverter and (2) track the Maximum Power Point (MPP). The three-phase VSI is used for (1) converting DC power to AC power, (2) controlling the active and reactive power flow from PV panel to bulk grid and (3) DC link voltage regulation by controlling active current injection based on the user-defined reference.

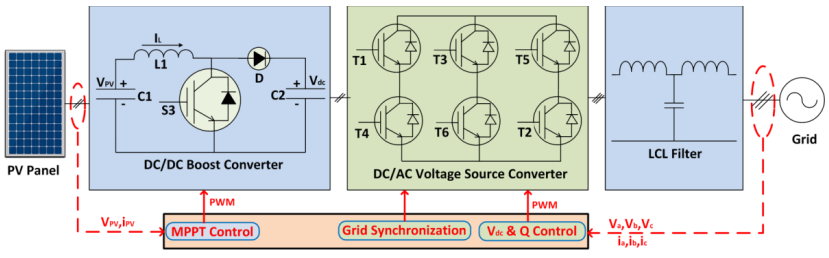

Figure 5-1: Two-stage PV inverter architecture

During day time and full sunshine condition, PV inverters continue to inject active power into the grid and contributes to serve the load. At night, without sunshine, PV inverters remain inactive. According to the current utility practice, if a PV inverter is subjected to PCC voltage disturbance as in Table 5-1, it is required to shut down for several minutes before attempting reconnection to the grid. This is a clear loss from revenue standpoint and can adversely affect the bulk system operation. So, now, recently introduced IEEE 1547a-2018 standard [5] strictly requires the inverter to ride through momentary faults for a certain period.

During abnormal voltage conditions, the inverter is required to inject the lowest short-circuit current possible to protect semiconductor switches inside it. One way to remain connected to the grid, and ride-through the temporary voltage disturbance, is to inject reactive current dynamically which reduces the active power contribution to the faulty location [90]. However, the inverter's DC-link voltage should be maintained nearly constant to accomplish the reactive current injection and react as fast as possible to the disturbance [91]. Therefore, finding the appropriate and optimal active and reactive current reference signals and successful interchange (within a few milli-seconds) between them during a momentary fault (duration<1s) is a challenge. Broadly speaking, typically three types of current control (CC) strategies [92]–[94], can be found in the context of dynamically supporting the grid voltage at times of faults, as shown in Figure 5-2. These are- (i) Vector Current Control (VCC), shown in Figure 5-2(a); (ii) Vector Current Control with Feedforward (VCCF), shown in Figure 5-2(b); and (iii) Dual Vector Current Control (DVCC), shown in Figure 5-2(c). In Figure 5-2, $\{V_a, V_b, V_c\}$ and $\{I_a, I_b, I_c\}$ are the measured grid voltages and currents at the PCC, respectively, V_{dq} and I_{dq} are the dq

components for the same after Park's transformation, θ_{ref} is the grid voltage angle tracked by the PLL for synchronization and (+) / (-) stands for the positive/negative sequences, respectively.

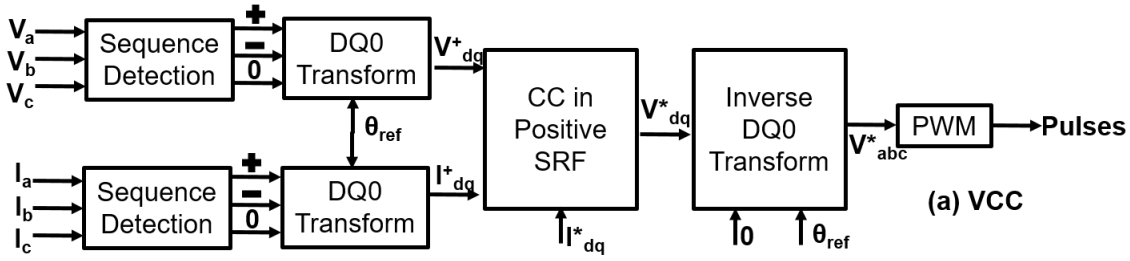

(a) Vector Current Control (VCC)

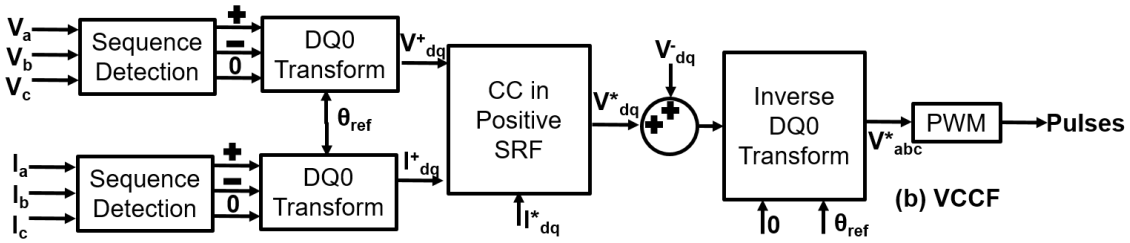

(b) Vector Current Control with Feedforward (VCCF)

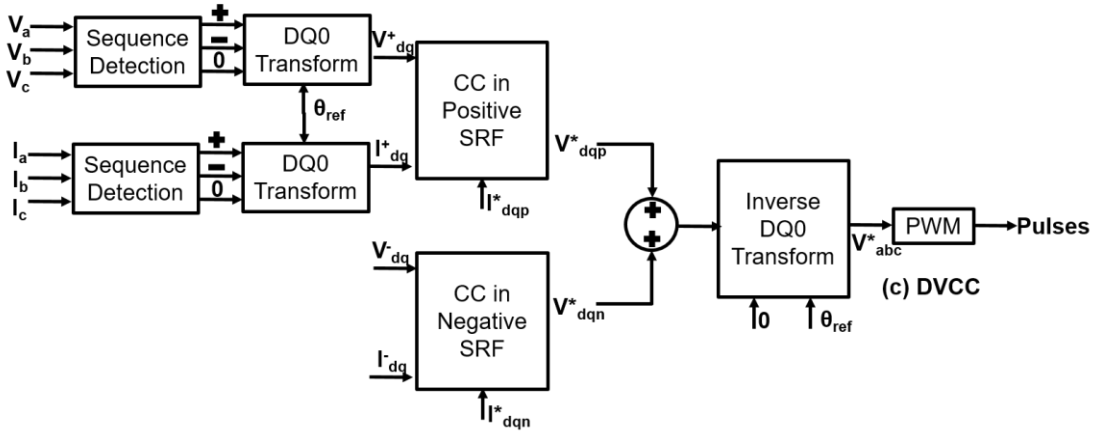

(c) Dual Vector Current Control (DVCC)

Figure 5-2: Different current control schemes of VSI (only the fundamental components have been shown)

As seen, VCC is implemented in the positive Synchronous Reference Frame (SRF), whereas VCCF is similar, but with an added negative sequence grid voltage as a feedforward term. The third controller, DVCC is implemented in both positive and negative SRF, where the objective is to reduce the ripple power of twice the grid frequency. Both stationary and synchronous reference frame implementation have been shown extensively in the literature [95]–[98]. However, inverter's optimal current reference calculation for a specific sequence is often not considered in the existing literature. During a voltage sag, smart inverters are required to support the grid voltage and thus remain connected for a brief period. However, this support depends on the X/R ratio at the PCC. The voltage support by reactive current injection is only applicable for inductive 'weak' grids such as a medium voltage (MV) distribution feeders. For low voltage (LV) distribution networks, the resistive component of the impedance is more dominant than its inductive counterpart. In such a case, dynamic active power management is more applicable [99].

Considering all the above, this chapter first proposes a mathematical formulation to calculate inverter's reference current signal based on- (1) the well-known Karush-Kuhn-Tucker (KKT) conditions to ensure optimality and (2) X/R ratio of the line to support weak and strong grid conditions. Existing MCCF based PLL is used to extract positive and negative sequence components as discussed. The proposed solution uses the existing DVCC approach to support grid voltage by controlling the current injection in positive and negative sequence SRF. This leads to propose the second contribution- a distributed 'ride-through coordination' approach for multiple inverter operation. The coordination approach utilizes one of the two different optimization goals for each inverter-(1) ride-through and

fundamental positive sequence voltage support and (2) ride through and fundamental negative sequence voltage support. To summarize, the key contributions of this work are given below:

1) We propose a dynamic voltage support strategy using smart inverters for a two-stage PV inverter architecture, which can be applied to different feeders with different X/R ratios. We use the Karush–Kuhn–Tucker (KKT) condition at the heart of the proposed approach to calculate and optimize the required active and reactive current references in both positive and negative sequence frames during a fault.

2) We propose a new coordination approach among multiple inverters to ride through the same fault event based on fundamental positive sequence voltage support and fundamental negative sequence voltage support. The approach is distributed in nature and does not need expensive communication structure. The justification for the distributed approach is that generally, with a centralized control scheme, the inverters must send and receive control signals from a centralized server which requires very fast and expensive reliable communication. Given the nature of the short-lived momentary faults, the signal exchange time might exceed the LVRT required time. Therefore, the inverters are assigned to take actions locally i.e. in distributed fashion.

5.3 Proposed control strategy

5.3.1 Measurement signals

During a fault, the three-phase grid voltage vector can be represented as positive, negative and zero sequence components as follows-

$$v_{abc} = \begin{bmatrix} v_a \\ v_b \\ v_c \end{bmatrix} = \sum_{n=1}^{\infty} (v_{abc}^{+n} + v_{abc}^{-n} + v_{abc}^{0n}). \tag{5.1}$$

Where,

$$v_{abc}^{+n} = V^{+n} \begin{bmatrix} \cos(n\omega t + \phi^{+n}) \\ \cos\left(n\omega t - \frac{2\pi}{3} + \phi^{+n}\right) \\ \cos\left(n\omega t + \frac{2\pi}{3} + \phi^{+n}\right) \end{bmatrix}$$

$$v_{abc}^{-n} = V^{-n} \begin{bmatrix} \cos(n\omega t + \phi^{-n}) \\ \cos\left(n\omega t + \frac{2\pi}{3} + \phi^{-n}\right) \\ \cos\left(n\omega t - \frac{2\pi}{3} + \phi^{-n}\right) \end{bmatrix}$$

$$v_{abc}^{0n} = V^{0n} \begin{bmatrix} \cos(n\omega t + \phi^{0n}) \\ \cos(n\omega t + \phi^{0n}) \\ \cos(n\omega t + \phi^{0n}) \end{bmatrix}$$

Similarly, the grid current vector can also be expressed as follows:

$$i_{abc} = \begin{bmatrix} i_a \\ i_b \\ i_c \end{bmatrix} = \sum_{n=1}^{\infty} (i_{abc}^{+n} + i_{abc}^{-n} + i_{abc}^{0n}). \tag{5.2}$$

Where,

$$i_{abc}^{+n} = I^{+n} \begin{bmatrix} \sin(n\omega t + \delta^{+n}) \\ \sin\left(n\omega t - \frac{2\pi}{3} + \delta^{+n}\right) \\ \sin\left(n\omega t + \frac{2\pi}{3} + \delta^{+n}\right) \end{bmatrix}$$

$$i_{abc}^{-n} = I^{-n} \begin{bmatrix} \sin(n\omega t + \delta^{-n}) \\ \sin\left(n\omega t + \frac{2\pi}{3} + \delta^{-n}\right) \\ \sin\left(n\omega t - \frac{2\pi}{3} + \delta^{-n}\right) \end{bmatrix}$$

$$i_{abc}^{0n} = I^{0n} \begin{bmatrix} \sin(n\omega t + \delta^{0n}) \\ \sin(n\omega t + \delta^{0n}) \\ \sin(n\omega t + \delta^{0n}) \end{bmatrix}$$

In (5.1) and (5.2), *n* is the number of harmonics, Φ is the corresponding voltage phase angle and $\boldsymbol{\delta}$ is the current phase angle. Plus (+), minus (-) and zero (0) stands for positive, negative and zero sequence components respectively.

5.3.2 Positive sequence reference frame transformation

The positive sequence components rotate in counter-clockwise direction with +ω angular frequency. Applying a power invariant Clarke's transformation to (5.1) and (5.2), two other expressions in stationary reference frame (αβ0) can be found, each for voltage and current vectors. Notice that the zero-sequence component is omitted considering a three-phase three-wire system.

$$\begin{bmatrix} v_\alpha \\ v_\beta \end{bmatrix} = \begin{bmatrix} \frac{2}{3} & \frac{-1}{3} & \frac{-1}{3} \\ 0 & \frac{1}{\sqrt{3}} & \frac{-1}{\sqrt{3}} \end{bmatrix} \begin{bmatrix} v_a \\ v_b \\ v_c \end{bmatrix} \tag{5.3}$$

$$\begin{bmatrix} i_\alpha \\ i_\beta \end{bmatrix} = \begin{bmatrix} \frac{2}{3} & \frac{-1}{3} & \frac{-1}{3} \\ 0 & \frac{1}{\sqrt{3}} & \frac{-1}{\sqrt{3}} \end{bmatrix} \begin{bmatrix} i_a \\ i_b \\ i_c \end{bmatrix} \tag{5.4}$$

The transformations of grid voltages and currents in the SRF are found using Park's transformation on (5.3) and (5.4).

$$\begin{bmatrix} v_d^+ \\ v_q^+ \end{bmatrix} = \begin{bmatrix} \cos(\omega t) & \sin(\omega t) \\ -\sin(\omega t) & \cos(\omega t) \end{bmatrix} \begin{bmatrix} v_\alpha \\ v_\beta \end{bmatrix} \tag{5.5}$$

$$\begin{bmatrix} i_d^+ \\ i_q^+ \end{bmatrix} = \begin{bmatrix} \cos(\omega t) & \sin(\omega t) \\ -\sin(\omega t) & \cos(\omega t) \end{bmatrix} \begin{bmatrix} i_\alpha \\ i_\beta \end{bmatrix} \tag{5.6}$$

It is to be noted that (5.5) and (5.6) can be further denoted as V^+_{dq} and I^+_{dq} for positive sequence components.

5.3.3 Negative sequence reference frame transformation

The negative sequence components rotate in clockwise direction with -ω angular frequency. Applying transposed Park's transformation to (5.3) and (5.4), two other expressions in SRF can be found, each for voltage and current vectors.

$$\begin{bmatrix} v_d^- \\ v_q^- \end{bmatrix} = \begin{bmatrix} \cos(\omega t) & -\sin(\omega t) \\ \sin(\omega t) & \cos(\omega t) \end{bmatrix} \begin{bmatrix} v_\alpha \\ v_\beta \end{bmatrix} \tag{5.7}$$

$$\begin{bmatrix} i_d^- \\ i_q^- \end{bmatrix} = \begin{bmatrix} \cos(\omega t) & -\sin(\omega t) \\ \sin(\omega t) & \cos(\omega t) \end{bmatrix} \begin{bmatrix} i_\alpha \\ i_\beta \end{bmatrix} \tag{5.8}$$

Note that (5.7) and (5.8) can be further denoted as V^-_{dq} and I^-_{dq} for negative sequence components.

5.3.4 Reference current calculation

Based on the instantaneous power theory, the output power of an inverter can be expressed as (5.9), where the asterisk (*) stands for complex conjugate.

$$S_{out} = \frac{3}{2} v_{\alpha\beta} i^*_{\alpha\beta} \tag{5.9}$$

The output power can be expressed in the SRF as in (5.10).

$$S_{out} = \frac{3}{2}(e^{jwt} v^+_{dq} + e^{-jwt} v^-_{dq})(e^{jwt} i^+_{dq} + e^{-jwt} i^-_{dq}) \tag{5.10}$$

Equation (5.10) can be further expressed as (5.11) after some algebraic manipulation. Note that, capital case notations denote power amplitudes.

$$\begin{aligned} S_{out} = {} & P_{out} + P_{oc1}\cos(2\omega t) + P_{oc2}\sin(2\omega t) \\ & + j(Q_{out} + Q_{oc1}\cos(2\omega t) + Q_{oc2}\sin(2\omega t)) \end{aligned} \tag{5.11}$$

Equation (5.11) contains four 2ω terms where ω is the angular frequency of the grid. Two

of them are associated with the active power (P) and the other two with the reactive power (Q). Using (5.5)-(5.8), it is possible to extract sequence components from (5.11), which is shown in (5.12) in matrix form.

$$\begin{bmatrix} P_{out} \\ Q_{out} \\ P_{oc1} \\ Q_{oc1} \\ P_{oc2} \\ Q_{oc2} \end{bmatrix} = \frac{3}{2} \begin{bmatrix} v_d^+ & v_q^+ & v_d^- & v_q^- \\ v_q^+ & -v_d^+ & v_q^- & -v_d^- \\ v_d^- & v_q^- & v_d^+ & v_q^+ \\ v_q^- & -v_d^- & v_q^+ & -v_d^+ \\ v_q^- & -v_d^- & -v_q^+ & v_d^+ \\ -v_d^- & -v_q^- & v_d^+ & v_q^+ \end{bmatrix} \begin{bmatrix} i_d^+ \\ i_q^+ \\ i_d^- \\ i_q^- \end{bmatrix} \tag{5.12}$$

From (5.12), four equations can be picked and solved for i_d^+, i_q^+, i_d^- and i_q^- as shown in (5.13)-(5.16) where P_{ref} is the desired power to be processed by the VSI. Given the P_{ref} and Q_{ref} values, solving (5.13)-(5.16) provides the current reference (I^*_{dq}) for both the positive and negative sequence reference frames.

$$P_{ref} = P_{out} = \frac{3}{2}(v_d^+ i_d^+ + v_q^+ i_q^+ + v_d^- i_d^- + v_q^- i_q^-) \tag{5.13}$$

$$Q_{ref} = Q_{out} = \frac{3}{2}(v_q^+ i_d^+ - v_d^+ i_q^+ + v_q^- i_d^- - v_d^- i_q^-) \tag{5.14}$$

$$P_{oc1} = \frac{3}{2}(v_d^- i_d^+ + v_q^- i_q^+ + v_d^+ i_d^- + v_q^+ i_q^-) \tag{5.15}$$

$$P_{oc2} = \frac{3}{2}(v_q^- i_d^+ - v_d^- i_q^+ - v_q^+ i_d^- + v_d^+ i_q^-) \tag{5.16}$$

For example, in normal condition, unity power factor operation will have $Q_{ref} = 0$. The oscillating terms in (5.15) and (5.16) can also be set to zero and solve for four current references. This ensures the DC link voltage to be constant and free of 2ω oscillations. There are two important points to note here [45]- (a) if just the injection of active power into the network is considered by (5.13), keeping the reactive power set-point to zero in (5.14), then the active power 2ω oscillations get cancelled in (5.15) and (5.16). This is since the oscillating component in the active power, depends on the reactive current

components i_q^+ and i_q^-. Similarly, reactive power oscillations (Q_{oc1}, Q_{oc2}) are nullified when the active power set-point is set to zero and (b) injection of any positive sequence creates an 2ω oscillation in the negative sequence reference frame and vice versa. This oscillation is cancelled by using a notch filter tuned at 2ω frequency in this work.

However, in an unbalanced voltage condition during a grid fault, the quantity P_{ref} in (5.13) should be minimized (as close to zero) to save the revenue generated by the solar power generators, whereas, for ride-through and dynamic grid support, the quantity Q_{ref} in (5.14) should be set to a value other than zero. The goal is to set the Q_{ref}–a function of i_q^+, i_q^-, in such a way that guarantees LVRT and no overcurrent tripping of the inverter. In this chapter, an optimal control strategy is proposed to find these current references using KKT conditions.

5.3.5 Solution strategy

A simple two bus test system is shown in Figure 5-3 to develop the proposed control strategy. The grid is modeled as an equivalent voltage source and is assumed to be under an unbalanced fault at bus 1. A PV inverter is connected to the PCC which injects both positive (I^+) and negative (I^-) sequence currents. DC link voltage is assumed to be constant inside the inverter.

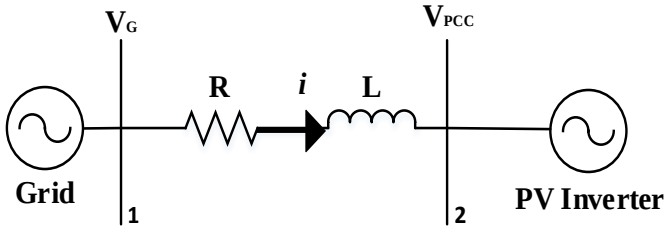

Figure 5-3: A simple illustrative two bus power system

From Figure 5-3, the following relationship between the grid voltage and the PCC voltage is derived-

$$v_{PCC} = v_G - Ri - L\frac{di}{dt}. \tag{5.17}$$

In the phasor domain, (5.17) can be expressed as-

$$V_{PCC} = V_G - RI - \omega LI. \tag{5.18}$$

Using positive and negative sequence information, (5.18) can be further expanded to (5.19) and (5.20) as follows-

$$V_{PCC}^{+} = V_G^{+} - RI^{+} - \omega LI^{+} \tag{5.19}$$

$$V_{PCC}^{-} = V_G^{-} - RI^{-} - \omega LI^{-} \tag{5.20}$$

The positive and negative sequence components can further be analyzed using (5.21)-(5.26).

$$I^{+} = \sqrt{I_d^{+2} + I_q^{+2}} \tag{5.21}$$

$$I^{-} = \sqrt{I_d^{-2} + I_q^{-2}} \tag{5.22}$$

$$V_G^{+} = \sqrt{V_{Gd}^{+\,2} + V_{Gq}^{+\,2}} \tag{5.23}$$

$$V_G^{-} = \sqrt{V_{Gd}^{-\,2} + V_{Gq}^{-\,2}} \tag{5.24}$$

$$V_{PCC}^{+} = \sqrt{V_{PCCd}^{+\,2} + V_{PCCq}^{+\,2}} \tag{5.25}$$

$$V_{PCC}^{-} = \sqrt{V_{PCCd}^{-\,2} + V_{PCCq}^{-\,2}} \tag{5.26}$$

Using (5.21)-(5.26) along with power magnitude calculation for each sequence

components from (5.13)-(5.14) leads to (5.27) and (5.28) after some algebraic manipulation-

$$V_{PCC}^{+} = RI_d^{+} + \omega LI_q^{+} + \sqrt{V_G^{+} + RI_q^{+} - \omega LI_d^{+}}\sqrt{V_G^{+} - RI_q^{+} + \omega LI_d^{+}} \tag{5.27}$$

$$V_{PCC}^{-} = RI_d^{-} + \omega LI_q^{-} + \sqrt{V_G^{-} + RI_q^{-} - \omega LI_d^{-}}\sqrt{V_G^{-} - RI_q^{-} + \omega LI_d^{-}} \tag{5.28}$$

To satisfy the condition of no overcurrent tripping, the phase currents,I_a, I_b, and, I_c of the inverter can be set as follows-

$$I_{max} = \sqrt{I^{+2} + I^{-2}} = \max(I_{a(peak)}, I_{b(peak)}, I_{c(peak)}) \tag{5.29}$$

Using (5.29) is a necessary condition to implement the proposed control strategy but is not a sufficient one i.e. it does not guarantee that the inverter will not trip due to over-current protection threshold which is not considered in [98]. Therefore, an inequality constraint is added as follows-

$$I_{max} \leq \mathrm{I_{oc}}. \tag{5.30}$$

Where, $\mathrm{I_{oc}}$ is the overcurrent protection threshold up to which the inverter switches sustain. Considering (5.19)-(5.30), two optimization problems are formulated as follows-

Optimization problem 1:

$$\textit{Maximize} \qquad f(x,y) = V_{PCC}^{+}$$

$$\textit{Subject to} \qquad I_{max} = \sqrt{I_d^{+2} + I_q^{+2}} \text{ and } I_{max} \leq \mathrm{I_{oc}}$$

Optimization problem 2:

$$\textit{Maximize} \qquad f(x,y) = -V_{PCC}^{-}$$

$$\textit{Subject to} \qquad I_{max} = \sqrt{I_d^{-2} + I_q^{-2}} \text{ and } I_{max} \leq \mathrm{I_{oc}}$$

The solution of optimization problem 1 can be obtained using KKT conditions as follows-

$$\mathcal{L}(x, y, \lambda, \mu) = f(x, y) - \mu g(x, y) - \lambda h(x, y) \tag{5.31}$$

Where,

$$\lambda, \mu = Lagrange\ multplier$$

$$h(x, y) = \sqrt{I_d^{+2} + I_q^{+2}} - I_{max} = 0 \tag{5.32}$$

$$g(x, y) = I_{max} - I_{oc} \leq 0 \tag{5.33}$$

As the formulation is done, the following KKT conditions can now be applied to find the optimal solution. Note that, (5.37)-(5.38) is same as (5.32)-(5.33). If (5.34)-(5.35) and (5.38) are solved, then only sub-gradient optimality conditions are met which are necessary but not sufficient. If (5.36) and (5.39) are solved with previous equations, then it provides necessary and sufficient conditions to find the optimal solution.

$$\nabla\mathcal{L}(x, y, \lambda, \mu) = 0 \tag{5.34}$$
$$\mu \geq 0 \tag{5.35}$$
$$\mu g(x, y) = 0 \tag{5.36}$$
$$h(x, y) = 0 \tag{5.37}$$
$$g(x, y) \leq 0 \tag{5.38}$$
$$\nabla^2\mathcal{L}(x, y, \lambda, \mu)\ is\ positive\ definite \tag{5.39}$$

Solving (5.34) – (5.39) provides the optimal solution-

$$(I_d^+)^* = I_{max} \frac{R}{\sqrt{R^2 + (\omega L)^2}} \tag{5.40}$$

$$(I_q^+)^* = I_{max} \frac{\omega L}{\sqrt{R^2 + (\omega L)^2}} \tag{5.41}$$

Similarly, for optimization problem 2, the optimal solution is-

$$(I_d^-)^* = -I_{max} \frac{R}{\sqrt{R^2 + (\omega L)^2}} \tag{5.42}$$
$$(I_q^-)^* = -I_{max} \frac{\omega L}{\sqrt{R^2 + (\omega L)^2}} \tag{5.43}$$

There are infinite combinations possible to set the current references during an unbalanced condition, as found in (5.40)-(5.43). For example, for an inductive grid, setting R=0 in (5.40)- (5.43) in conjunction with (5.21) and (5.22) produces the following set of references in per unit-

$$(I_d^+)^* = 0, (I_q^+)^* = 1, (I_d^-)^* = 0 \; and \; (I_q^-)^* = 0 \tag{5.44}$$

Similarly, for a resistive grid, the following set of references can be calculated in per unit-

$$(I_d^+)^* = 1, (I_q^+)^* = 0, (I_d^-)^* = 0 \; and \; (I_q^-)^* = 0 \tag{5.45}$$

Other solutions provide sub-optimal solutions that does not take X/R ratio into account and can be calculated from the inverter rating as in (5.46).

$$Q_{ref} = \sqrt{S_{rated}^2 - P_{ref}^2} \tag{5.46}$$

5.3.6 Sequence extraction

When a voltage sag occurs due to an unbalanced grid fault, the voltage and current can be decomposed into positive, negative and zero sequence components. To extract these components, the PLL design demands modification which is extensively discussed in the literature [60], [100]–[105]. In 2011, Guo *et al.* presented a MCCF based PLL which structure is used for synchronization and sequence detection purposes in this study. For a detailed discussion about the robustness and performance of this PLL see [61] and the references therein.

5.3.7 Current controller

As both the positive and negative sequence current are injected to support the grid dynamically, the DVCC method [94] is used for implementing the current control. This is shown in Figure 5-4. The power references are transformed to equivalent positive and negative sequence components. For positive and negative d-axis and q-axis components, a total of four PI controllers are used to regulate the current. Finally, inverse dq0 transformation is used to generate the inverter's PWM pulses.

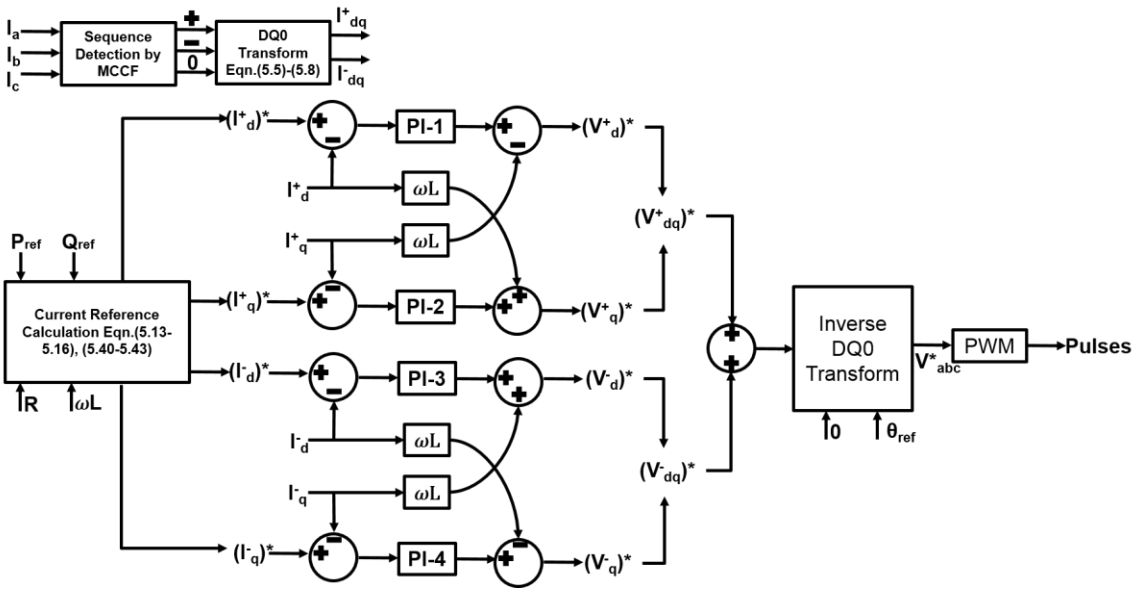

Figure 5-4: Current controller for the proposed strategy

5.3.8 Online impedance estimation

The optimal solution uses the impedance information to set the current references in (5.40)-(5.43). In this work, grid impedance is set using predefined look-up tables of the known positive sequence impedance values. For a robust method to estimate it online, see [106] and the references therein. There are other methods such as in [107] that provide the same estimation.

5.4 Distributed ride-through coordination among multiple inverters

Consider a modified IEEE-13 bus test feeder to demonstrate the dynamic grid support when multiple inverters are connected as shown in Figure 5-5.

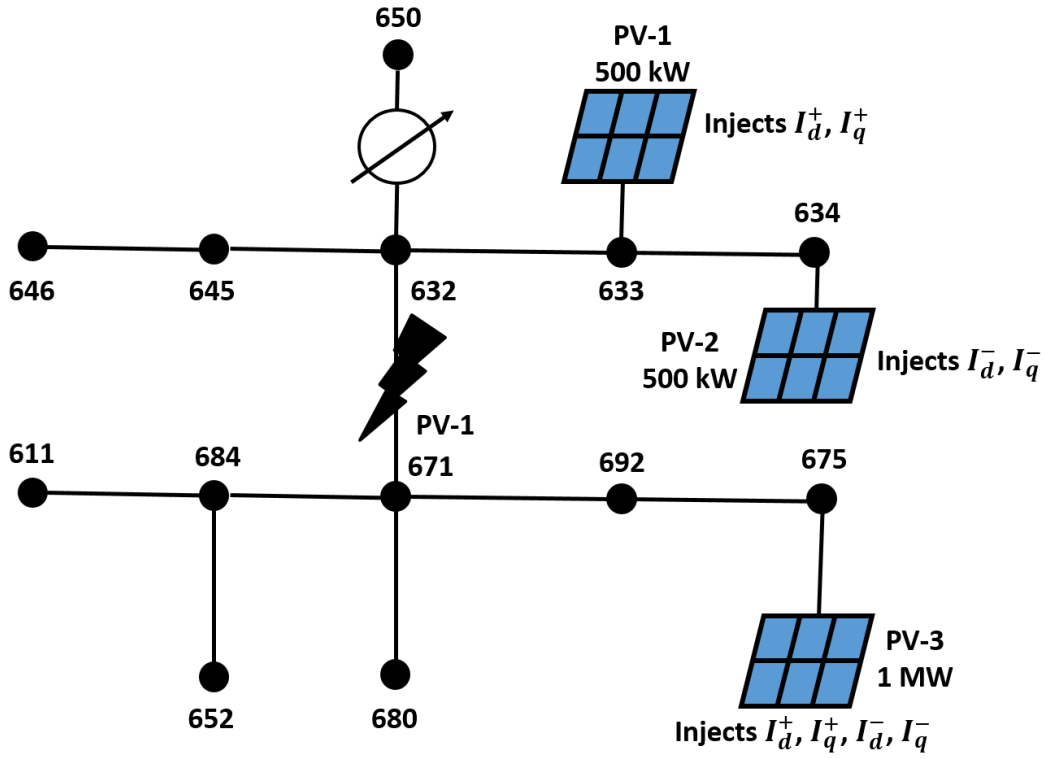

Figure 5-5: Modified IEEE-13 bus test system

The IEEE-13 bus test system is an unbalanced MV distribution network with a total load of 3.46+j1.4 MVA. An unbalanced, phase A to ground fault occurs between bus 632 and 671. This creates a voltage sag condition in the upstream and downstream buses. Two solar generators (PV-1 & PV-2) each rated at 500kW are installed at buses 633 and 634. Another 1 MW PV inverter is installed at bus 675 (PV-3). The goal of these three inverters during this fault is to ride through the event and support the voltage by injecting reactive currents

only. As the test system in Figure 5-5 is mainly inductive in nature, it is assumed that injecting reactive currents only should be enough.

Notice that there are four degrees of freedom in terms of four sequence current components in d and q axes. If PV-1 inverter is chosen to carry out the optimization problem 1 i.e. to support the fundamental positive sequence voltage, then it simultaneously ride-through the fault and injects the maximum reactive current into the fault using i_d^+ and i_q^+ components calculated by (5.40)-(5.41). Alternatively, it could be chosen to ride-through and support the fundamental negative sequence voltage by minimizing it with the reactive current injection using (5.42)-(5.43). Other inverters can also choose the same. There are three inverters shown in Figure 5-5. Therefore, total 6 combinations are possible to ride-through the same fault between bus 632 and 671. For *n*-number of inverters, there will be 2*n* possible ways of riding through the fault event. If an inverter pair is selected to be coordinated by utilizing both the optimization problem 1 and 2, then there will be $\frac{n}{2}$ and $\frac{n+1}{2}$ ways to ride through the same fault event with even and odd number of inverters in the system, respectively. In this case, a peer-to-peer connection is needed to exchange control signals between the inverter pairs. Using this proposed coordination scheme, both PV-1 and 2 will not only be compliant with LVRT requirement but will also support the grid voltage by injecting the maximum current to the faulted point with no oscillations and no tripping of the overcurrent protection scheme. A stand-alone operation scheme is shown where PV-3 is connected to bus 675, can inject all the sequence current components. As the inverter is injecting both the positive and negative sequence current components simultaneously, there will always be an optimal solution which can be changed using

current references derived from (5.46) in conjunction with (5.21) and (5.22) to drive the inverter.

5.5 Simulation results and analysis

The proposed strategy is modelled and simulated in the test system, shown in Figure 5-5, to validate its performance during an unbalanced grid fault. MATLAB-SIMULINK is used as a simulation platform. Five cases are shown in total.

5.5.1 Case I: Transient performance test of MCCF based PLL

As the sequence extraction and synchronization technique needs to be quite fast to validate the claims, first the transient performance of the MCCF based PLL [61] is tested with a phase A to ground fault of 200ms duration. This short duration is chosen intentionally to check the transient and steady-state performance of the designed controllers.

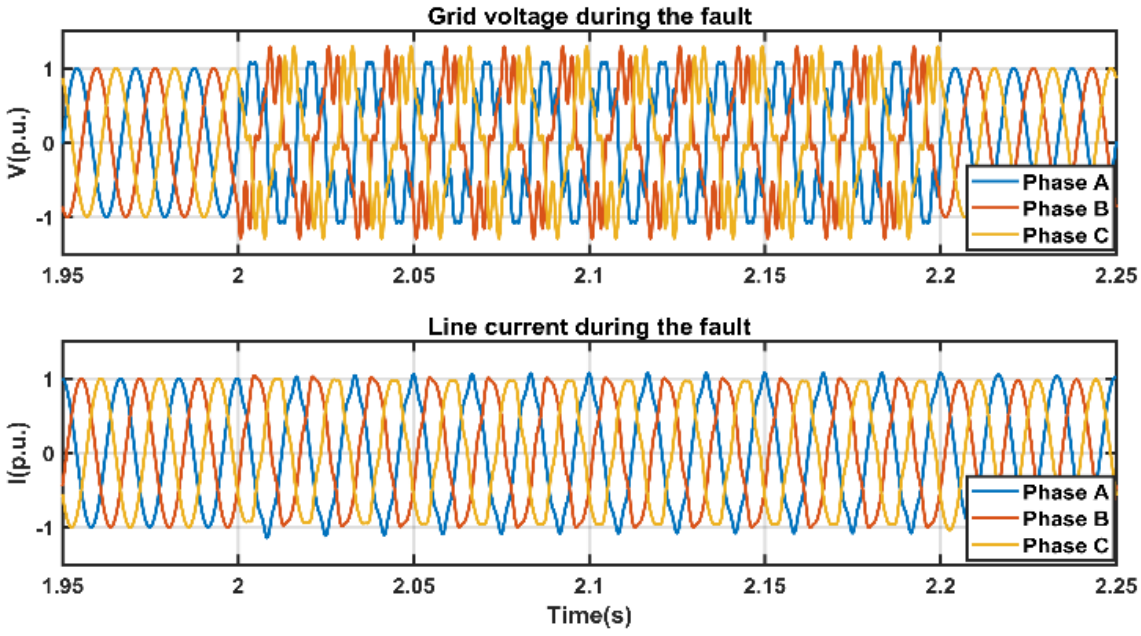

Figure 5-6: Testing voltage and line current for the MCCF based PLL

In Figure 5-6, fault starts at t=2s and during the grid fault, to test it more rigorously for distorted grid voltage, controlled positive sequence 5th and controlled negative sequence 7th harmonics are applied as shown. As can be seen from Figure 5-7, MCCF-PLL identifies the disturbance within 5ms and tracks the harmonic sequence and magnitude with a settling time of 30ms. For a short-lived momentary fault, this timing is quite good and therefore, MCCF-PLL can safely be applied to test the control strategy. Also note, it reveals that the controlled 5th and 7th harmonics have a 0.25 and 0.20 per unit magnitude, respectively, as seen from Figure 5-7.

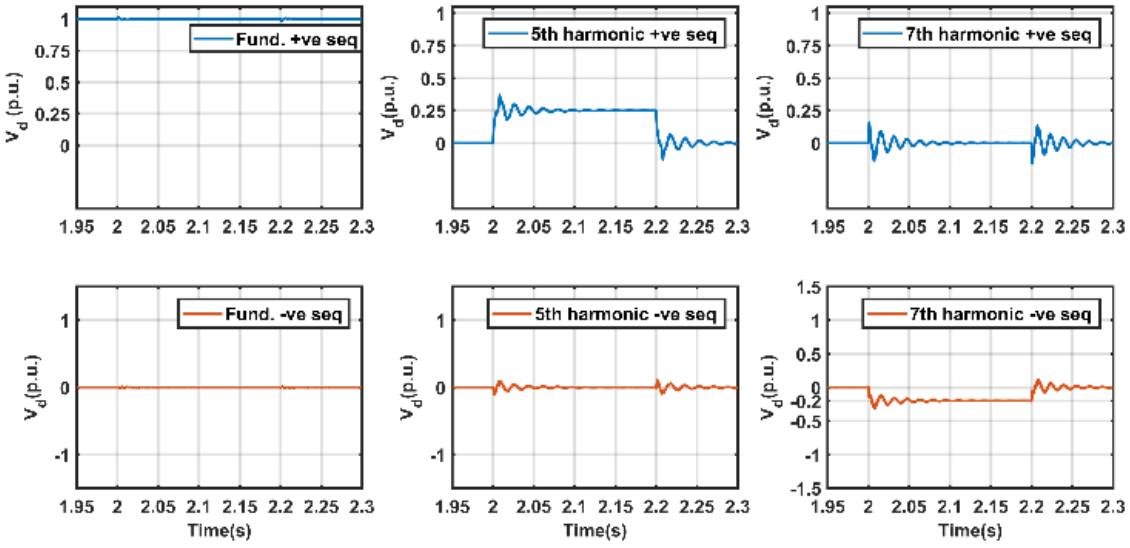

Figure 5-7: MCCF output for testing voltage

5.5.2 Case II: Ride through and fundamental positive sequence voltage support

PV-1, rated at 500kW, is connected at bus 633, and programmed to inject only positive sequence current components, i.e. I_d^+ and I_q^+. The inverter is set to inject 400kW at unity power factor at normal condition. So, for normal operating condition, $(I_d^+)^* = 0.4\ p.u.\ and\ (I_q^+)^* = 0$ as calculated from (5.13)-(5.16). The phase A to ground fault is

initiated at t=0.5s and has now a duration of 300ms. This creates a remaining voltage sag of 0.88 p.u. at buses 633. The top graph in Figure 5-8 shows the case. As expected, PV-1 inverter rides through for the entire 300ms by injecting positive sequence reactive current only. This is shown in the middle graph plot. The current references for the inverter during this event is calculated as$(I_d^+)^* = 0.05\ p.u. and\ (I_q^+)^* = 0.99\ p.u$ from (5.40)-(5.41). I_{oc} is equal to $\sqrt{2}I_{rated}$ as suggested by [108]. By setting$(I_d^+)^* = 0.05\ p.u.$ during the fault, the active power reference P_{ref} is set to be minimized. It physically means that the short circuit current contribution from PV-1 is to be minimized. Moreover, the excess DC-link power is rerouted to a dump load during this momentary interruption. By doing this, the overvoltage fluctuation is minimized at the DC link as seen from the bottom graph in Figure 5-8.

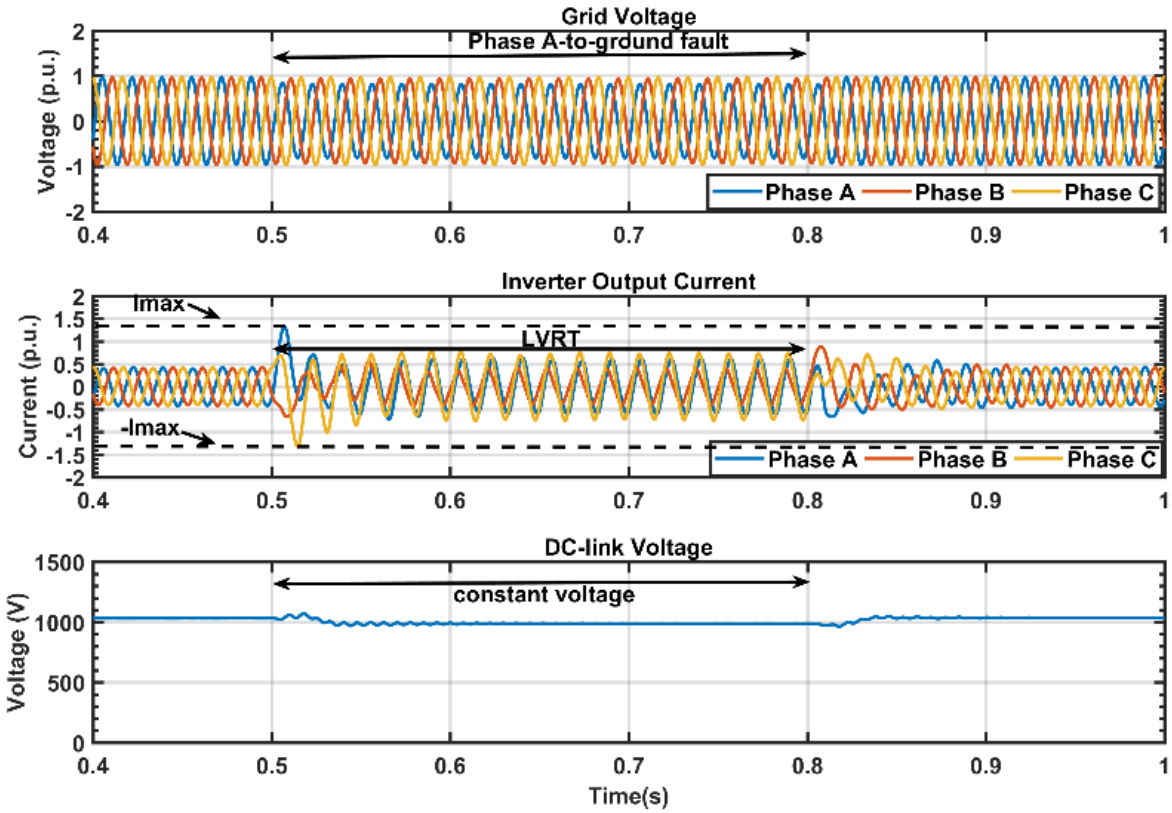

Figure 5-8: LVRT at bus 633

Similarly, by setting $(I_q^+)^* = 0.99\,p.u$, the fundamental positive sequence reactive power reference is set to be maximized to boost up the positive sequence grid voltage. The transition of current references from normal to fault condition is assumed to be instantaneous, i.e. without any significant time delay which is experimentally verified later in this section. As mentioned before, the test system is inductive, and therefore requires reactive power compensation to boost up the positive sequence voltage. This assumption is validated and shown in Figure 5-9. During the fault, the positive sequence grid voltage component, V_d^+ is at 0.88 p.u. By injecting full rated active current equivalent to 500kW from PV-1 boosts up V_d^+ by only 1%. This proves that there is negligible effect of active

power injection to boost up V_d^+. The positive sequence q-axis grid voltage component, V_q^+ is also unaffected, which is clear from Figure 5-9.

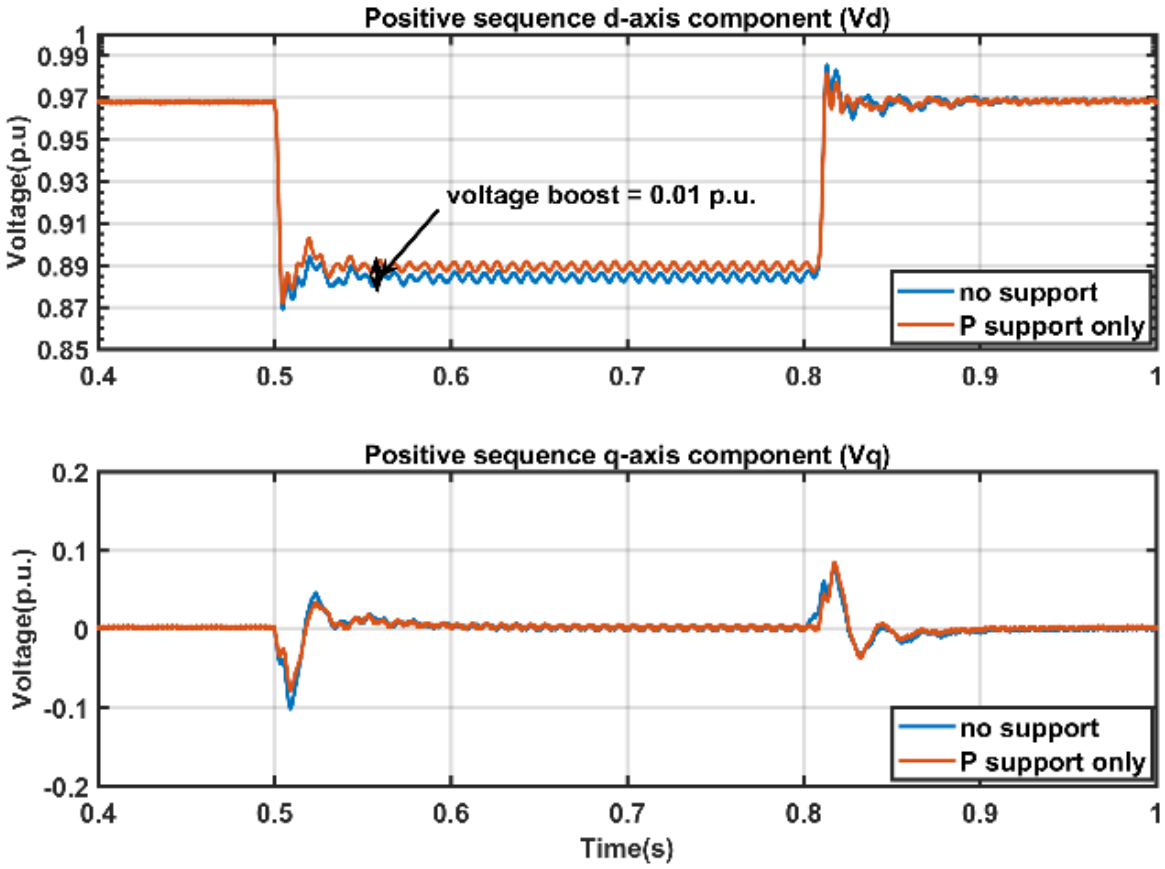

Figure 5-9: Injecting full rated active current at bus 633

A more realistic case, considering a time delay, is simulated and shown in Figure 5-10. From the inception of the fault at t=0.5s, the inverter references took a time delay of 100ms to change from their settings at normal operating condition to those at faulted condition. At t=0.6s, the current references changed, and Q injection starts. The inverter responds immediately to the control signal and boost up V_d^+ for the remaining 200ms of the fault duration, which is critical for the LVRT requirement. By injecting the positive sequence reactive current only, V_d^+ increases by 4% and settles at the average value of 0.92 p.u.

Compared to the dynamic active power support condition shown in Figure 5-9, this is a significant improvement in a MV distribution system. It also validates the assumptions used in deriving (5.40)-(5.43). Notice that the positive sequence voltage is oscillating because of the presence of negative sequence components as discussed in section 5.3.4.

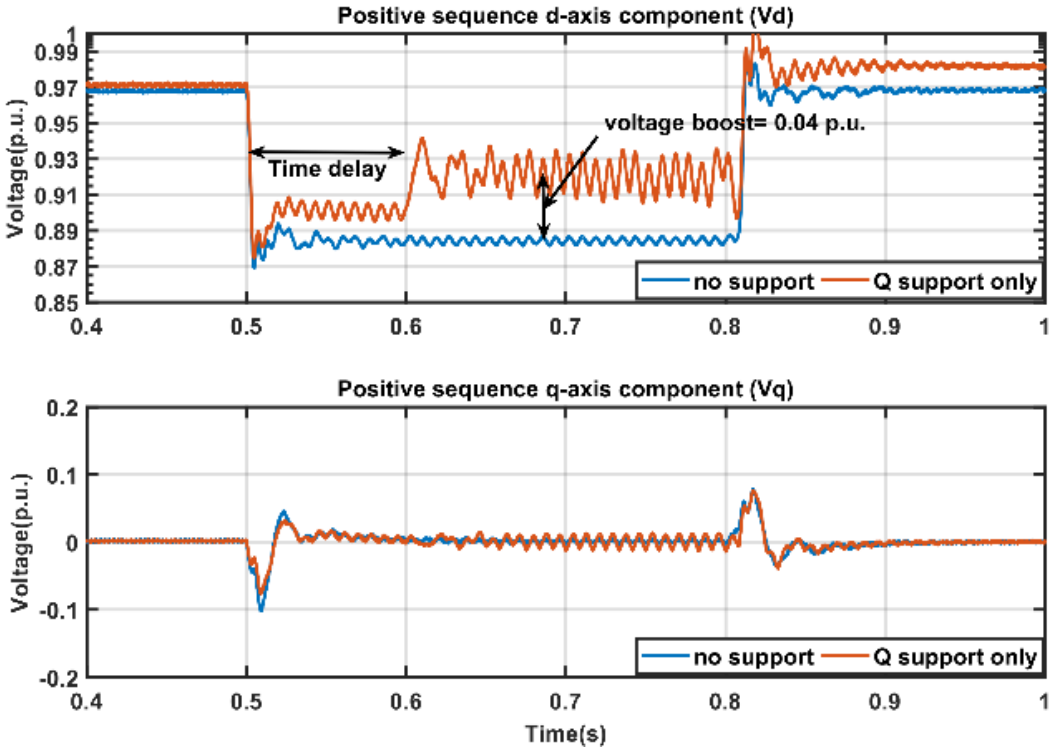

Figure 5-10: V_d^+ and V_q^+ components at bus 633 with time delay

5.5.3 Case III: Ride through and fundamental negative sequence voltage support

The PV-2 inverter installed at bus 634 is programmed to inject only the negative sequence currents i.e. I_d^- and I_q^-. Therefore, it rides through the unbalanced voltage sag event by injecting reactive current in the negative sequence reference frame. Physically it means that the unbalance from the grid voltage is reduced. The negative sequence grid voltage components, V_d^- and V_q^- are shown in Figure 5-11.

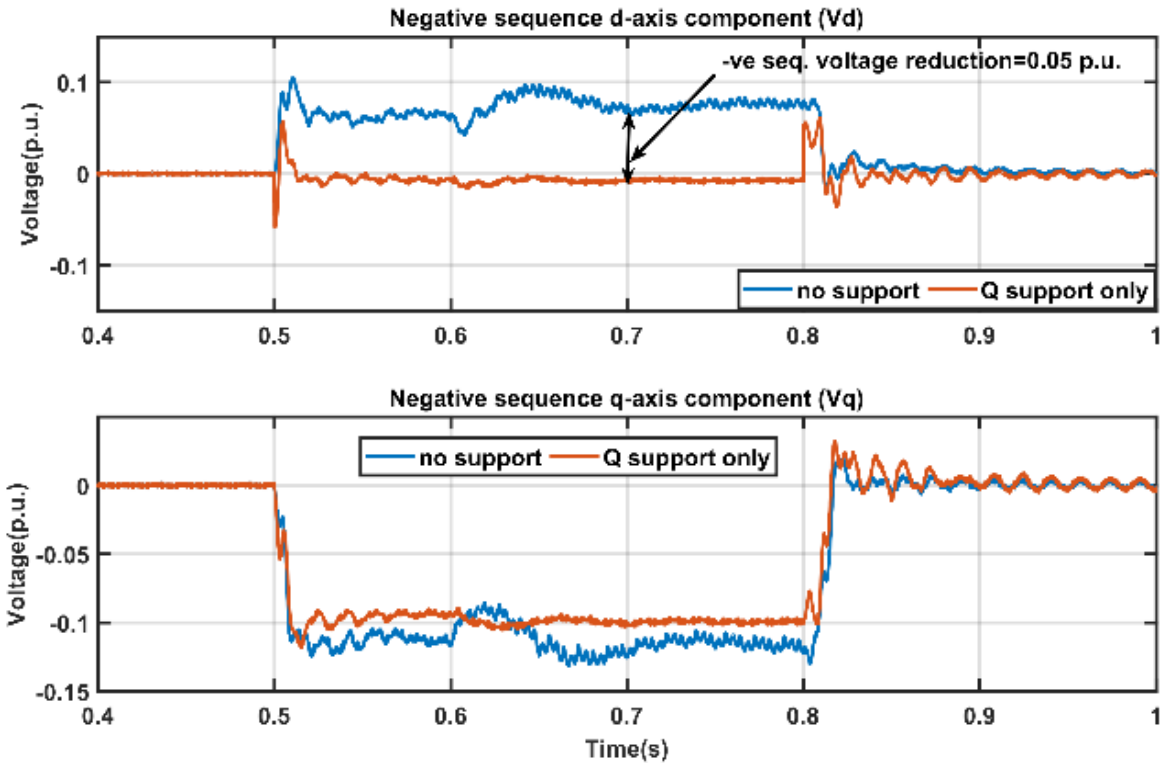

Figure 5-11: V_d^- and V_q^- components at bus 634

In this case, as the target is to inject only negative sequence components, the positive sequence current references can be set to zero i.e. $(I_d^+)^* = 0\ and\ (I_q^+)^* = 0$. This leads to $(I_d^-)^* = 0\ and\ (I_q^-)^* = -1$. To implement this coordination between a pair of inverters, say PV-1 and PV-2, a peer-to-peer communication scheme, as in distributed voltage control, is needed. As seen from the Figure 5-11, the negative sequence voltage is reduced by 5%. The q-axis component remains almost the same. The performance index to measure the impact of this result is to calculate the Voltage Unbalance Factor (VUF) which is defined as the ratio of negative sequence voltage to positive sequence voltage as shown in (5.47). The solution to the optimization problem 2 thus reduced the voltage unbalance by 5.68% as calculated below-

$$\%\,VUF = \frac{negative\ sequence\ voltage\ component}{positive\ sequence\ voltage\ component} X100\% \qquad (5.47)$$

$$\%\,VUF = \frac{-0.05}{0.88} X100\% = -5.68\%$$

5.5.4 Case IV: Sub-optimal current injection

A 1 MW inverter is installed at bus 675 for the PV-3 generation. This inverter is a standalone case where it can be controlled to inject both positive and negative sequence active and reactive current components. The phase A to ground fault between bus 632 and 671 leads to a voltage of 0.88 p.u. at bus 675. However, a different sub-optimal solution is intentionally chosen to verify whether a sub-optimal solution from (5.46) would ride through the momentary disturbance as explained in Figure 5-12 and Figure 5-13. Note that by doing it, dynamic grid support will not be optimal but LVRT can be tested. This is important because it justifies that the sub-optimal values might still make the inverter ride-through. For this case, the reference currents are set as $(I_d^+)^* = 0.08, (I_q^+)^* = 0.7, (I_d^-)^* = -0.08, (I_q^-)^* = 0.7$ p.u. which is not optimal and arbitrarily chosen. As shown in Figure 5-12, the inverter successfully rides through the fault event. DC link voltage remains constant because of the excessive energy dumping into the dump load. Notice that, a boost of 4% for the positive sequence grid voltage is achieved, which is like Case I, as shown in the top graph of Figure 5-13. The bottom graph shows that the q-axis components are unaffected.

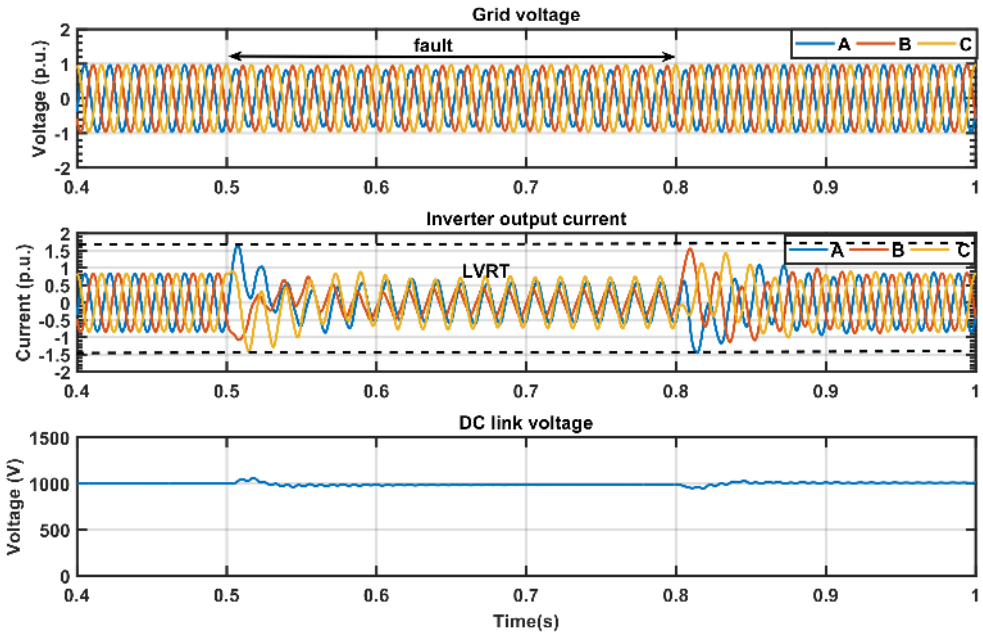

Figure 5-12: LVRT at bus 675 with suboptimal solution

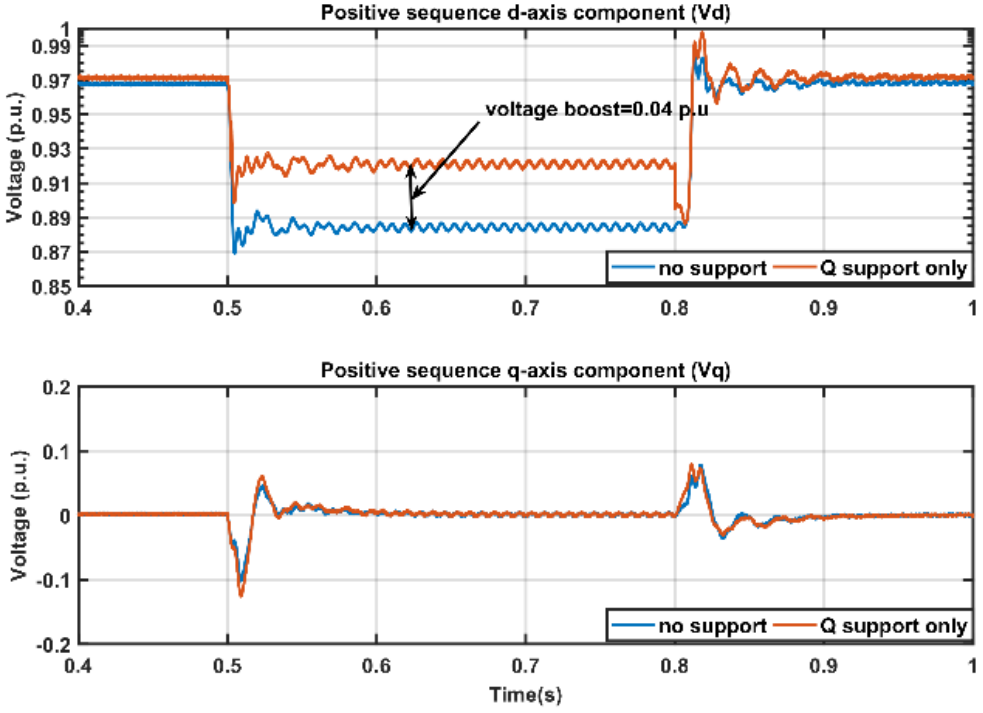

Figure 5-13: V_d^+ and V_q^+ components at bus 675

5.5.5 Case V: Impact of X/R ratio change

As the mathematical formulation shows the dependency of inverter's optimal current references on the line's X/R ratio, the impact of X/R ratio change is investigated. The performance index to measure the effectiveness of the proposed strategy for change in X/R ratio, is selected to be the VUF as defined in (5.47). Rather than varying the X/R ratio randomly, all the locations inside the IEEE-13 bus test system are chosen and tested with a 1MW inverter's full rated reactive current injection at each bus in each iteration. The goal is to find the amount of reduction in VUF for each bus if it is affected by a phase A to ground fault located near the substation at bus 650, which affects all the buses. The results are shown in Figure 5-14. In this figure, bus no 645, 646, 611, 652 and 684 are shown to have zero VUF as these buses contain single and two phases connection for which VUF is not defined. Notice that the bus 675 is the farthest location from the substation at bus 650. Therefore, it has the 'weak grid' characteristics and the proposed strategy can reduce the VUF up to 1.902% if optimal current references are used which can be calculated by (5.40)-(5.43). However, this result may vary based on the fault location, fault impedance and fault type.

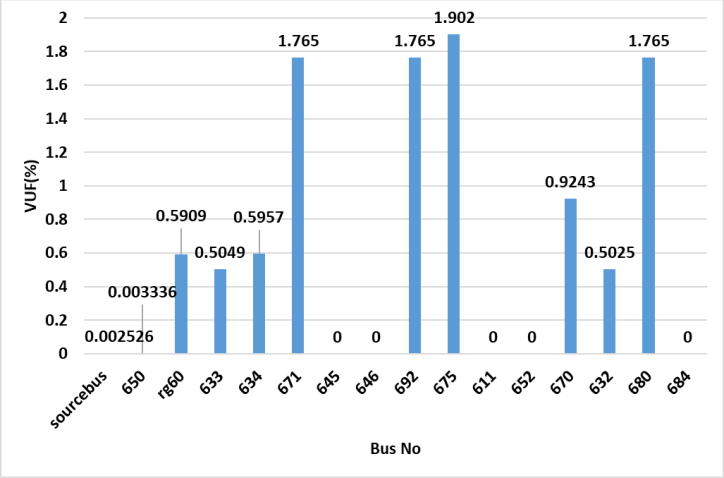

Figure 5-14: VUF reduction by changing X/R ratio

5.6 Controller's transient performance: experimental verification

The designed controller's transient performance is experimentally validated to test the timing constraint using a Controller Hardware-in-the-loop (C-HIL) approach. A TMS320F28335 microcontroller-based DSP control card is programmed to provide the PWM pulses to the inverter at bus 675. Typhoon HIL 600 is used to emulate the test system in a high fidelity, high resolution environment. The fault scenario in the modified IEEE-13 bus test system is mimicked in the testing platform. A single-phase to ground fault, with a duration of 300ms, is depicted in Figure 5-15. Here, phase A of bus 675 is chosen to be grounded through a fault resistance of 0.1 Ω. The sag depth shown is 50%.

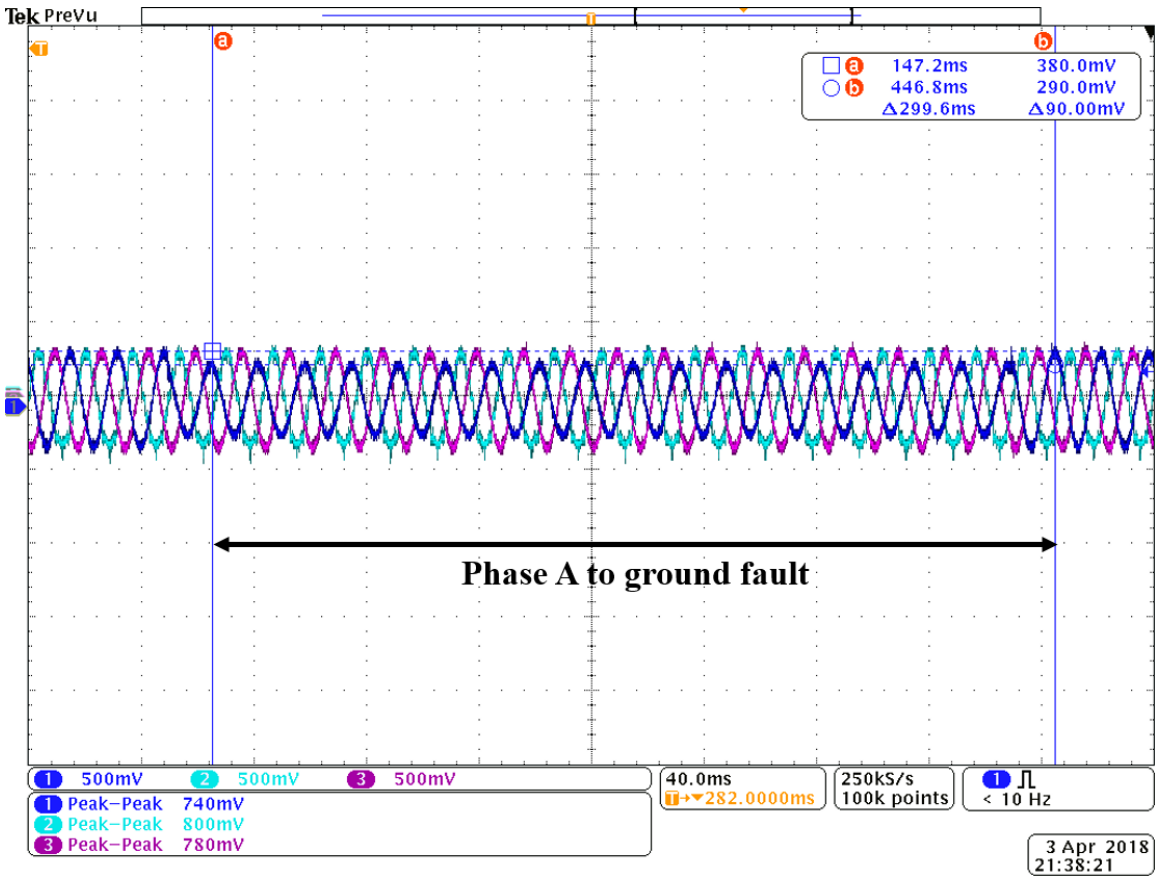

Figure 5-15: Phase A to ground fault at bus 675

As expected from the proposed control strategy, the fundamental active and reactive currents in the positive sequence change their references respectively as calculated by the KKT conditions discussed in Section 5.3.5. Figure 5-16 captures the transition moments of the references.

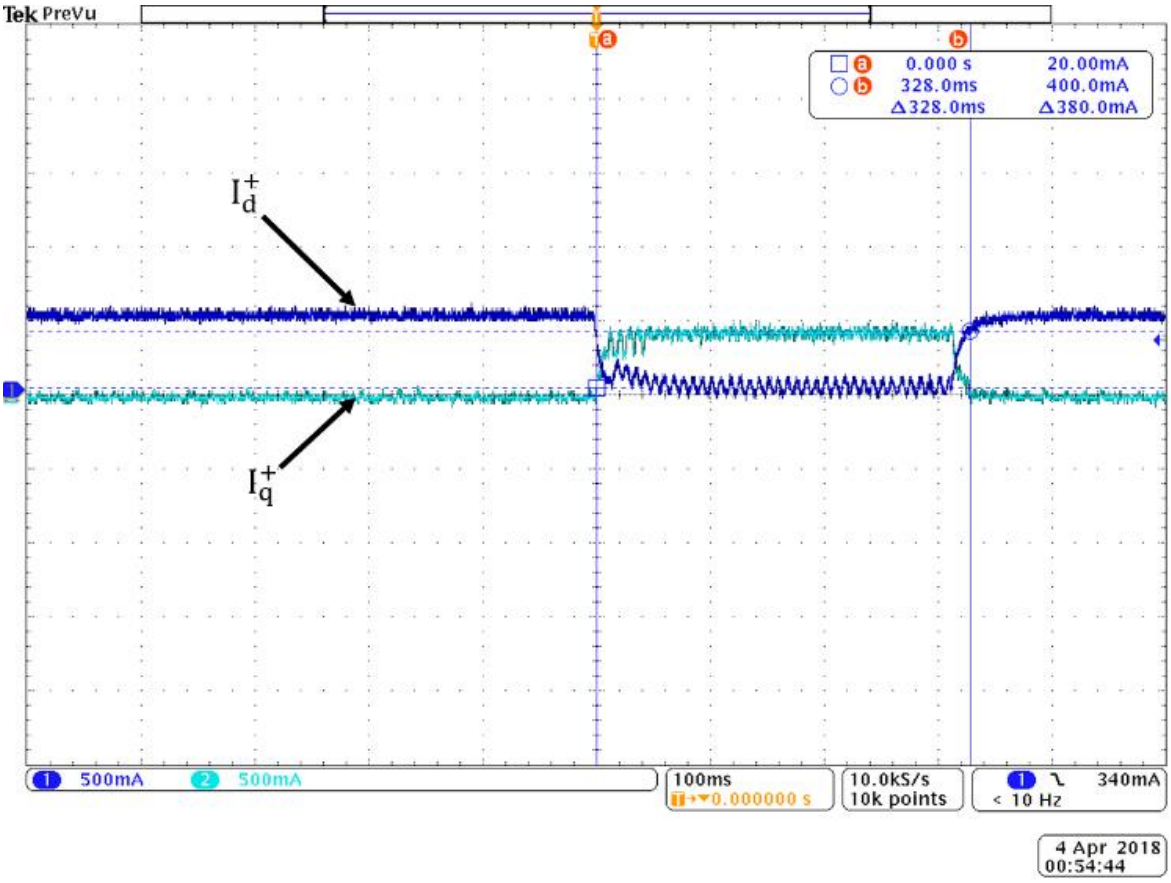

Figure 5-16: I_d^+ and I_q^+ components during the entire fault duration

Figure 5-17 shows the controller's transient performance in setting the required references. Using a zoomed version of Figure 5-16, we can observe that it took around 45ms for the current references in the positive sequence reference frame to settle down to steady state. This includes sequence detection using MCCF based PLL and using (5.40)-(5.43) directly. It is important to note that this short time is achieved because none of the non-linear

optimization problems is solved in real-time rather, as mentioned before, the known positive sequence impedance values, R and X are set using predefined look-up tables to calculate (5.40)-(5.43). According to the LVRT requirement imposed by IEEE 1547-2014 listed in Table 5-1, for a sag of 50%, the minimum ride through time is 160ms. The proposed strategy changes the current references within 45ms which seems satisfactory. Table 5-2 shows the system parameters.

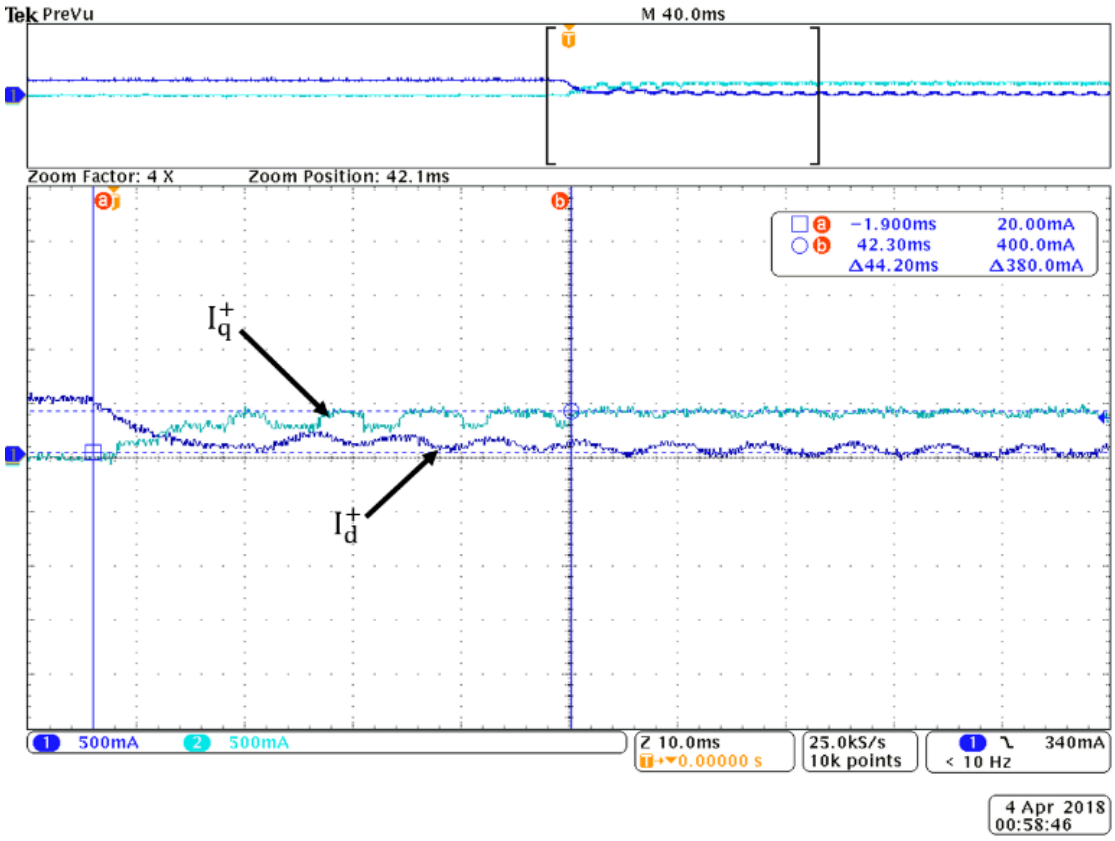

Figure 5-17: Transient performance of the controller

Table 5-2: System parameters

Parameters	**PV Inverter-1, 2, 3**
Rated power	500kW and 1000kW
DC link voltage	1kV
[Kp1, Ki1]	[3e-6, 3e-6]
[Kp2, Ki2]	[4e-6, 7e-6]
[Kp3, Ki3]	[3e-6, 3e-6]
[Kp4, Ki4]	[10e-6, 10e-6]

5.7 Conclusion

A control strategy proposed for the dynamic grid support condition which satisfies the LVRT code - a bulk system support requirement defined by IEEE 1547a-2014. A detailed mathematical formulation was shown using KKT conditions for both equality and inequality constraints. The constraints were found to be necessary and sufficient to find the optimal solution. The advantage of the proposed solution is that it is applicable for different X/R ratios. Furthermore, it takes care of the maximum overcurrent limit an inverter can handle. The proposed solution is aimed at providing the maximum positive sequence voltage boost during fault and minimizing the voltage unbalance. This provides a better controllability during the fault condition. A distributed coordination scheme using a two optimization goals are also described. This coordination scheme provides flexibility to multiple inverters to ride through the same fault utilizing different sequence components. Finally, the strategy was simulated, and controller's transient validity is experimentally validated using a C-HIL approach on the IEEE 13 bus test system. The results show that the proposed control strategy could effectively rides through the disturbance, thus meeting the transient performance expectation and providing dynamic grid support during an unbalanced grid fault condition.

CHAPTER 6: CONCLUSION AND FUTURE WORK

6.1 Concluding remarks

In this thesis, the application of smart PV inverters and battery energy storage systems in various scenarios were addressed. First, the control methodology of smart inverters in grid connected and islanded modes was introduced. A case study for transition from one mode to another was shown. After that, a directional power factor based distributed voltage control methodology is proposed. The methodology utilizes volt-var characteristics of a smart inverter. Next, a frequency regulation scheme with the frequency-watt characteristics is proposed and a coordination approach is presented that utilizes Inverse Definite Minimum Time (IDMT) characteristics of a relay.

The control of the smart inverter with BESS has a significant impact on grid-friendly features. In this thesis, two scenarios were reviewed: 1- the role of BESS as a power sink to enable the solar PV plant to ride through the momentary disturbance; 2- the role of smart inverter as a Shunt Active Power Filter (SAPF) for Selective Harmonic Compensation (SHC). In the first scenario, it is shown that the BESS provides auxiliary support to the solar PV system to successfully follow the IEEE 1547 standard and ride through grid side faults. In addition, the BESS is assumed to provide energy during times solar power is less than the required power to stabilize the DC link voltage. In the second scenario, a new value proposition is presented as to operate the smart inverter just like a SAPF. The concept is extended to extreme cases even under the grid fault.

Based on the findings in normal and fault time operation of smart inverter, a reconfigurable and flexible voltage control strategy is proposed. A novel solar-storage circuit topology is proposed, and dynamic analysis is carried out to validate its performance. The proposed

topology has the advantage of reconfiguring itself in case of BESS maintenance and overhauling. The flexible control strategy is achieved by using active and reactive power based on the sensitivity index of the connected feeder. The proposed control strategy is shown to be effective in regulating the voltage.

For the fault operation, the smart inverter is required to inject the lowest short circuit to the faulty location and ride through momentary sags with a duration of maximum one second. This requirement is made mandatory by IEEE 1547a-2018 standard. Therefore, the thesis attempts to calculate the optimum current references using Karush-Kuhn-Tucker (KKT) optimal condition. The non-linear conditions are solved, and an analytical expression is found to be applicable for strong and weak grid. The transient performance of the smart inverter controller is experimentally verified, and the results shown are found to be satisfactory. Five cases are discussed in details and the physical and operational constraints were investigated. Existing Dual Vector Current Control (DVCC) scheme is used. The methodology may be used in Low Voltage Ride Through (LVRT) implementation.

Previous approaches often did not support the unification of droop settings in smart inverters. The proposed unified P-f and Q-V control supports remote on/off feature of the smart inverter with adjustable droop settings. The unified approach can enable voltage and frequency regeneration in islanded condition. It also enables the smart inverter to switch to different modes when needed. Next, it is shown that a unique yet simple OLTC and inverter coordination based on the leading and lagging var direction can be achieved that mitigates voltage rise or drop effectively and allow high PV penetration. Most of the existing methodologies used costly and complex communication infrastructure with a single point-of-failure. A reconfigurable voltage control strategy is proposed for the two-stage utility

owned PV and integrated BESS technology. Then, a novel topology is introduced to incorporate a BESS which is safe and easy to reconfigure from an operational standpoint, not possible in existing literature and industry practice. The proposed algorithm is implemented by device level controllers and local voltage control is guaranteed. Flexible voltage control can be achieved using active and reactive power in a network cognizant manner. Finally, a coordinated FWC scheme for multiple inverters is proposed which mimics the principle of inverse definite minimum time (IDMT) characteristics for frequency regulation aiding bulk grid in the upstream. The novelty of this work lies in the fact that the existing frequency regulation approaches require BESS and a centralized communication network to solve this classical issue.

Dynamic voltage support and low voltage ride through using dc link voltage stabilization with BESS is proposed. The novelty of this work is in the application of BESS for extended period of operation in strong and weak grid conditions which is not considered in existing literature. Investigation on PLL performance under fault condition found room for improvement inside its structure for synchronization and sequence extraction which is solved by MCCF. A dynamic voltage support strategy using smart inverters for a two-stage PV inverter architecture, which can be applied to different feeders with different X/R ratios, is proposed. Karush–Kuhn–Tucker (KKT) condition is implemented at the heart of the proposed approach to calculate and optimize the required active and reactive current references in both positive and negative sequence frames during a fault. A new distributed coordination approach among multiple inverters to ride through the same fault event based on fundamental positive and negative sequence voltage support is also proposed which is non-existent in current literature.

6.2 Future Work

Interesting research directions for future work are recommended in this section. In what follows, detailed recommendations are discussed:

1. In Chapter 2, the autonomous control of smart inverters in grid connected and islanded modes were addressed. The main challenge here is the issue of transition from one mode to another. A good research direction would be to study seamless transition methods with appropriate control algorithms in a hardware testbed. The distributed voltage control may be achieved using the proposed methodology discussed in chapter 2. The voltage regulating devices may be coordinated with the smart inverter based on the power factor direction. However, detail simulations on a larger test network are required to verify the performance of the method and clarify possible challenges of utilizing this distributed voltage control strategy. The frequency regulation using FWC of smart inverter is also presented in this chapter. The coordination proposed for multiple inverters to participate in the frequency regulation is presented. The main challenge here is to optimize the droop setting so that active power curtailment to regulate the frequency can be kept to a minimum. A mathematical formulation along with a larger test network for validation may be a good future work.
2. In Chapter 3, control of smart inverter during grid side faults is presented. The BESS can act as a sink to remove the excess energy from the DC link capacitor at times of fault. This prevents the DC link from hitting the over voltage limit, thus allowing it to remain operational for implementing the LVRT. The BESS can work properly in this application but the idea to absorb the excess energy using BESS is

not safe from the operational point of view. The BESS circuit could be severely damaged by doing this for a long time. Therefore, finding a safe operational approach for managing the DC link voltage might be a future work in this case. For the SAPF technology, different types of PLLs may be used and compared to find the best approach for selective harmonic compensation.

3. Chapter 4 could be extended by adding forecasted solar power and load demand in the control strategy. Stochasticity in solar energy may be considered, and it should be noted that an optimization algorithm can be formulated based on the targeted voltage profile. Measurement and prediction errors may also be incorporated into the study. Larger IEEE test networks like 8500 bus may be used for further validation.
4. In Chapter 5, it was assumed that the dc link voltage source is constant. In other words, the voltage of the dc link capacitor remains the same throughout the entire fault duration. The assumption can be relaxed and further research on this is possible. A detailed simulation could be done by putting more solar PV power-plants at different buses with a larger test network. Therefore, dynamic grid support could be performed at more locations with different X/R ratio and the results could be used in the optimization constraints. In actual systems, the distributed coordination needs a robust communication scheme which is an attractive future research direction.
5. Impact of location and seasonality could be an interesting factor to evaluate the effectiveness of the BESS in solar PV deployment in advanced distribution networks. Different locations in a network have different patterns of applicability.

Moreover, BESS materials and physics may also be considered to understand the application further.

6. After several consecutive hurricanes and super typhoons around different parts of the world, resiliency in distribution networks are getting paramount importance. To move forward with this topic, microgrids with DERs and distributed storages might be a good research direction. Demand response with controllable loads are also getting tremendous attention which can be a great field to work on.

REFERENCES

[1] M. A. Green, K. Emery, Y. Hishikawa, W. Warta, and E. D. Dunlop, "Solar cell efficiency tables (Version 45)," *Prog. Photovoltaics Res. Appl.*, vol. 23, no. 1, pp. 1–9, Jan. 2015.

[2] "2014 SunShot Initiative Portfolio Book | Department of Energy." [Online]. Available: https://www.energy.gov/eere/solar/2014-sunshot-initiative-portfolio-book. [Accessed: 18-Sep-2018].

[3] "Solar Energy Technologies Office | Department of Energy." [Online]. Available: https://www.energy.gov/eere/solar/solar-energy-technologies-office. [Accessed: 18-Sep-2018].

[4] B. Kaun, "Cost-Effectiveness of Energy Storage in California: Application of the EPRI Energy Storage Valuation Tool to Inform the California Public Utility Commission Proceeding R. 10-12-007."

[5] *IEEE Std 1547-2018 (Revision of IEEE Std 1547-2003) IEEE Standard for Interconnection and Interoperability of Distributed Energy Resources with Associated Electric Power Systems Interfaces.* IEEE.

[6] A. F. Hoke, M. Shirazi, S. Chakraborty, E. Muljadi, and D. Maksimovic, "Rapid Active Power Control of Photovoltaic Systems for Grid Frequency Support," *IEEE J. Emerg. Sel. Top. Power Electron.*, vol. 5, no. 3, pp. 1154–1163, Sep. 2017.

[7] M. Guan, W. Pan, J. Zhang, Q. Hao, J. Cheng, and X. Zheng, "Synchronous Generator Emulation Control Strategy for Voltage Source Converter (VSC) Stations," *IEEE Trans. Power Syst.*, vol. 30, no. 6, pp. 3093–3101, Nov. 2015.

[8] A. Nelson, G. Martin, and J. Hurtt, "Experimental evaluation of grid support enabled PV inverter response to abnormal grid conditions," in *2017 IEEE Power & Energy Society Innovative Smart Grid Technologies Conference (ISGT)*, 2017, pp. 1–5.

[9] Fang Gao and M. R. Iravani, "A Control Strategy for a Distributed Generation Unit in Grid-Connected and Autonomous Modes of Operation," *IEEE Trans. Power Deliv.*, vol. 23, no. 2, pp. 850–859, Apr. 2008.

[10] E. Serban, M. Ordonez, and C. Pondiche, "Voltage and Frequency Grid Support Strategies Beyond Standards," *IEEE Trans. Power Electron.*, vol. 32, no. 1, pp. 298–309, Jan. 2017.

[11] I. Serban and C. Marinescu, "Control Strategy of Three-Phase Battery Energy Storage Systems for Frequency Support in Microgrids and with Uninterrupted Supply of Local Loads," *IEEE Trans. Power Electron.*, vol. 29, no. 9, pp. 5010–5020, Sep. 2014.

[12] R. Yokoyama, Y. Hida, K. Koyanagi, and K. Iba, "The role of battery systems and expandable distribution networks for smarter grid," in *2011 IEEE Power and Energy Society General Meeting*, 2011, pp. 1–6.

[13] T. Fenimore, “McAlpine Microgrid – A Distribution System Based Microgrid on Vimeo.” [Online]. Available: https://vimeo.com/233701320. [Accessed: 18-Sep-2018].

[14] C. L. Masters, “Voltage rise: the big issue when connecting embedded generation to long 11 kV overhead lines,” *Power Eng. J.*, vol. 16, no. 1, pp. 5–12, Feb. 2002.

[15] R. Tonkoski, D. Turcotte, and T. H. M. El-Fouly, “Impact of High PV Penetration on Voltage Profiles in Residential Neighborhoods,” *IEEE Trans. Sustain. Energy*, vol. 3, no. 3, pp. 518–527, Jul. 2012.

[16] R. A. Shayani and M. A. G. de Oliveira, “Photovoltaic Generation Penetration Limits in Radial Distribution Systems,” *IEEE Trans. Power Syst.*, vol. 26, no. 3, pp. 1625–1631, Aug. 2011.

[17] W. G. Hartmann, “Implementing VVO with DER penetration,” in *2017 IEEE Power & Energy Society Innovative Smart Grid Technologies Conference (ISGT)*, 2017, pp. 1–5.

[18] P. M. S. Carvalho, P. F. Correia, and L. A. F. Ferreira, “Distributed Reactive Power Generation Control for Voltage Rise Mitigation in Distribution Networks,” *IEEE Trans. Power Syst.*, vol. 23, no. 2, pp. 766–772, May 2008.

[19] M. Brenna, E. De Berardinis, L. Delli Carpini, F. Foiadelli, P. Paulon, P. Petroni, G. Sapienza, G. Scrosati, and D. Zaninelli, “Automatic Distributed Voltage Control Algorithm in Smart Grids Applications,” *IEEE Trans. Smart Grid*, vol. 4, no. 2, pp. 877–885, Jun. 2013.

[20] P. N. Vovos, A. E. Kiprakis, A. R. Wallace, and G. P. Harrison, “Centralized and Distributed Voltage Control: Impact on Distributed Generation Penetration,” *IEEE Trans. Power Syst.*, vol. 22, no. 1, pp. 476–483, Feb. 2007.

[21] P. IEEE Standards Coordinating Committee 21 (Fuel Cells, Institute of Electrical and Electronics Engineers., and IEEE-SA Standards Board., *IEEE standard for interconnecting distributed resources with electric power systems. Amendment 1*. .

[22] Z.-S. Zhang, Y.-Z. Sun, J. Lin, and G.-J. Li, “Coordinated frequency regulation by doubly fed induction generator-based wind power plants,” *IET Renew. Power Gener.*, vol. 6, no. 1, p. 38, 2012.

[23] J. Johnson, J. C. Neely, J. J. Delhotal, and M. Lave, “Photovoltaic Frequency–Watt Curve Design for Frequency Regulation and Fast Contingency Reserves,” *IEEE J. Photovoltaics*, vol. 6, no. 6, pp. 1611–1618, Nov. 2016.

[24] M. Datta and T. Senjyu, “Fuzzy Control of Distributed PV Inverters/Energy Storage Systems/Electric Vehicles for Frequency Regulation in a Large Power System,” *IEEE Trans. Smart Grid*, vol. 4, no. 1, pp. 479–488, Mar. 2013.

[25] H. Bevrani, A. Ghosh, and G. Ledwich, “Renewable energy sources and frequency regulation: survey and new perspectives,” *IET Renew. Power Gener.*, vol. 4, no. 5, p. 438, 2010.

[26] G. Delille, B. Francois, and G. Malarange, “Dynamic frequency control support: A virtual inertia provided by distributed energy storage to isolated power systems,” in *2010 IEEE PES Innovative Smart Grid Technologies Conference Europe (ISGT Europe)*, 2010, pp. 1–8.

[27] F. Zhang, Z. Hu, X. Xie, J. Zhang, and Y. Song, “Assessment of the Effectiveness of Energy Storage Resources in the Frequency Regulation of a Single-Area Power System,” *IEEE Trans. Power Syst.*, vol. 32, no. 5, pp. 3373–3380, Sep. 2017.

[28] A. Hoke, M. Elkhatib, A. Nelson, J. Johnson, J. Tan, R. Mahmud, V. Gevorgian, J. Neely, C. Antonio, D. Arakawa, and K. Fong, “The Frequency-Watt Function: Simulation and Testing for the Hawaiian Electric Companies,” 2017.

[29] E. H. Camm and S. E. Williams, “Solar power plant design and interconnection,” in *2011 IEEE Power and Energy Society General Meeting*, 2011, pp. 1–3.

[30] C. H. Benz, W.-T. Franke, and F. W. Fuchs, “Low voltage ride through capability of a 5 kW grid-tied solar inverter,” in *Proceedings of 14th International Power Electronics and Motion Control Conference EPE-PEMC 2010*, 2010.

[31] X. Wang, M. Yue, and E. Muljadi, “Modeling and control system design for an integrated solar generation and energy storage system with a ride-through capability,” in *2012 IEEE Energy Conversion Congress and Exposition (ECCE)*, 2012, pp. 3727–3734.

[32] M. Mirhosseini and V. G. Agelidis, “Performance of large-scale grid-connected photovoltaic system under various fault conditions,” in *2013 IEEE International Conference on Industrial Technology (ICIT)*, 2013, pp. 1775–1780.

[33] A. Marinopoulos, F. Papandrea, M. Reza, S. Norrga, F. Spertino, and R. Napoli, “Grid integration aspects of large solar PV installations: LVRT capability and reactive power/voltage support requirements,” in *2011 IEEE Trondheim PowerTech*, 2011, pp. 1–8.

[34] *519-1992 IEEE Recommended Practices and Requirements for Harmonic Control in Electrical Power Systems.* .

[35] H. Akagi, “Control strategy and site selection of a shunt active filter for damping of harmonic propagation in power distribution systems,” *IEEE Trans. Power Deliv.*, vol. 12, no. 1, pp. 354–363, 1997.

[36] Y. F. Wang and Y. W. Li, “Three-Phase Cascaded Delayed Signal Cancellation PLL for Fast Selective Harmonic Detection,” *IEEE Trans. Ind. Electron.*, vol. 60, no. 4, pp. 1452–1463, Apr. 2013.

[37] X. Wang, F. Blaabjerg, and P. C. Loh, “Virtual RC]]> Damping of,” *IEEE Trans. Power Electron.*, vol. 30, no. 9, pp. 4726–4737, Sep. 2015.

[38] S.-W. Kang and K.-H. Kim, “Sliding mode harmonic compensation strategy for power quality improvement of a grid-connected inverter under distorted grid condition,” *IET Power Electron.*, vol. 8, no. 8, pp. 1461–1472, Aug. 2015.

[39] Hua Zhou, Yun Wei Li, N. R. Zargari, Zhongyaun Cheng, Ruoshui Ni, and Ye Zhang, "Selective Harmonic Compensation (SHC) PWM for Grid-Interfacing High-Power Converters," *IEEE Trans. Power Electron.*, vol. 29, no. 3, pp. 1118–1127, Mar. 2014.

[40] F. D. Freijedo, J. Doval-Gandoy, O. Lopez, and E. Acha, "Tuning of Phase-Locked Loops for Power Converters Under Distorted Utility Conditions," *IEEE Trans. Ind. Appl.*, vol. 45, no. 6, pp. 2039–2047, 2009.

[41] F. D. Freijedo, A. G. Yepes, Ó. López, A. Vidal, and J. Doval-Gandoy, "Three-Phase PLLs With Fast Postfault Retracking and Steady-State Rejection of Voltage Unbalance and Harmonics by Means of Lead Compensation," *IEEE Trans. Power Electron.*, vol. 26, no. 1, pp. 85–97, Jan. 2011.

[42] R. H. Lasseter, "MicroGrids," in *2002 IEEE Power Engineering Society Winter Meeting. Conference Proceedings (Cat. No.02CH37309)*, vol. 1, pp. 305–308.

[43] J. S. L. Senanayaka, "Power dispatching of active generators using droop control in grid connected micro-grid," *VIII, 81 p.*, 2014.

[44] R. W. (Robert W. Erickson and D. Maksimović, *Fundamentals of power electronics*. Kluwer Academic, 2001.

[45] R. Teodorescu, M. Liserre, and P. Rodríguez, *Grid Converters for Photovoltaic and Wind Power Systems*. Chichester, UK: John Wiley & Sons, Ltd, 2011.

[46] S. L. Lorenzen, A. B. Nielsen, and L. Bede, "Control of a grid connected converter during weak grid conditions," in *2016 IEEE 7th International Symposium on Power Electronics for Distributed Generation Systems (PEDG)*, 2016, pp. 1–6.

[47] F. Katiraei and M. R. Iravani, "Power Management Strategies for a Microgrid With Multiple Distributed Generation Units," *IEEE Trans. Power Syst.*, vol. 21, no. 4, pp. 1821–1831, Nov. 2006.

[48] S. Conti, S. Raiti, and G. Vagliasindi, "Voltage sensitivity analysis in radial MV distribution networks using constant current models," in *2010 IEEE International Symposium on Industrial Electronics*, 2010, pp. 2548–2554.

[49] "SRRL BMS September 2018 Solar Calendar." [Online]. Available: https://midcdmz.nrel.gov/apps/calendar.pl?site=BMS&year=2018&month=9. [Accessed: 18-Sep-2018].

[50] Shengyi Liu and R. A. Dougal, "Dynamic multiphysics model for solar array," *IEEE Trans. Energy Convers.*, vol. 17, no. 2, pp. 285–294, Jun. 2002.

[51] M. Ceraolo, "New dynamical models of lead-acid batteries," *IEEE Trans. Power Syst.*, vol. 15, no. 4, pp. 1184–1190, 2000.

[52] C.-J. Zhan, X. G. Wu, S. Kromlidis, V. K. Ramachandaramurthy, M. Barnes, N. Jenkins, and A. J. Ruddell, "Two electrical models of the lead–acid battery used in a dynamic voltage restorer," *IEE Proc. - Gener. Transm. Distrib.*, vol. 150, no. 2, p. 175, 2003.

[53] H. Wang, G. Li, M. Li, Z. Jiang, X. Wang, and Q. Zhao, “Third-order dynamic model of a lead acid battery for use in fuel cell vehicle simulation,” in *2011 International Conference on Mechatronic Science, Electric Engineering and Computer (MEC)*, 2011, pp. 715–720.

[54] G. J. Kish, J. J. Lee, and P. W. Lehn, “Modelling and control of photovoltaic panels utilising the incremental conductance method for maximum power point tracking,” *IET Renew. Power Gener.*, vol. 6, no. 4, p. 259, 2012.

[55] A. D. Clarke, H. A. Bihani, E. B. Makram, and K. A. Corzine, “Analysis of the Impact of Different PEV Battery Chargers during Faults,” *J. Power Energy Eng.*, vol. 02, no. 08, pp. 31–44, Aug. 2014.

[56] Se-Kyo Chung, “A phase tracking system for three phase utility interface inverters,” *IEEE Trans. Power Electron.*, vol. 15, no. 3, pp. 431–438, May 2000.

[57] M. Wei and Z. Chen, “A Fast PLL Method for Power Electronic Systems Connected to Distorted Grids,” in *IECON 2007 - 33rd Annual Conference of the IEEE Industrial Electronics Society*, 2007, pp. 1702–1707.

[58] P. Rodriguez, R. Teodorescu, I. Candela, A. V. Timbus, M. Liserre, and F. Blaabjerg, “New Positive-sequence Voltage Detector for Grid Synchronization of Power Converters under Faulty Grid Conditions,” in *37th IEEE Power Electronics Specialists Conference*, pp. 1–7.

[59] M. Karimi-Ghartemani and M. R. Iravani, “A nonlinear adaptive filter for online signal analysis in power systems: applications,” *IEEE Trans. Power Deliv.*, vol. 17, no. 2, pp. 617–622, Apr. 2002.

[60] P. Rodriguez, J. Pou, J. Bergas, J. I. Candela, R. P. Burgos, and D. Boroyevich, “Decoupled Double Synchronous Reference Frame PLL for Power Converters Control,” *IEEE Trans. Power Electron.*, vol. 22, no. 2, pp. 584–592, Mar. 2007.

[61] X. Guo, W. Wu, and Z. Chen, “Multiple-Complex Coefficient-Filter-Based Phase-Locked Loop and Synchronization Technique for Three-Phase Grid-Interfaced Converters in Distributed Utility Networks,” *IEEE Trans. Ind. Electron.*, vol. 58, no. 4, pp. 1194–1204, Apr. 2011.

[62] C. Lascu, L. Asiminoaei, I. Boldea, and F. Blaabjerg, “Frequency Response Analysis of Current Controllers for Selective Harmonic Compensation in Active Power Filters,” *IEEE Trans. Ind. Electron.*, vol. 56, no. 2, pp. 337–347, Feb. 2009.

[63] S. J. Finney, G. Connor, and C. E. Jones, “End user voltage regulation to ease urban low-voltage distribution congestion,” *IET Gener. Transm. Distrib.*, vol. 8, no. 8, pp. 1453–1465, Aug. 2014.

[64] D. A. Quijano, J. Wang, M. R. Sarker, and A. Padilha-Feltrin, “Stochastic assessment of distributed generation hosting capacity and energy efficiency in active distribution networks,” *IET Gener. Transm. Distrib.*, vol. 11, no. 18, pp. 4617–4625, Dec. 2017.

[65] D. Santos-Martin, S. Lemon, J. D. Watson, A. R. Wood, A. J. V. Miller, and N. R.

Watson, “Impact of solar photovoltaics on the low-voltage distribution network in New Zealand,” *IET Gener. Transm. Distrib.*, vol. 10, no. 1, pp. 1–9, Jan. 2016.

[66] E. Romero-Cadaval, P. González-Castrillo, V. Miñambres-Marcos, and M. Á. Guerrero-Martínez, “Grid-connected photovoltaic power plants for helping node voltage regulation,” *IET Renew. Power Gener.*, vol. 9, no. 3, pp. 236–244, Apr. 2015.

[67] B. Bakhshideh Zad, J. Lobry, and F. Vallée, “Impacts of the model uncertainty on the voltage regulation problem of medium-voltage distribution systems,” *IET Gener. Transm. Distrib.*, vol. 12, no. 10, pp. 2359–2368, May 2018.

[68] P. Jahangiri and D. Aliprantis, “Distributed Volt/VAr control by PV inverters,” in *2014 IEEE PES General Meeting | Conference & Exposition*, 2014, pp. 1–1.

[69] A. O’Connell and A. Keane, “Volt–var curves for photovoltaic inverters in distribution systems,” *IET Gener. Transm. Distrib.*, vol. 11, no. 3, pp. 730–739, Feb. 2017.

[70] R. A. Jabr and I. Dzafic, “Sensitivity-Based Discrete Coordinate-Descent for Volt/VAr Control in Distribution Networks,” *IEEE Trans. Power Syst.*, vol. 31, no. 6, pp. 4670–4678, Nov. 2016.

[71] S. Ghosh, S. Rahman, and M. Pipattanasomporn, “Distribution Voltage Regulation Through Active Power Curtailment With PV Inverters and Solar Generation Forecasts,” *IEEE Trans. Sustain. Energy*, vol. 8, no. 1, pp. 13–22, Jan. 2017.

[72] F. Olivier, P. Aristidou, D. Ernst, and T. Van Cutsem, “Active Management of Low-Voltage Networks for Mitigating Overvoltages Due to Photovoltaic Units,” *IEEE Trans. Smart Grid*, vol. 7, no. 2, pp. 926–936, Mar. 2016.

[73] S. Hashemi and J. Østergaard, “Methods and strategies for overvoltage prevention in low voltage distribution systems with PV,” *IET Renew. Power Gener.*, vol. 11, no. 2, pp. 205–214, Feb. 2017.

[74] T. K. Saha, M. I. Hossain, and R. Yan, “Investigation of the interaction between step voltage regulators and large-scale photovoltaic systems regarding voltage regulation and unbalance,” *IET Renew. Power Gener.*, vol. 10, no. 3, pp. 299–309, Mar. 2016.

[75] A. Samadi, R. Eriksson, L. Soder, B. G. Rawn, and J. C. Boemer, “Coordinated Active Power-Dependent Voltage Regulation in Distribution Grids With PV Systems,” *IEEE Trans. Power Deliv.*, vol. 29, no. 3, pp. 1454–1464, Jun. 2014.

[76] S. Alyami, Y. Wang, C. Wang, J. Zhao, and B. Zhao, “Adaptive Real Power Capping Method for Fair Overvoltage Regulation of Distribution Networks With High Penetration of PV Systems,” *IEEE Trans. Smart Grid*, vol. 5, no. 6, pp. 2729–2738, Nov. 2014.

[77] A. Thomas, T. K. Saha, S. R. Deeba, D. Chakraborty, and R. Sharma, “Evaluation of technical and financial benefits of battery-based energy storage systems in distribution networks,” *IET Renew. Power Gener.*, vol. 10, no. 8, pp. 1149–1160, Sep. 2016.

[78] H. Fallahzadeh-Abarghouei, M. Nayeripour, S. Hasanvand, and E. Waffenschmidt, "Online hierarchical and distributed method for voltage control in distribution smart grids," *IET Gener. Transm. Distrib.*, vol. 11, no. 5, pp. 1223–1232, Mar. 2017.

[79] M. E. Elkhatib, R. El Shatshat, and M. M. A. Salama, "Decentralized Reactive Power Control for Advanced Distribution Automation Systems," *IEEE Trans. Smart Grid*, vol. 3, no. 3, pp. 1482–1490, Sep. 2012.

[80] E. Demirok, P. C. González, K. H. B. Frederiksen, D. Sera, P. Rodriguez, and R. Teodorescu, "Local Reactive Power Control Methods for Overvoltage Prevention of Distributed Solar Inverters in Low-Voltage Grids," *IEEE J. Photovoltaics*, vol. 1, no. 2, pp. 174–182, Oct. 2011.

[81] N. Yorino, Y. Zoka, M. Watanabe, and T. Kurushima, "An Optimal Autonomous Decentralized Control Method for Voltage Control Devices by Using a Multi-Agent System," *IEEE Trans. Power Syst.*, vol. 30, no. 5, pp. 2225–2233, Sep. 2015.

[82] W. Zhang, W. Liu, X. Wang, L. Liu, and F. Ferrese, "Distributed Multiple Agent System Based Online Optimal Reactive Power Control for Smart Grids," *IEEE Trans. Smart Grid*, vol. 5, no. 5, pp. 2421–2431, Sep. 2014.

[83] M. E. Baran and I. M. El-Markabi, "A Multiagent-Based Dispatching Scheme for Distributed Generators for Voltage Support on Distribution Feeders," *IEEE Trans. Power Syst.*, vol. 22, no. 1, pp. 52–59, Feb. 2007.

[84] A. Engler and N. Soultanis, "Droop control in LV-grids," in *2005 International Conference on Future Power Systems*, 2005, p. 6 pp.-6.

[85] M. A. Kashem and G. Ledwich, "Multiple Distributed Generators for Distribution Feeder Voltage Support," *IEEE Trans. Energy Convers.*, vol. 20, no. 3, pp. 676–684, Sep. 2005.

[86] K. Khalid Mehmood, S. U. Khan, S.-J. Lee, Z. M. Haider, M. K. Rafique, and C.-H. Kim, "Optimal sizing and allocation of battery energy storage systems with wind and solar power DGs in a distribution network for voltage regulation considering the lifespan of batteries," *IET Renew. Power Gener.*, vol. 11, no. 10, pp. 1305–1315, Aug. 2017.

[87] A. Datta, D. Saha, A. Ray, and P. Das, "Evaluation of anti-islanding techniques for renewable energy powered distributed generators using analytic network process," *IET Renew. Power Gener.*, vol. 10, no. 9, pp. 1245–1254, Oct. 2016.

[88] P. Wang and T.-Z. Bei, "Robust frequency-locked loop algorithm for grid synchronisation of single-phase applications under distorted grid conditions," *IET Gener. Transm. Distrib.*, vol. 10, no. 11, pp. 2593–2600, Aug. 2016.

[89] X.-Q. Guo and W.-Y. Wu, "Simple synchronisation technique for three-phase grid-connected distributed generation systems," *IET Renew. Power Gener.*, vol. 7, no. 1, pp. 55–62, Jan. 2013.

[90] A. Molina-García, A. Honrubia-Escribano, T. García-Sánchez, E. Gómez-Lázaro, and E. Muljadi, "Power quality surveys of photovoltaic power plants:

characterisation and analysis of grid-code requirements," *IET Renew. Power Gener.*, vol. 9, no. 5, pp. 466–473, Jul. 2015.

[91] B. Weise, "Impact of K-factor and active current reduction during fault-ride-through of generating units connected via voltage-sourced converters on power system stability," *IET Renew. Power Gener.*, vol. 9, no. 1, pp. 25–36, Jan. 2015.

[92] S. Alepuz, S. Busquets-Monge, J. Bordonau, J. A. Martinez-Velasco, C. A. Silva, J. Pontt, and J. Rodriguez, "Control Strategies Based on Symmetrical Components for Grid-Connected Converters Under Voltage Dips," *IEEE Trans. Ind. Electron.*, vol. 56, no. 6, pp. 2162–2173, Jun. 2009.

[93] G. Saccomando and J. Svensson, "Transient operation of grid-connected voltage source converter under unbalanced voltage conditions," in *Conference Record of the 2001 IEEE Industry Applications Conference. 36th IAS Annual Meeting (Cat. No.01CH37248)*, vol. 4, pp. 2419–2424.

[94] F. A. Magueed, A. Sannino, and J. Svensson, "Transient performance of voltage source converter under unbalanced voltage dips," in *2004 IEEE 35th Annual Power Electronics Specialists Conference (IEEE Cat. No.04CH37551)*, pp. 1163–1168.

[95] P. Shanthi, G. Uma, and M. S. Keerthana, "Effective power transfer scheme for a grid connected hybrid wind/photovoltaic system," *IET Renew. Power Gener.*, vol. 11, no. 7, pp. 1005–1017, Jun. 2017.

[96] M. I. Milanés-Montero, V. Miñambres-Marcos, M. Á. Guerrero-Martínez, and E. Romero-Cadaval, "Cooperative converter for improving the performance of grid-connected photovoltaic power plants," *IET Renew. Power Gener.*, vol. 7, no. 2, pp. 110–117, Mar. 2013.

[97] G. Ding, F. Gao, H. Tian, C. Ma, M. Chen, G. He, and Y. Liu, "Adaptive DC-Link Voltage Control of Two-Stage Photovoltaic Inverter During Low Voltage Ride-Through Operation," *IEEE Trans. Power Electron.*, vol. 31, no. 6, pp. 4182–4194, Jun. 2016.

[98] A. Camacho, M. Castilla, J. Miret, L. G. de Vicuna, and R. Guzman, "Positive and Negative Sequence Control Strategies to Maximize the Voltage Support in Resistive–Inductive Grids During Grid Faults," *IEEE Trans. Power Electron.*, vol. 33, no. 6, pp. 5362–5373, Jun. 2018.

[99] P.-H. Huang, M. S. El Moursi, W. Xiao, and J. L. Kirtley, "Fault Ride-Through Configuration and Transient Management Scheme for Self-Excited Induction Generator-Based Wind Turbine," *IEEE Trans. Sustain. Energy*, vol. 5, no. 1, pp. 148–159, Jan. 2014.

[100] R. E. Best, *Phase-locked loops : design, simulation, and applications*. McGraw-Hill, 2007.

[101] W. Du, X. Chen, and H. Wang, "Parameter tuning of the PLL to consider the effect on power system small-signal angular stability," *IET Renew. Power Gener.*, vol. 12, no. 1, pp. 1–8, Jan. 2018.

[102] M. Chen, L. Peng, B. Wang, and J. Kan, "PLL based on extended trigonometric function delayed signal cancellation under various adverse grid conditions," *IET Power Electron.*, vol. 11, no. 10, pp. 1689–1697, Aug. 2018.

[103] Z. Ali, N. Christofides, L. Hadjidemetriou, and E. Kyriakides, "Design of an advanced PLL for accurate phase angle extraction under grid voltage HIHs and DC offset," *IET Power Electron.*, vol. 11, no. 6, pp. 995–1008, May 2018.

[104] H. A. Hamed, A. F. Abdou, E. Bayoumi, and E. E. EL-Kholy, "Effective design and implementation of GSS-PLL under voltage dip and phase interruption," *IET Power Electron.*, vol. 11, no. 6, pp. 1018–1028, May 2018.

[105] R. K. Agarwal, I. Hussain, and B. Singh, "Dual-function PV-ECS integrated to 3P4W distribution grid using 3M-PLL control for active power transfer and power quality improvement," *IET Renew. Power Gener.*, vol. 12, no. 8, pp. 920–927, Jun. 2018.

[106] L. Asiminoaei, R. Teodorescu, F. Blaabjerg, and U. Borup, "Implementation and Test of an Online Embedded Grid Impedance Estimation Technique for PV Inverters," *IEEE Trans. Ind. Electron.*, vol. 52, no. 4, pp. 1136–1144, Aug. 2005.

[107] S. Cobreces, E. J. Bueno, D. Pizarro, F. J. Rodriguez, and F. Huerta, "Grid Impedance Monitoring System for Distributed Power Generation Electronic Interfaces," *IEEE Trans. Instrum. Meas.*, vol. 58, no. 9, pp. 3112–3121, Sep. 2009.

[108] C.-T. Lee, C.-W. Hsu, and P.-T. Cheng, "A Low-Voltage Ride-Through Technique for Grid-Connected Converters of Distributed Energy Resources," *IEEE Trans. Ind. Appl.*, vol. 47, no. 4, pp. 1821–1832, Jul. 2011.

APPENDIX: PERMISSIONS

Chapter 2 References

Chapter 3 References

Chapter 4 Reference

M. A. Shuvra and B. H. Chowdhury, " A Reconfigurable and Flexible Voltage Control Strategy with Integrated Energy Storage for Advanced Distribution System," *IET Journal of Renewable Power Generation* (in review)

Chapter 5 Reference

M. A. Shuvra and B. H. Chowdhury, "Distributed Dynamic Grid Support using Smart PV Inverters during Unbalanced Grid Faults," *IET Journal of Renewable Power Generation* (in review)